ELECTROCHEMICAL, KINETIC AND MOLECULAR MECHANIC ASPECTS OF RHODIUM(I) AND RHODIUM(III) COMPLEXES

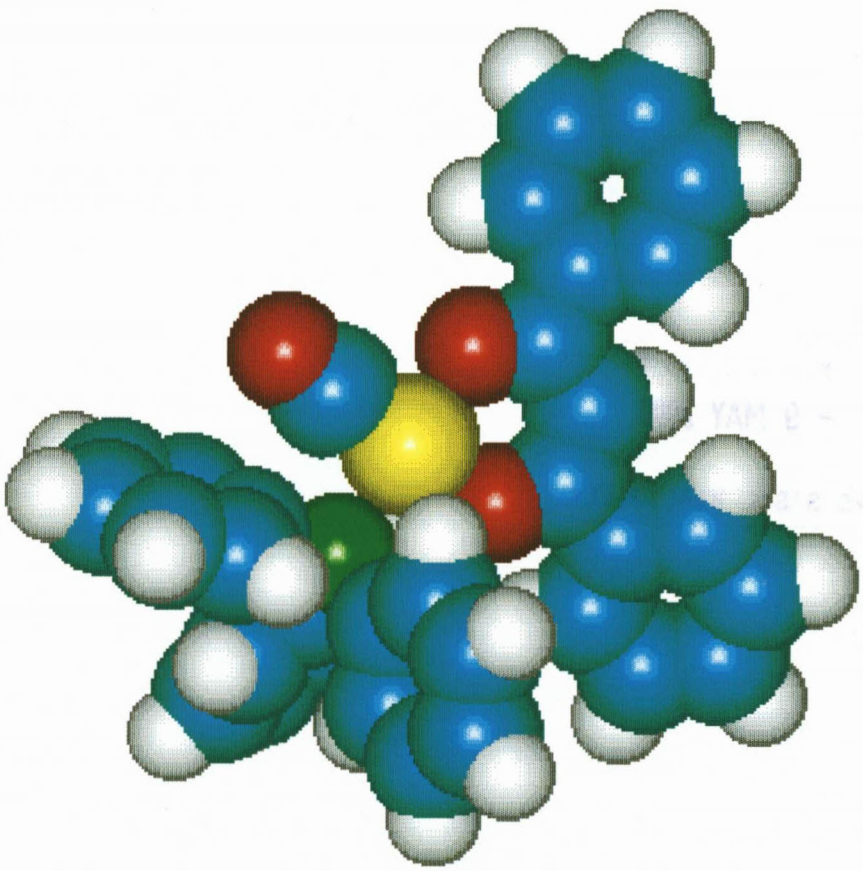

Computed structure of
1,3-Diphenyl-1,3-Propanedionato-κO, κO-Triphenyl Phosphine Rhodium(I)

ELECTROCHEMICAL, KINETIC AND MOLECULAR MECHANIC ASPECTS OF RHODIUM(I) AND RHODIUM(III) COMPLEXES

DELANIE LAMPRECHT

A thesis submitted to meet the requirements for the degree of

PHILOSOPHIAE DOCTOR

November 1998

In the

FACULTY OF SCIENCE
DEPARTMENT OF CHEMISTRY

At the

UNIVERSITY OF THE ORANGE FREE STATE

PROMOTER

PROF. G.J. LAMPRECHT

ACKNOWLEDGEMENTS

Looking back at my childhood days, playing with molecular structure models, I wonder whether I had any choice other than to become a scientist.

I would like to thank my parents for introducing me to the world of science, creating in me an interest in the unseen mechanisms of the everyday life. To my dad, there are no words to describe my appreciation for everything - for giving me wisdom that nobody can take away from me. I thank you from the bottom of my heart and am proud to be your daughter.

TABLE OF CONTENTS

INTRODUCTION

PART 1
CHEMICAL KINETICS

OXIDATIVE ADDITION KINETICS OF METHYL IODIDE TO RHODIUM(I) β-DIKETONATO CARBONYL PHOSPHINE COMPLEXES

CHAPTER 4:
CHEMICAL OXIDATION AND REACTION MECHANISM

PART 2
ELECTROCHEMISTRY

ELECTROCHEMICAL OXIDATION OF RHODIUM(I) β-DIKETONATO CARBONYL PHOSPHINE COMPLEXES

CHAPTER 5:
STATIONARY-ELECTRODE CYCLIC VOLTAMMETRY

CHAPTER 6:
ELECTROCHEMICAL MECHANISTIC STUDIES

PART 3
MOLECULAR MECHANICS

THE DEVELOPMENT AND APPLICATIONS OF A RHODIUM(I) CARBONYL PHOSPHINE FORCE FIELD

INTRODUCTION

BACKGROUND AND OBJECTIVES:

The thesis is submitted in three independent but interrelated parts, namely:

Part 1: **Chemical Kinetics**

Part 2: **Electrochemistry**

Part 3: **Molecular Mechanics**

Background

The original impetus for the study of Rh(I) complexes was their use as homogeneous catalysts in the chemical industry. The study of the oxidative addition kinetics of CH_3I to Rh(I) complexes was a logical outflow since these reactions play an important role in many catalytic cycles such as carbonylation[1,2,3,] and the conversion of methanol into acetic acid[4,5] where a Rhodium Iodide - Methyl Iodide promoted catalyst is used.

The synthesis of organometallic compounds, of the type as formulated below, with anti-neoplastic properties and the anchoring of these complexes onto water soluble polymer carriers, forms part of the research of the polymer branch (Prof. J. C. Swarts) of the Physical Chemistry section.

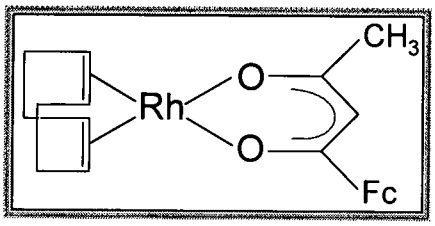

It is in fact the ferricenium ion, and not the ferrocene itself, that is the active anti-neoplastic agent in cancer treatment, and this phenomenon led to the introduction of electrochemical studies on Rh(I) complexes.

---

[1] Stille J.K., Lau S.Y., *Acc. Chem. Res.*, **10**, 434, (1977)
[2] Collman J.P., *Acc. Chem. Res.*, **1**, 136, (1968)
[3] Webster D.E., *Adv. Organomet. Chem.*, **15**, 147, (1977)
[4] Foster D., Adv. *Organomet. Chem.*, **17**, 255, (1979)
[5] Foster D., Singleton T.D., *J. Mol. Catal.*, **17**, 299, (1982)

During chemical kinetic and electrochemical investigations, knowledge of the molecular structures of reagents and products is required for the meaningful interpretation of results, and consequently X-ray crystallography followed as part of the study. The latter developed into a molecular mechanics investigation with the purpose to predict future structures and also to help with the formulation of the intermediates obtained during oxidative addition.

Objectives

Consider the oxidative addition of CH_3I to Rh(I)(β-diketonato) complexes. In contrast to the diphosphite complexes[6,7] of Rh(I)[(A)], the presence of a carbonyl ligand[(B)] offers the interesting possibility of giving a *trans* co-ordinated alkyl[(C)], and/or via isomerisation (carbonyl insertion) the acyl species[(D)], and/or the *cis* co-ordinated alkyl[(E)], which is formed by isomerisation of either the *trans* co-ordinated alkyl[(C)] or the acyl[(D)].

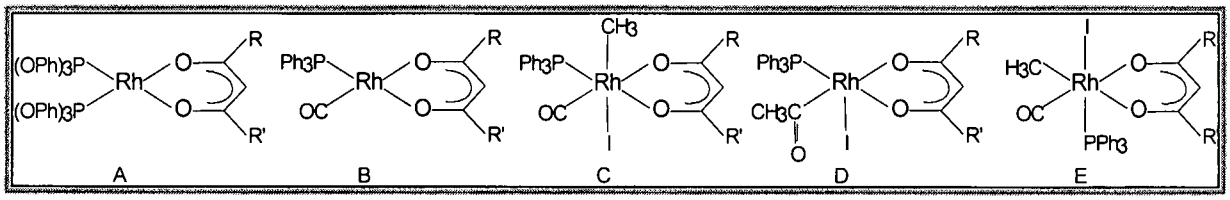

The preferred choice as well as the reactivity of the complex is influenced by the nucleophilicity of the metal ion. The latter is determined by, and can be changed by, the electron donating or electron withdrawing properties of the substituents R and R' of the β-diketonato ligands. The fact that only one CO group in the Rh(I) Dicarbonyl complex is substituted by PPh_3[(B)] can be used to determine the relative *trans* influence of the oxygen bonding atoms. This electronic effect may however be dominated by the bulkiness, or steric hindrance, of the groups R and R'. Steric effects can be important in controlling the rate of oxidative addition reactions. A relation between electrochemical oxidation (oxidation potential by means of cyclic voltammetry) and the pKa values of the various β-diketones co-ordinated onto the Rhodium is expected to be independent of steric parameters. The relation between chemical oxidation by means of CH_3I and the pKa values of the various β-diketones

[6] van Zyl G.J., Lamprecht G.J., Swaddle T.W., *Inorg. Chim. Acta*, **143**, 223, (1988)
[7] Lamprecht G.J., Beetge J.H., *S. Afr. J. Chem.*, **40(2)**, 131, (1987)

co-ordinated onto the Rhodium, is expected to be influenced by steric parameters. Electrochemical investigations can also offer numerous new ways to explore the chemistry of these Rhodium complexes, in particular the role of solvent co-ordination.

Two possible intermediates, a concerted three centred or a linear polar transition state, are postulated during the oxidative addition of CH_3I reaction to Rh(I) Carbonyl Phosphine complexes[8,9].

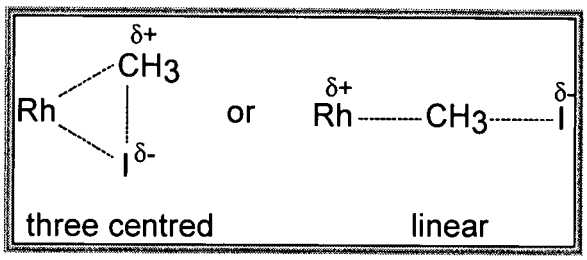

It is further speculated[8,9] that a concerted three centred intermediate will lead to *cis* co-ordination(E) and a linear polar transition state will lead to *trans* co-ordination(C). The development of a Rh(I) force field, with the aid of molecular mechanics, should offer a better alternative to address the question of intermediates.

Against this background the following goals were set for this study:

- The synthesis and characterisation of at least four Rh(I)(β-diketonato)(CO)(PPh_3) complexes(B) with different electron donating properties, where the pKa values of the free β-diketones were known.
- The use of X-ray crystallography to determine the molecular structure of at least one Rh(I)(β-diketonato)(CO)(PPh_3) complex.
- The study of the oxidation addition kinetics of CH_3I to all Rh(I)(β-diketonato)(CO)(PPh_3) complexes, by means of Visible spectroscopy, to obtain the reaction rate constants and to correlate the latter with the electronic and steric parameters of the various Rh(I)(β-diketonato)(CO)(PPh_3) complexes.

[8] Venter J.A., Leipoldt J.G., van Eldik R, *Inorg. Chem.*, **30**, 2207, (1991)
[9] Leipoldt J.G., Basson S.S., Botha L.J., *Inorg. Chim. Acta.*, **168**, 215, (1990)

- The use of Infrared and NMR kinetics to justify the Visible results as well as to link the reaction rate constants obtained to specific intermediate reaction paths and to postulate the oxidative addition reaction mechanism.
- The use of variable temperature and high pressure kinetics to determine the thermodynamic activation parameters of enthalpy, entropy and volume.
- The investigation of the effect of solvent polarity on the oxidative addition reaction rate.
- The use of activation parameters and solvent effects for the formulation of an intermediate during the oxidative addition of Rh(I) to Rh(III).
- The use of cyclic voltammetry to determine the oxidation potentials of Rh(I) to Rh(III) during electrochemical oxidation and to determine the relationship of these oxidation potentials obtained with the pKa values of the respective β-diketones as well as with the reaction rate constants that were obtained during chemical oxidation.
- The technique of bulk electrolysis to prove the two electron electrochemical oxidation of Rh(I) to Rh(III).
- Solvent co-ordination during the electrochemical oxidation of Rh(I) to Rh(III).
- The use of known molecular structures to develop a molecular mechanics force field for the Rh(I) complexes and its use to predict unknown Rh(I) structures.
- The possible use of the molecular mechanics force field to help with the formulation of the reaction intermediate obtained during the chemical oxidation of Rh(I) to Rh(III).

PART 1
CHEMICAL KINETICS

OXIDATIVE ADDITION KINETICS OF METHYL IODIDE TO RHODIUM(I) β-DIKETONATO CARBONYL PHOSPHINE COMPLEXES

CHAPTER 1:

CO-ORDINATION COMPOUNDS

1.1 Introduction

The chemistry of metals in solution is essentially the chemistry of their complexes. A metal ion in solution is co-ordinated to the solvent molecules and/or to other ligands. Metal ions are almost never encountered without effective shielding from one another. The shielding in solution is provided either by the solvent or by some other ligands, and in the solid state, cations are surrounded by anions. A co-ordination compound or metal complex can be defined as a central atom or ion attached to a sheath of molecules[1]. These molecules bonded directly to the metal ion are called ligands. For example, acetylacetone is a bidentate ligand that displays keto-enol tautomerism (Figure 1.1).

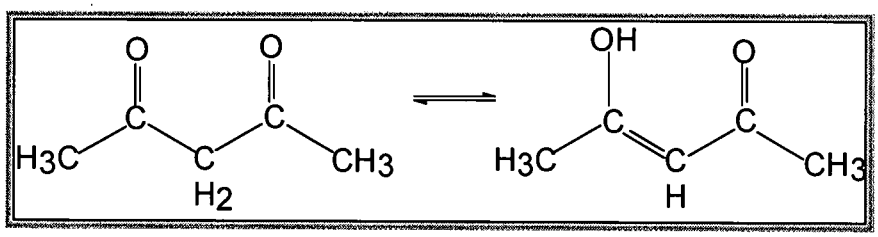

Figure 1.1: Keto-enol tautomerism in acetylacetone.

[1] Douglas B., McDaniel D., Alexander J., *Concepts and Models of Inorganic Chemistry, Chapter 9*, Third Edition, Wiley, New York, (1993)

The enol form can lose a proton and co-ordinates to the metal ion through both oxygen atoms, with a resulting chelate ring (Figure 1.2). The term metal chelate is used to refer to a compound formed as a result of chelation. Chelating ligands must have two or more points of attachment.

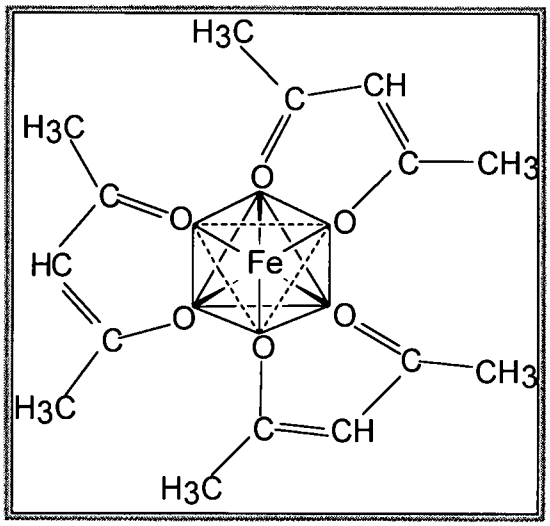

Figure 1.2: Chelate rings in the tris(acetylacetonato)iron(III) compound.

1.2 Stability of Co-ordination Complexes

The co-ordination process is in effect an acid-base reaction. In general, an increase in the basicity of a ligand or an increase in the acidity of the metal enhances the stability of the complex formed.

Stability of a compound refers to either thermodynamic stability with respect to the formation from its elements, or to kinetic stability with respect to the decomposition of the compound.

Ligands are Lewis bases. For consistency, the basicity of a ligand is expressed in terms of pKa (-logKa), the dissociation constant of its conjugate acid.

1.2.1 Effect of the Metal Ion

Thermodynamic stability of the complexes formed by various metals follows some regular trends, such as those including size and charge effects, factors that determine the Lewis acid strength of a metal ion. Generally, the stability

of complexes decreases with the increasing atomic number of the electropositive metal.

1.2.2 Basicity and Structure of Ligands

With a given donor atom, the stability of the metal complex generally increases as the basicity of the ligand increases. Generally, the complexes of chelate ligands are much more stable than those of monodentate ligands. This enhanced stability is referred to as the chelate effect.

The chelate effect can be largely an entropy effect for non-transition metal ions, but there may be a significant enthalpy effect for transition metal ions[2].

$\Delta G° = -RT\ln K$. K increases as $\Delta G°$ becomes more negative. From $\Delta G° = \Delta H° - T\Delta S°$ a more negative $\Delta G°$ can result from making $\Delta H°$ more negative or from making $\Delta S°$ more positive.

Consider the thermodynamic data[3] of the following two reactions (Table 1.1):

$$Cd^{2+}(aq) + 4CH_3NH_2(aq) \rightleftharpoons [Cd(NH_2CH_3)_4]^{2+}(aq)$$

$$Cd^{2+}(aq) + 2H_2NCH_2NH_2(aq) \rightleftharpoons [Cd(H_2NCH_2NH_2)_2]^{2+}(aq)$$

Ligands	$\Delta H°(kJ.mol^{-1})$	$\Delta S°(J.mol^{-1}.deg^{-1})$	$-T\Delta S°(kJ.mol^{-1})$	$\Delta G°(kJ.mol^{-1})$
$4CH_3NH_2$	-57.3	-67.3	20.1	-37.2
$2H_2NCH_2NH_2$	-56.5	14.1	-4.2	-60.7

Table 1.1: Two reactions illustrating a purely entropy based chelate effect.

The enthalpy difference of the two reactions under consideration is well within experimental error. The chelate effect can thus be traced entirely to the entropy difference. The main cause of the large entropy increase in the latter reaction is due to the increase in the number of unbound molecules.

[2] Frausto de Silva J.J.R, *J.Chem.Ed.*, **60**, 390, (1983)
[3] Cotton F.A., Wilkinson G., *Advanced Inorganic Chemistry, Chapter 2*, Fifth Edition, Wiley, New York, (1988)

1.3 Valence Bond Models

1.3.1 Effective Atomic Number

The formulas of co-ordination compounds are complex. According to Sidgwick[4], the co-ordination process provides the opportunity for a transition metal ion to reach a noble gas configuration. The effective atomic number of a metal ion is calculated by adding the electrons of the metal ion to those shared with it through co-ordination. The effective atomic number concept has been particularly successful for complexes of low valent metals (oxidation number $\leq$ II). This electron counting scheme is also called the eighteen-electron rule, in contrast with the visual octet rule for "simple" compounds.

1.3.2 Hybridisation and Orbital Occupancy

According to the valence bond theory, co-ordination compounds result from the use of available empty bonding orbitals on the metal ion for the formation of co-ordinate covalent bonds. The geometries are determined in part by size and charge effects, but also by the orbitals available for bonding.

Planar complexes are common for d^8-ions, for example: Pd(II), Pt(III), Au(III), Rh(I) and Ir(I). The empty d-orbitals necessary for forming dsp^2-hybrid orbitals are available, or can be made available by paring electrons in the four other d-orbitals.

1.4 The Ligand Field Theory

The five d-orbitals are degenerate (of equal energy) in gaseous metal ions. The simple electrostatic model fails to predict differences of bond energies among complexes of different transition metals, because it ignores the fact that the degeneracy of the d-orbitals may be removed in the presence of ligands.

There are two aspects that set the study of the electronic structures of transition metal compounds apart from the remaining body of the valence theory. One is the

[4] Elshenbrauch Ch., Salzer A., *Organometallics, a Concise Introduction, Chapter 12*, New York, VCH, (1989)

presence of partly filled d- and f-shells. The second is that there is a crude but effective approximation, called crystal field theory, which provides a way of determining how the energies of the metal ion orbitals will be affected by a set of surrounding atoms or ligands.

Let us consider a metal ion, M^{n+}, lying at the centre of an octahedral set of point charges (Figure 1.3).

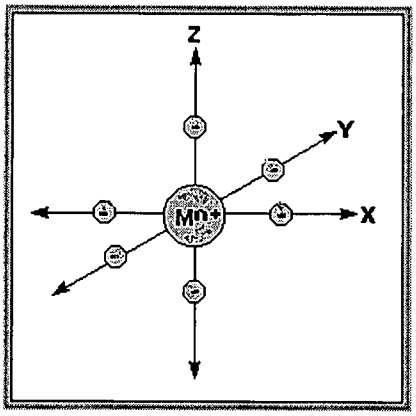

Figure 1.3: Six negative charges arranged octahedrally around a centre M^{n+} ion.

If some d-orbitals are filled with electrons, the d-orbitals will not be equivalent. The electrons will prefer to occupy the orbitals in which they can get as far as possible from the negative charges. Both the d_{Z^2}- and $d_{X^2-Y^2}$-orbitals have lobes that are concentrated in the vicinity of the charges, whereas the d_{XY}-, d_{YZ}-, and d_{XZ}-orbitals have lobes that project between the charges (Figure 1.4).

D_{XY}-, d_{YZ}- and d_{XZ}-orbitals are equally favourable for an electron and have equivalent environments in the octahedral complex. The two unfavourable orbitals, d_{Z^2} and $d_{X^2-Y^2}$, are also equivalent and of higher energy. The energy difference values between the two energy states depend on the identity of the ligand co-ordinating on the metal ion and follow the order known as the spectrochemical series:

Weak d-orbital splitting ligands - $I^- < Br^- < Cl^- < F^- < OH^- < C_2O_4^{2-} < H_2O < NCS^- <$ py $< NH_3 <$ en $<$ bipy $<$ o-phen $< NO_2^- < CN^-$ - strong d-orbital splitting ligands.

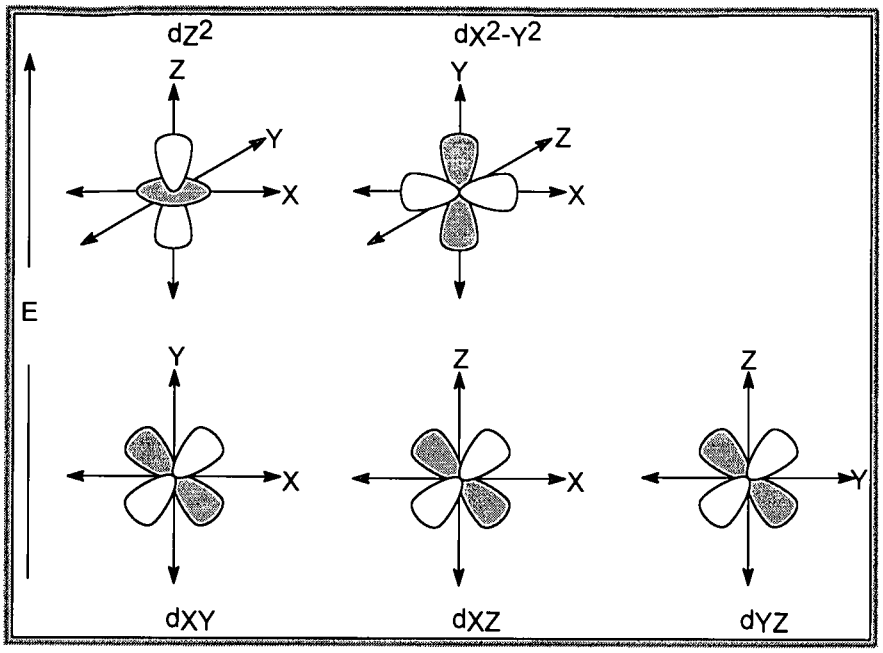

Figure 1.4: *The distribution of electron density in the five d-orbitals and its orientation with respect to the set of octahedrally arranged negative charges.*

1.4.1 Planar Complexes

Metal ions with d^8-configuration (Au(III), Ni(II), Pd(II), Pt(II), Rh(I) and Ir(I)) usually form four co-ordinate square planar complexes, in which splitting can be great enough to bring about paring of all electrons. The very high-energy $d_{X^2-Y^2}$-orbital is left vacant.

The ideal radius ratio ($r^+/r^- \geq 0.414$) for square planar arrangement is identical to that of an octahedral complex. The square planar arrangement is encountered only in cases where the additional splitting of the levels is most advantageous or where the planar configuration is imposed by the geometry of the ligands.

1.5 Rhodium: Group VIII

The chemistry of Rhodium centres around the oxidation states I, II and III. The II oxidation state is best characterised by complexes with metal-metal bonds, as exemplified by $Rh_2(O_2CCH_3)_4$.

The chemistry of Rh(I) usually involves π-complexing ligands such as CO, PR_3, alkenes and arenes. Square, tetrahedral and five co-ordinate species are found. The criteria for relative stability of five and four co-ordinate species are by no means fully established. Substitution reactions of square species are therefore rapid and proceed by an associative pathway including a five co-ordinate intermediate[5].

The Rh(I) complexes are prepared by some form of reduction, either by similar Rh(III) complexes or by halide complexes such as $RhCl_3.3H_2O$ in the presence of the complexing ligand.

Most of the square Rh(I) complexes undergo oxidative addition reactions and this constitutes a way of preparing Rh(III) complexes. Rh(III) forms octahedral complexes, which are diamagnetic.

[5] Cotton F.A., Wilkinson G, *Advanced Inorganic Chemistry, Chapter 17,* Fifth Edition, Wiley, New York, (1988)

CHAPTER 2:

REACTION MECHANISMS OF CO-ORDINATION COMPOUNDS

2.1 The Kinetic Model

The model that chemists currently use to rationalise and predict what goes on during chemical reactions was developed during the 1930's from the transition state theory[1]. The cause of a reaction is seen as involving collisions of reactants sufficiently energetic to form an activated complex or transition state. Along the path from reactants to products, kinetic energy is converted to potential energy by such processes as bond stretching, partial bond formation and angular distortion. The exact processes that occur depend on the particular reaction. The transition state is the species with maximum potential energy resulting from these motions. The energy required to reach the transition state from the reactant ground state is called the activation energy. After the transition state, the collection of atoms rearranges towards a more stable species.

2.1.1 Activation Parameters

By studying a reaction at different temperatures, values of ΔH^*, which relates to the energy required for reaching the transition state (enthalpy of activation), and values of ΔS^*, which relates to the change in ordering on reaching the transition state (entropy of activation), may be extracted.

Examining activation parameters provides added information on the mechanism for a series of related complexes. Measurements at various pressures, P, have been employed to obtain volume of activation, ΔV^*. The reaction rate, k, is proportional to $e^{(-P\Delta V^*/RT)}$ and a plot of ln(k) *versus* P gives therefore a straight line of slope $-\Delta V^*/RT$ (Chapter 4). The naïve expectation is that dissociative mechanisms should lead to $\Delta V^* > 0$ because a ligand is

[1] Douglas B., McDaniel D., Alexander J., *Concepts and Models of Inorganic Chemistry, Chapter 11,* Third Edition, Wiley, New York, (1993)

released into the bulk solution in the transition state. On the other hand, an associative mechanism partially bonds species formerly present in the bulk solution and thus might be expected to lead to $\Delta V^* < 0$. This is probably true insofar as only the bond angles and bond distances intrinsic to the reacting species are concerned. Solvent effects are also important. However, any process that creates charge leads to solvent electrostriction and a negative contribution to ΔV^*. Conversely, charge neutralisation gives a positive contribution. The volume of activation is thus partitioned into two contributions:

$\Delta V^* = \Delta V^*_{intrinsic} + \Delta V^*_{solvent}$

Another factor not yet assessed is the contribution by the non-labile ligands whose bond strengths and bond distances will surely change during the formation of the transition state.

2.1.2 Theories of the *trans* effect

Ligands in square planar complexes show distinct preferences for the site *trans* to one ligand than to another. This phenomenon is known as the *trans* effect and the approximate ordering of ligands is[2]:

$CO, CN^-, C_2H_4 > PR_3, H^- > CH_3^-, SC(NH_2)_2 >> C_6H_5^-, NO_2^-, I^-, SCN^- > Br^- > Cl^- > py > NH_3, OH^-, H_2O$

The *trans* effect is essentially an empirical observation on reaction rates. All theorising about the *trans* effect must recognise that since it is a kinetic phenomenon, depending on the activation energies, the stability of both the ground state and activated complex is relevant. A good *trans* directing ligand could weaken the bond between the metal and the *trans* ligand. This is a thermodynamic effect that has been called the *trans* influence to distinguish it from the kinetic *trans* effect[3]. Several theories exist as to how a ligand might weaken the bond *trans* to itself. One of the earliest was the polarisation theory of Grinberg in which a good *trans* directing ligand was visualised as being very polarisable and forming an ionic bond to the metal[1]. A dipole then

[2] Cotton F.A., Wilkinson G., *Advanced Inorganic Chemistry, Chapter 29*, Fifth Edition, Wiley, New York, (1988)
[3] Appleton T.G., Clark H.C., Manzer L.E., *Co-ord. Chem. Rev*, **10**, 335, (1973)

serves to repel the *trans* ligand, thus weakening the bond. This could account for the presence of H^- and CH_3^- high in the *trans* effect series.

A second view emphasises the effectiveness of good σ-donor ligands in weakening the *trans* bond. With dsp^2-hybrids, *trans* ligands share the $d_{X^2-Y^2}$-, s- and one p-orbital. A good σ-donor ligand claims a larger share of the metal σ-orbitals, leaving a lesser share to bond the *trans* ligand. The order of some important ligands with regard to their *trans* influence is[2]:
$H^- > PR_3 > SCN^- > I^-, CH_3^-, CO^-, CN^- > Br^- > Cl^- > NH_3 > OH^-$

The sequence is generally similar to the *trans* effect sequence, with certain striking exceptions, such as the positioning of CN^- and CO. This can be traced to the ability of these ligands to produce a *trans* effect by participating in π-bonding in the transition state.

Ligands capable of a high degree of σ-donation or π-acceptance can confer stability and are good *trans* directors. In brief, π-acceptor ligands can help to drain off some of the extra electron density provided by the addition of a fifth ligand, while good σ-donors claim a large share of metal orbitals for bonding.

Ligands high in the *trans* effect series are both good entering groups and poor leaving groups.

2.2 Oxidative Addition Reactions

An ubiquitous reaction in organometallic chemistry is oxidative addition in which a low-valent transition metal complex, behaving simultaneously as a Lewis acid and Lewis base, reacts with a molecule XY to yield a product in which both the oxidation number and co-ordination number of the metal are increased.
$L_yM^n + XY \rightarrow L_yM^{n+2}(X)(Y)$

The reverse reaction can be termed reductive elimination. These terms merely describe a reaction and have no mechanistic implication. The mechanisms can be

extremely complicated and vary with the nature of the metal-ligand system and the reactant that is oxidatively added.

For an oxidative reaction to proceed there must be[4]:

a.) nonbonding electron density on the metal,

b.) two vacant co-ordination sites on the complex L_yM to allow the formation of two new bonds to X and Y,

c.) a metal with its oxidation state separated by two units.

Oxidative addition of 16-electron systems such as the co-ordinated unsaturated square planar complexes of Rh(I), Ir(I) or Pt(II) produces 18-electron systems. Compounds of 18-electron systems cannot undergo oxidative addition reactions without expulsion of a ligand.

For oxidative addition of 16-electron complexes where no ligand loss is involved, there may be an equilibrium reaction.

$$L_yM^n + XY \rightleftharpoons L_yM^{n+2}(X)(Y)$$

Whether the equilibrium lies on the reduced or the oxidised side depends on:

a.) the nature of the metal and its ligands,

b.) the nature of the added molecule XY and of the bonds M-X and M-Y ,

c.) the medium in which the reaction is conducted.

Qualitatively, for the oxidative addition to proceed, $E_{MX} + E_{MY}$ must exceed E_{XY}, where E_{MX} and E_{MY} are the free energy of the new bonds to the metal and E_{XY} is the free energy for bond dissociation of XY. Usually only E_{XY} is known.

The higher oxidation states are usually more stable for the heavier than for the lighter metals. For example, Ir(III) species are generally more stable than Rh(III) species.

[4] Cotton F.A., Wilkinson G., Gous P.L, *Basic Inorganic Chemistry, Chapter 30,* Second Edition, Wiley, New York, 1987

Factors that tend to increase the electron density on the metal increase the oxidisability. High electron density on the metal atom, of necessity in low oxidation states, can be delocalised onto the ligand. Ligands with the ability to accept electron density into low-lying empty π-orbitals are called π-acids.

CO provides a paradigm for bonding of π-acid ligands to metals. The valence-bond structure of CO shows two non-bonding electron pairs: :C ≡ O:

The molecular orbital energy diagram of CO (Figure 2.1) shows that the electron pair in the molecular orbital localised on C is more loosely bonded and is the one available for electron donation to a metal.

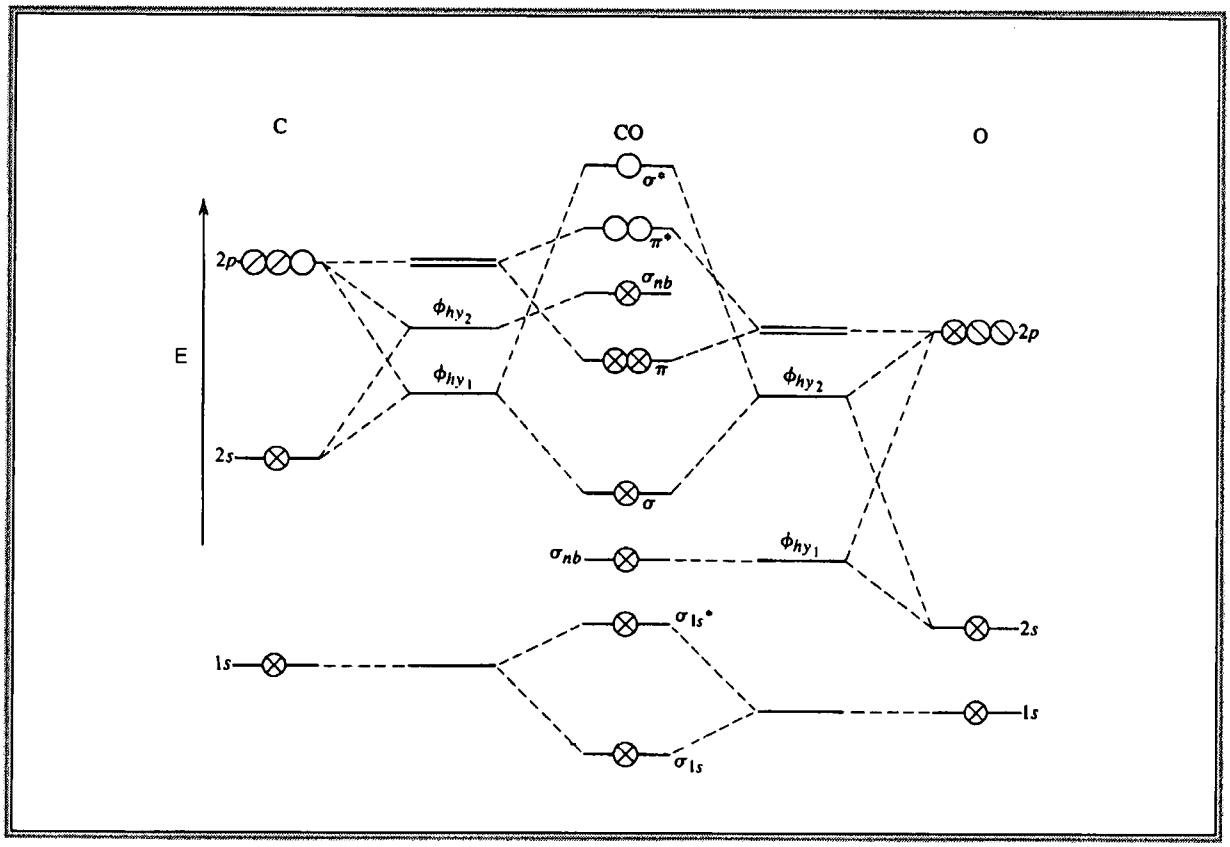

Figure 2.1: The molecular orbital energy-level diagram for CO.

CO also has a pair of empty, mutually perpendicular, π*-orbitals that overlap with filled metal orbitals of π-symmetry and help to drain excess negative charge from the metal onto the ligand. Metal-to-ligand electron donation is referred to as back bonding (Figure 2.2).

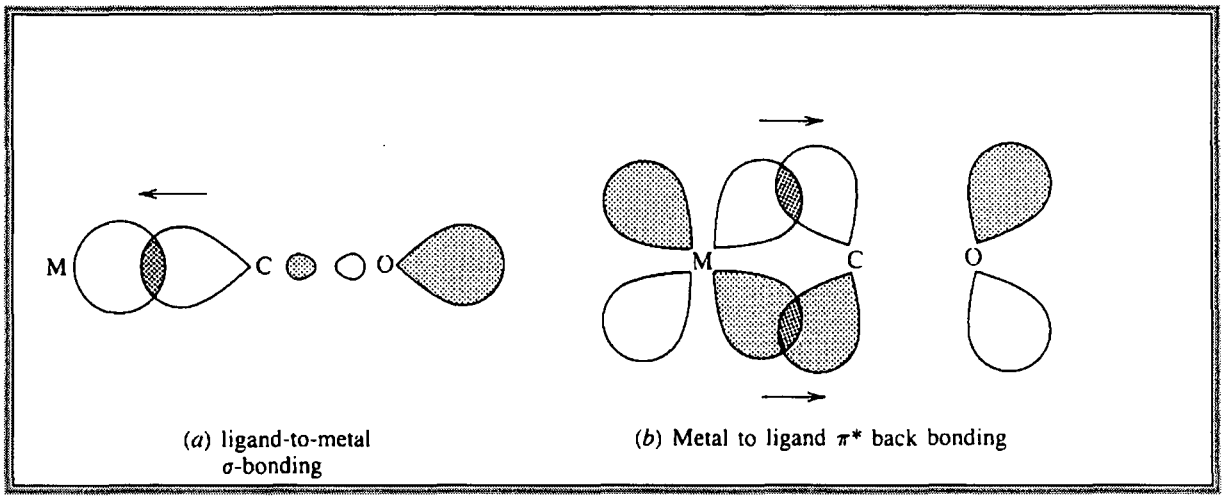

Figure 2.2: Orbital overlap in M-CO bonding.

Energetically, the most important bonding component is σ L → M donation. Back bonding, the π-component, assumes greater importance when the metal has many electrons to dissipate. Thus low oxidation states are stabilised by π-acid ligands.

Steric properties of ligands are also important. Very bulky ligands tend to decrease the ease of oxidative addition. Compounds of type PX_3, as well as AsX_3, SbX_3, SX_2 and SeX_2 are also important π-bonding ligands. Tertiary phosphines and phosphites are much better Lewis bases than CO and can replace any CO group in a CO containing molecule. PR_3 ligands compete with CO groups for metal dπ-electrons. The significant σ-donor ability[5] and steric requirements[6] are therefore of great importance in the structures of $M(CO)_x(PR_3)_y$ type molecules.

P(III) ligands have a lone pair for σ-donation and filled π-orbitals, as well as empty anti-bonding π*-orbitals. The donor and acceptor ability of these ligands are influenced by the identity of R. π-Acidity is promoted by electron withdrawing groups, such as F and OR groups bonded to the Phosphor. The electronegative substituent will reduce the σ-donor character so that there will be less Phosphor→Metal electron transfer and Metal dπ → Phosphor dπ transfer will be needed. The general order of π-acidity for P(III) is:

$PF_3 > PCl_3 > P(OAr)_3 > P(OR)_3 > PAr_3 > PR_3$

[5] Einstein F.W.B. *et al.*, *Inorg. Chem.*, **23**, 4361, (1984)
[6] Cotton F.A. *et al.*, *Inorg. Chem.*, **21**, 294, (1982)

Steric factors of the Phosphor ligand, measured by the cone angle θ, also affect the bonding ability to the metal. Tolman[7] obtained values for the apex angle θ of cones centred 228 pm from the P atom and tangent to the van der Waals' radii of the R groups by constructing molecular models to scale and measuring the angle (Figure 2.3).

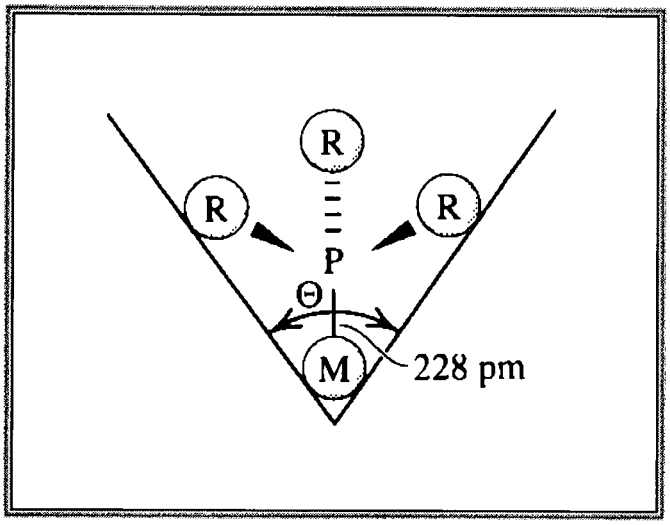

Figure 2.3: Tolman cone angle for PR_3.

All other factors being equal, small cone angles should lead to better bonding by permitting closer ligand approach, but since such compounds are stronger bases, it is not always possible to distinguish steric effects from electronic factors.

2.2.1 Mechanisms of Oxidative Addition Reactions

Pearson[8] has pointed out that reactions proceeding with reasonable low activation energies involve electron flow between orbitals with the same symmetry properties. For oxidative addition, electrons must flow from a filled metal orbital into an anti-bonding X-Y orbital. This allows the X-Y bond to be broken and new bonds to the metal to be formed. The X-Y anti-bonding orbital must overlap in phase with a filled metal orbital (Figure 2.4).

[7] Tolman C.A., *Chem. Rev.*, **77**, 313, (1977)
[8] Pearson R.G., *Symmetry rules for Chemical Reactions*, Wiley, New York, 1976

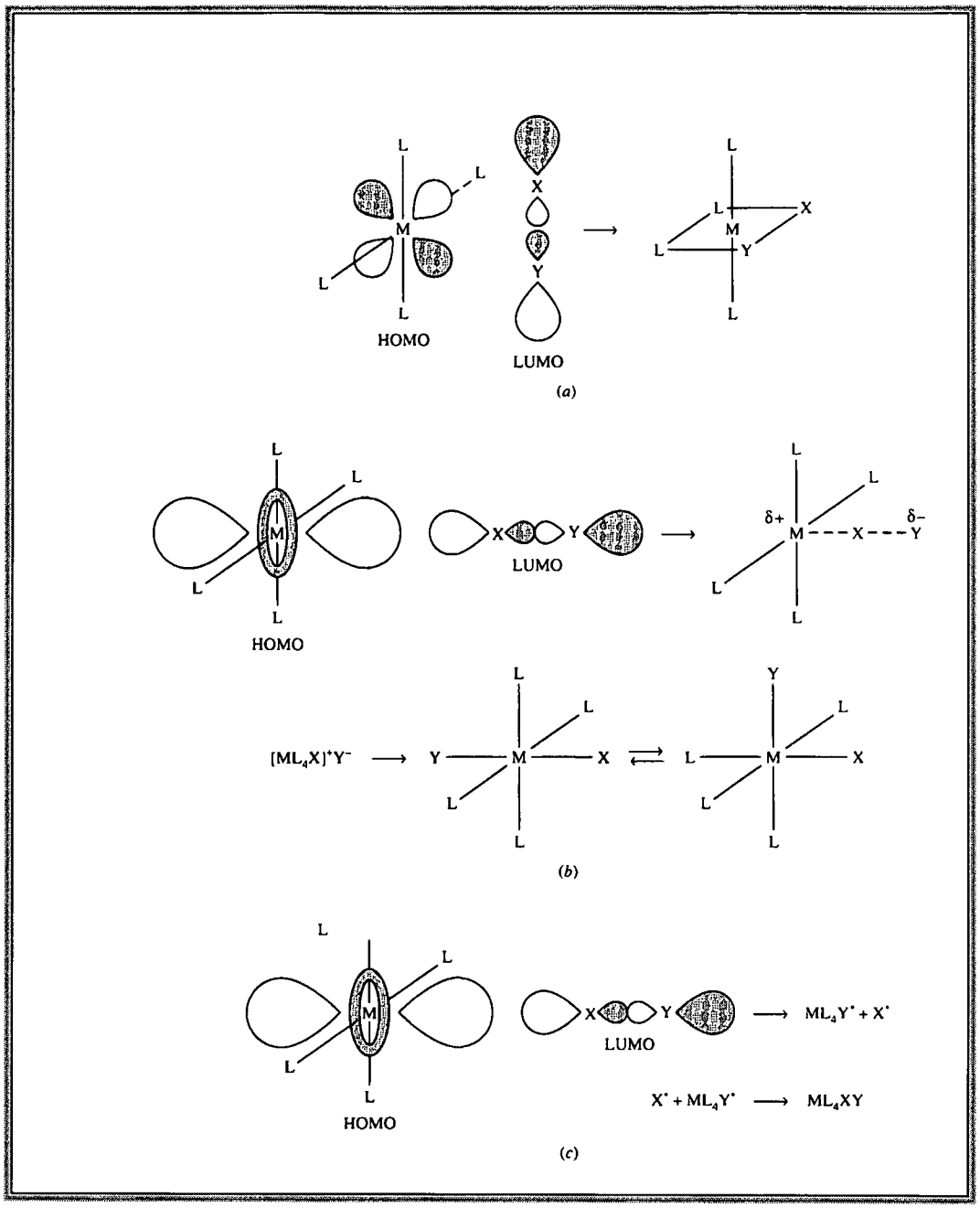

Figure 2.4: Symmetry-allowed overlap of orbitals for electron transfer in oxidative addition to 16 e⁻ ML_4 complexes.

a.) concerted addition

b.) S_n2-type addition

c.) free radical addition

The different possibilities for such overlap lead to the different mechanisms for oxidative addition of X-Y to square planar ML_4 complexes.

The mechanisms of oxidative addition reactions are of four general types:

a.) Ionic b.) S_N2 c.) One step, concerted d.) Free radical

Ionic mechanism:

In polar media, HCl or HBr will dissociate and protonation of a square complex will first produce a five-co-ordinate intermediate. Intramolecular isomerisation is followed by co-ordination of X^-.

S_n2 mechanism:

The transition metal complex attacks an alkyl halide. A polar transition state appears to be involved[9], since there is promotion by polar solvents (Figure 2.5).

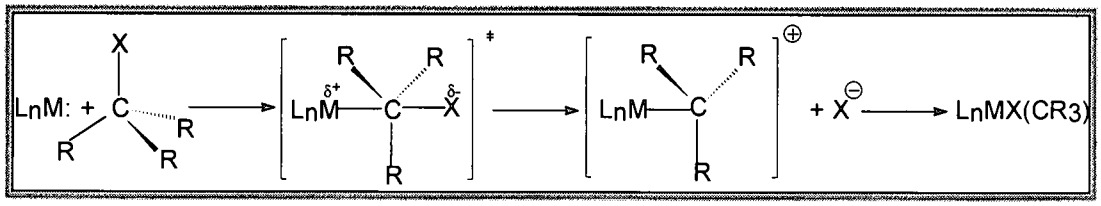

One step, concerted mechanism:

Under non-polar conditions, *cis* addition takes place during oxidative addition (Figure 2.5). For example:

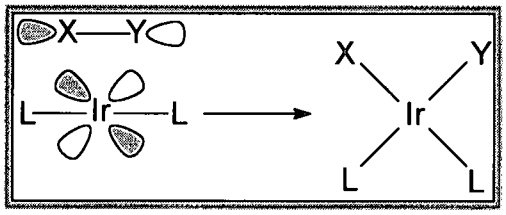

Free radical mechanism:

This is initiated by free radical sources such as peroxides. The chain mechanism involves a one-electron rather than a two-electron step:

$L_nM + R^\bullet \rightarrow L_nMR^\bullet + RX \rightarrow L_nMXR + R^\bullet$

The non-chain process is probably initiated by electron transfer to alkyl halides:

[9] Cotton F.A., Wilkinson G., *Advanced Inorganic Chemistry, Chapter 27*, Fifth Edition, (1988)

$L_nM + RX \rightarrow L_nM^{+\bullet}RX^{-\bullet} \rightarrow L_nMX^{\bullet} + R^{\bullet} \rightarrow L_nMXR$

The majority of simple Bromides and Iodides react with Ir(I), Pd(0) and Pt(0) by one-electron paths, although it seems that CH_3I, $C_6H_5CH_2Cl$ and CH_2=CH-CH_2Cl are generally non-radical.

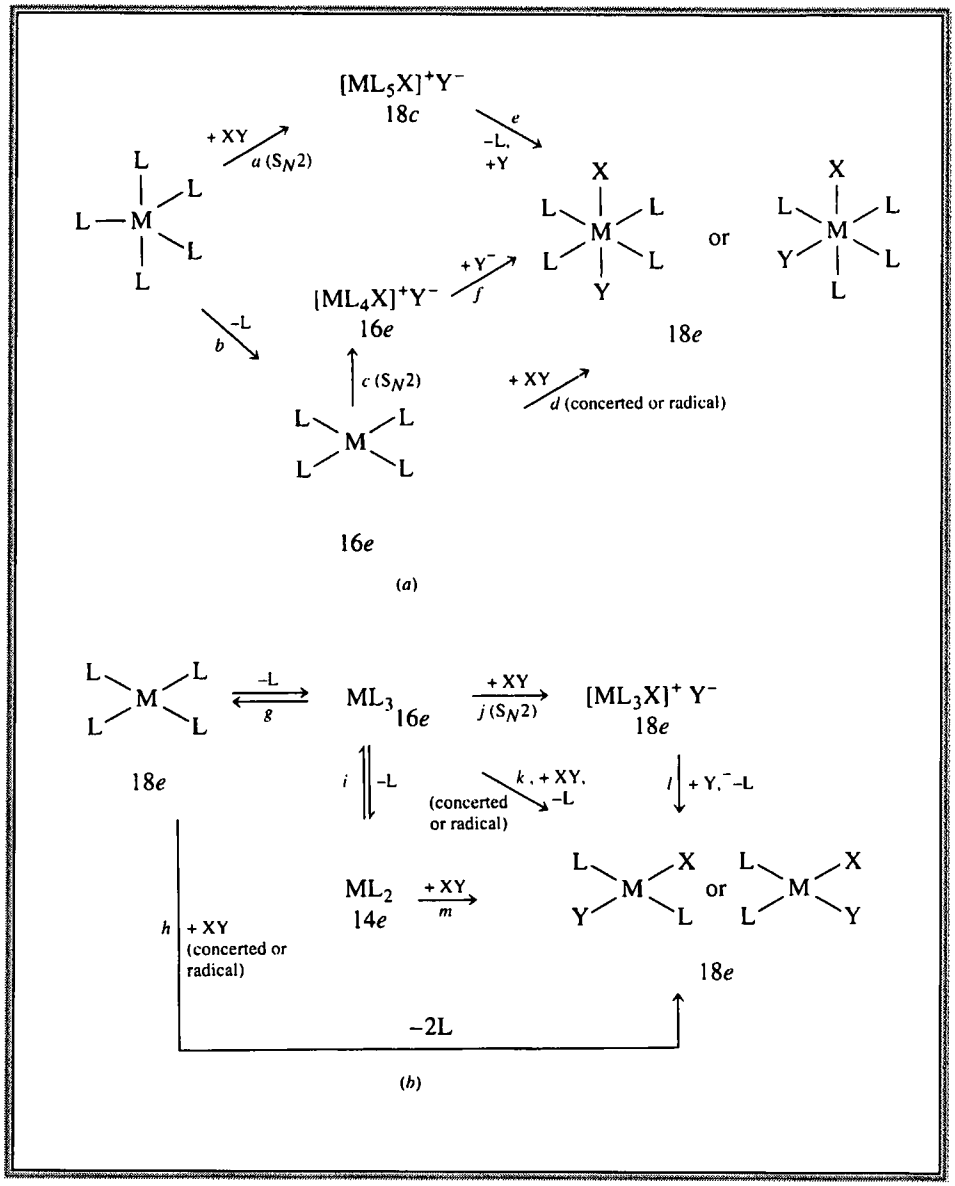

Figure 2.5: Oxidative addition mechanisms.

The final product of oxidative addition will be an isomer that is the most stable thermodynamically under the conditions used. The nature of the final product does therefore not necessarily give a guide to the initial product of the oxidative addition, since isomerisation of the initial products may occur.

2.3 Migration (Insertion) Reactions

The concept of "insertion" is defined as a reaction wherein any atom or group of atoms is inserted between two atoms initially bonded together. Both 1,1- and 1,2-insertions are possible:

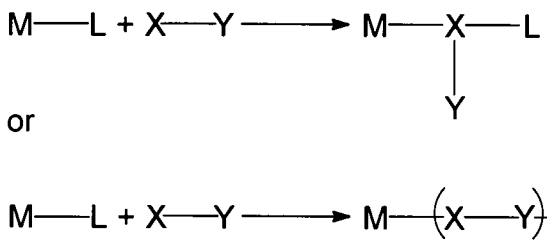

The term "insertion" describes only the result of the reaction and has no mechanistic significance.

2.3.1 Insertion of Carbon Monoxide

Mechanistic studies have shown that the CO molecule that becomes the acyl carbon, is not derived from external CO, but is a CO molecule already co-ordinated to the metal atom. The conversion of an alkyl into an acyl can be effected by the addition of ligands to the metal atom. The first step involves equilibrium between the octahedral alkyl and a five co-ordinated acyl, which is probably square pyramidal with a basal acetyl group[10]. The co-ordinated unsaturated acyl then adds the incoming ligand (L) to reform an octahedral complex.

The CO insertion is a 1,2-insertion of an alkyl group to a co-ordinated CO ligand in a *cis* position, proceeding through a three-centred transition state (Figure 2.6).

[10] Wright S.C. and Baird M.C., *J. Am. Chem. Soc.*, **107**, 6899, (1985)

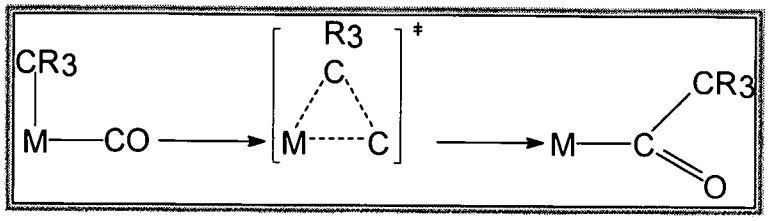

Figure 2.6: An accepted mechanism for CO insertion.

The *cis* complex can equilibrate with the *trans* isomer. Both basicity and size of L influence its ability to capture the intermediate before it reverts back to the alkyl.

CHAPTER 3:

SYNTHESES AND CHARACTERISATION OF RHODIUM(I) β-DIKETONATO CARBONYL PHOSPHINE COMPLEXES

3.1 Introduction

Square planar Rh(I) complexes, being co-ordinatively unsaturated, undergo oxidative addition reactions with various organic and inorganic molecules. Since oxidative addition reactions can proceed via different reaction pathways and because the addition can be either *cis* or *trans*, it is imperative to know the molecular structure of the reactants and products in order to propose suitable reaction mechanisms.

The impetus for these investigations has been the desire to gain a greater understanding of the electronic and steric factors influencing the oxidative addition reactions, which are vital steps in the functioning of many of these compounds as homogeneous catalysis.

Four Rh(I)(β-diketonato)(CO)(PPh_3) complexes, in which the β-diketone has different electronegativities and steric hindrances, were prepared (Table 3.1).

Electronic properties		**Relative bulkiness**
β-diketone	**pK_a**	tfaa < ba < btfa < dbm
dbm	9.4	
ba	8.7	
btfa	6.3	
tfaa	6.3	

Table 3.1: *The electronegativities and relative bulkiness of the various β-diketones used*

β-diketones: *dibenzoylmethane (dbm)*
benzoylacetone (ba)
benzoyltriflouroacetone (btfa)
trifluoroacetone (tfaa)

3.2 Preparation of Rhodium(I) Dicarbonyl Complexes

Rhodium(III) Chloride Trihydrate ($RhCl_3.3H_2O$) (0.05 g) was dissolved in a few drops of water because of the weak solubility in the reaction solvent and reduction agent, N,N-Dimethylformamide (DMF). Distilled DMF (2 ml) was added to the $RhCl_3.3H_2O$ solution and refluxed for approximately 20 minutes until the reaction mixture colour changed from dark red to yellow[1]. The yellow colour[2] was due to the formation of the Rh(I) dimer (Figure 3.1).

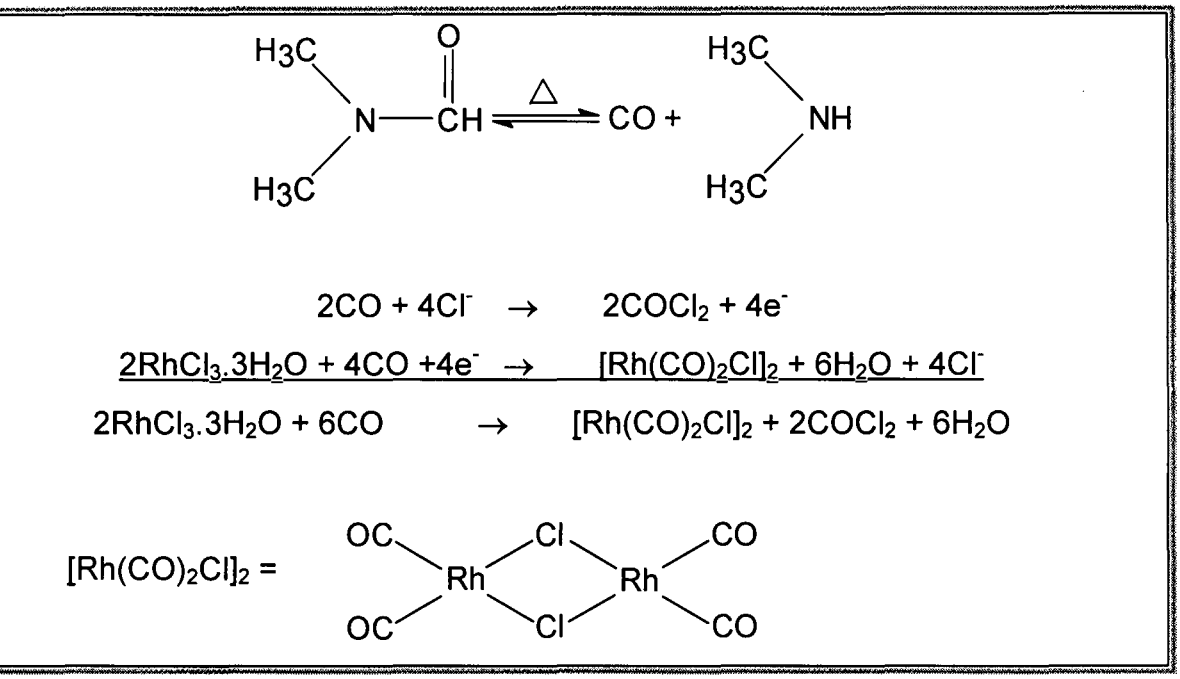

Figure 3.1: Proposed mechanism for the formation of the Rh(I) dimer.

DMF can be used as a source of CO, because DMF decomposes into CO and $HN(CH_3)_2$ upon thermolysis[3].

When using a new clean flask for the preparation of the Rh(I) dimer it was observed that the rate of the colour change from dark red to yellow was very slow (45 minutes to 1 hour) and there was an uncontrolled reduction of Rh(I) to black Rh(0). When the same flask was used repeatedly (after rinsing it with DMF) consistent reaction rates and yields were obtained. The only possible explanation is that absorbed Rhodium and/or its complexes on the glass surface are engaged in some catalytic

[1] Leipoldt J.G., Basson S.S., Bok L.D.C. and Gerber T.I.A., *Inorg. Chim. Acta*, **26**, L35, (1978)
[2] McCleverty J.A., Wilkinson G., *Inorg. Synth.*, **211**, (1966)
[3] Davies J.A., Hockensmith C.M., Kukushkin V Yu and Kukushkin Yu N, *Synthetic Coordination Chemistry, Principles and Practice*, Chapter 9, Singapore, (1996)

activity in decomposing the DMF (Figure 3.1). Under normal circumstances DMF does not decompose upon refluxing.

The respective β-diketones (dbm, ba, btfa, tfaa) were added to the Rh(I) dimer solution in a 1:1 mole ratio. The Rh(I) Carbonyl complexes were precipitated by the addition of ice cold water. The precipitate was centrifuged, washed with ice cold water, dried and characterised by means of infrared spectrophotometry (Figure 3.2), showing two[1] Rh-CO stretching frequencies (Table 3.4).

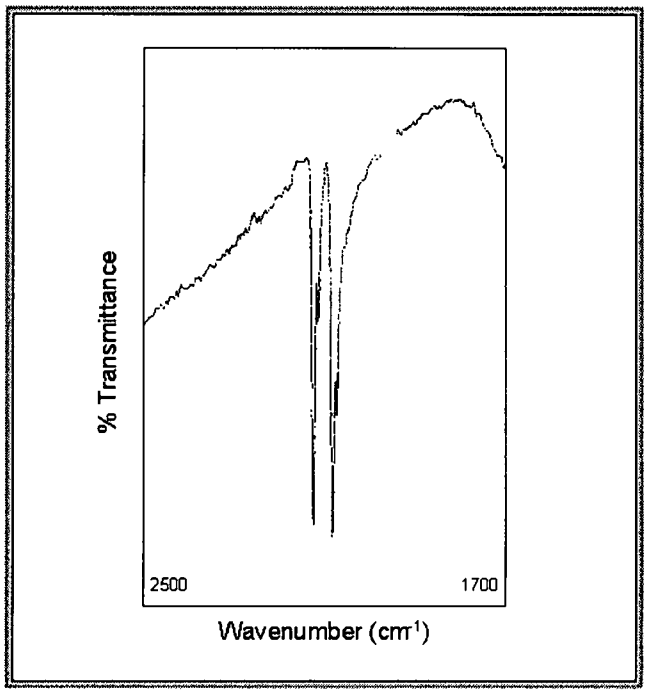

Figure 3.2: Infrared Spectrum of Rh(dbm)(CO)$_2$

The best % yields were obtained when freshly distilled DMF was used (Table 3.2).

Rh(β-diketonato)(CO)$_2$	% Yield
dbm	83
ba	74
btfa	53
tfaa	-

Table 3.2: % Yields obtained for the preparation of the various Rh(I) Dicarbonyl complexes. (Rh(tfaa)(CO)$_2$ was not isolated as a result of sublimation and Rh(tfaa)(CO)(PPh$_3$) was therefore prepared in situ.)

3.3 Preparation of Rhodium(I) Carbonyl Phosphine Complexes

The Rh(I) Dicarbonyl complexes were dissolved in a minimal quantity of methanol with the addition of a few drops of acetone to complete solubility. The Rh(I) Dicarbonyl complexes are highly soluble in acetone, but less soluble in methanol. Solid Triphenyl Phosphine (PPh_3) was added to the reaction mixture in a 1:1 mole ratio Rh(I) Dicarbonyl:PPh_3. The Rh(I) Carbonyl Phosphine complexes precipitated out of the solution. The formation of CO gas during the reaction can be used as a means to monitor the reaction (Figure 3.3).

The precipitated complexes were recrystallised (Table 3.3) from acetone, dried and characterised by means of infrared spectrophotometry (Figure 3.4) and NMR (Figure 3.5).

Rh(β-diketonato)(CO)(PPh_3)	% Yield
dbm	69
ba	64
btfa	52
tfaa	31

Table 3.3: % Yields obtained during the preparation of the Rh(I) Carbonyl Phosphine complexes.

The PPh_3 will substitute the CO *trans* to the co-ordinated oxygen with the largest *trans* influence, in accordance with the polarisation theory and the σ-*trans* effect (Section 2.1.2). The crystal structure determination of Rh(tfdmaa)(CO)(PPh_3)[4] and Rh(tftmaa)(CO)(PPh_3)[5], however, indicated that substituents of the β-diketone may cause steric hindrance and can dominate the electronic effect to result in the isomer with the PPh_3 group *trans* to the co-ordinated oxygen nearest to the strong electron attracting CF_3 group.

[4] Leipoldt J.G., Basson S.S., Nel J.T., *Inorg. Chim. Acta*, **74**, 85, (1983)
[5] Leipoldt J.G., Basson S.S. Potgieter J.H., *Inorg. Chim. Acta*, **117**, L3, (1986)

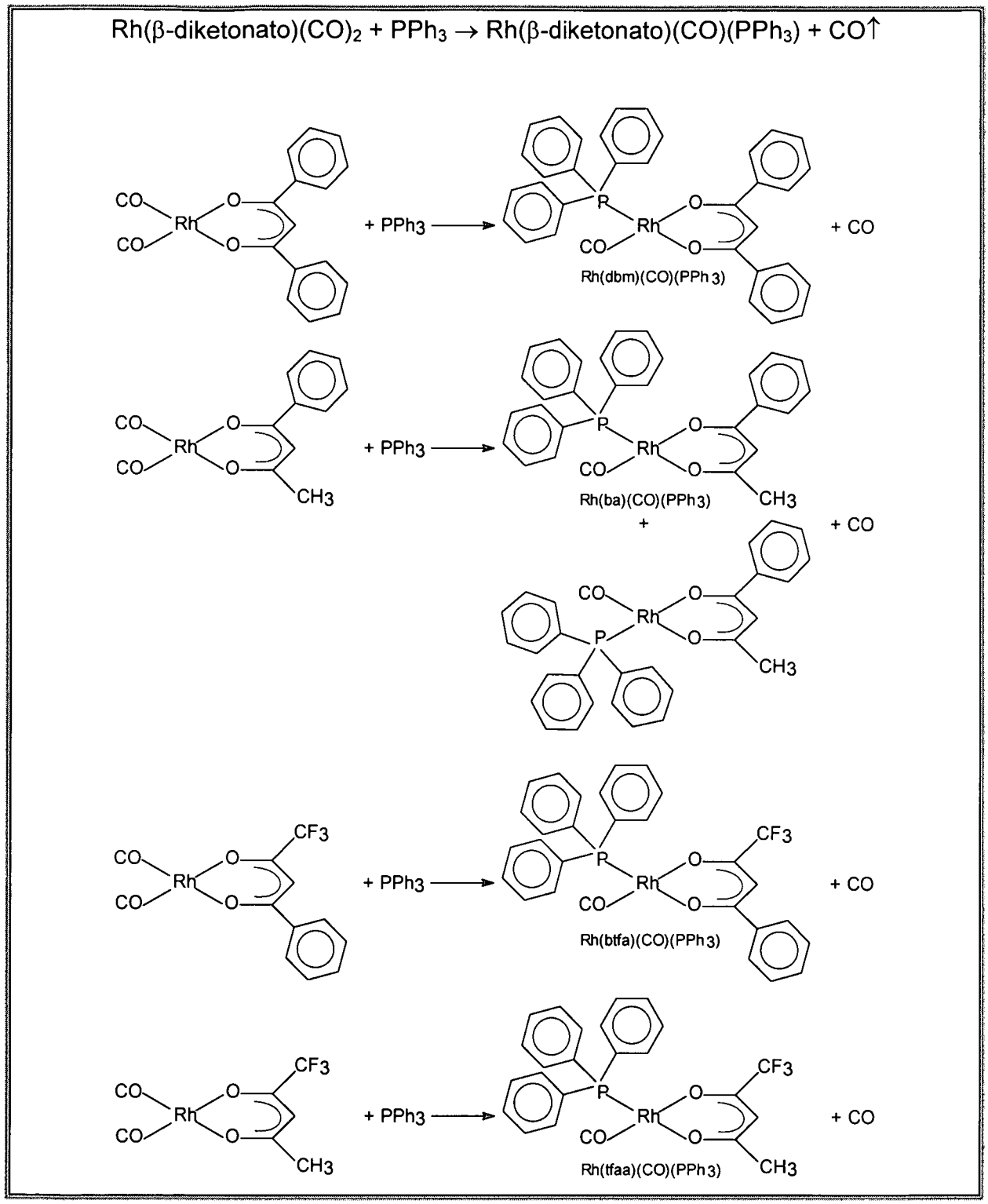

Figure 3.3: *Substitution of one CO group by PPh_3 in Rh(β-diketone)$(CO)_2$ to form Rh(dbm)$(CO)(PPh_3)$[6], Rh(ba)$(CO)(PPh_3)$[7], Rh(btfa)$(CO)(PPh_3)$ and Rh(tfaa)$(CO)(PPh_3)$.*

[6] Lamprecht Delanie, Lamprecht G.J., Botha J.M., Umakoshi K., Sasaki Y, *Acta Cryst.* **C53**, 1403, (1997)
[7] Purcell W, Basson S.S., Leipoldt J.G. Roodt A., Preston H., *Inorg. Chim. Acta*, **234**, 153, (1995)

Square planar substitution reactions are thought to proceed through a trigonal bipyrimidal transition state in which the entering ligand, the leaving ligand and the group *trans* to the leaving ligand occupy the trigonal plane[8]. If the group *trans* to the expected leaving ligand were too bulky, the intermediate would be relatively unstable and the unexpected isomer, which is in accordance with the polarisation theory, would rather form.

The crystal structures of both $Rh(btfa)(CO)(PPh_3)$ and $Rh(tfaa)(CO)(PPh_3)$ are unknown, but it can be expected that the substitution of the one CO in $Rh(btfa)(CO)_2$ and $Rh(tfaa)(CO)_2$ will follow the polarisation theory.

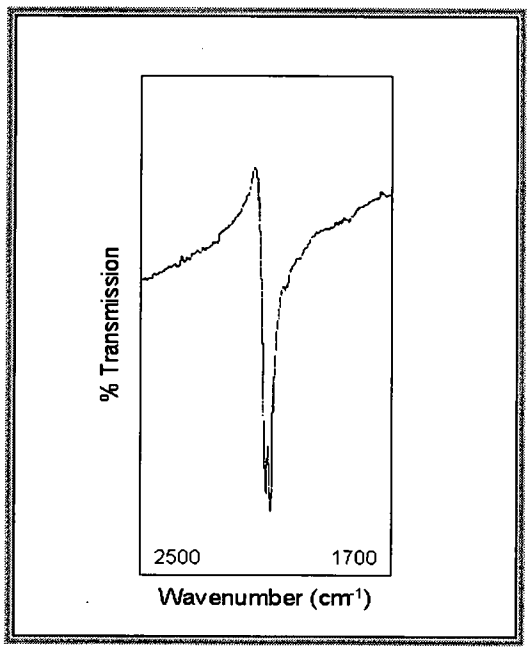

Figure 3.4: Infrared Spectrum of Rh(dbm)(CO)(PPh_3)

[8] Purcell K.F., Kotz J.C., *Inorganic Chemistry*, Holt-Saunders, Philadelphia, (1977)

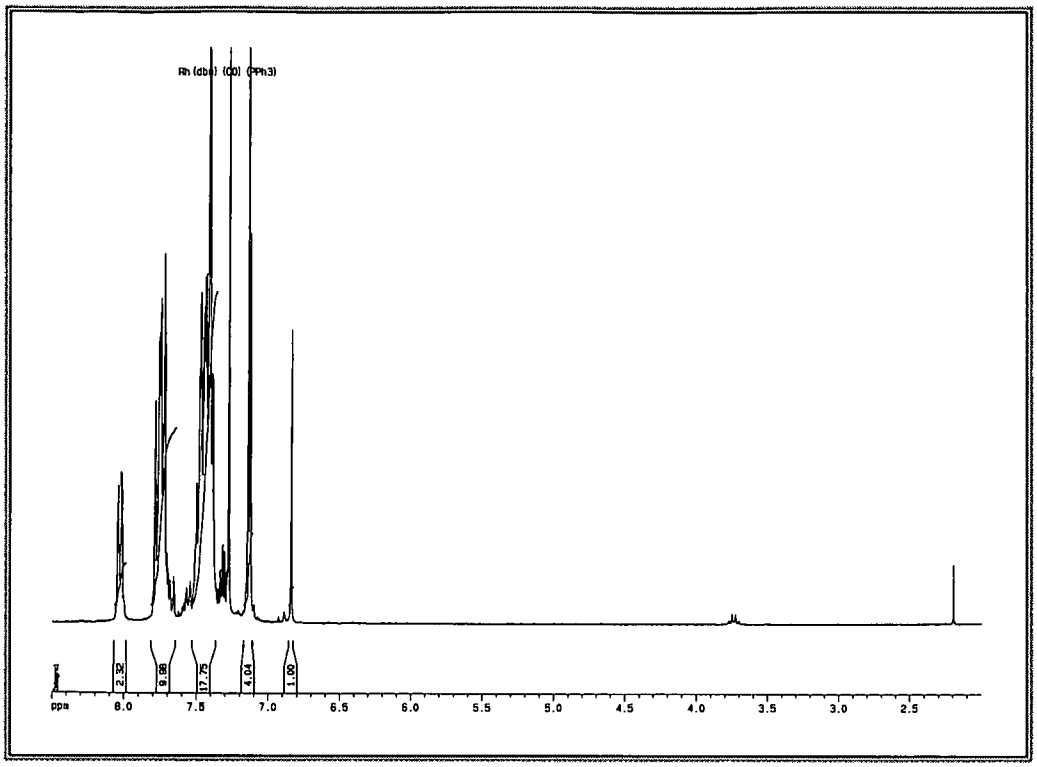

Figure 3.5 (a): NMR Spectrum of Rh(dbm)(CO)(PPh_3)

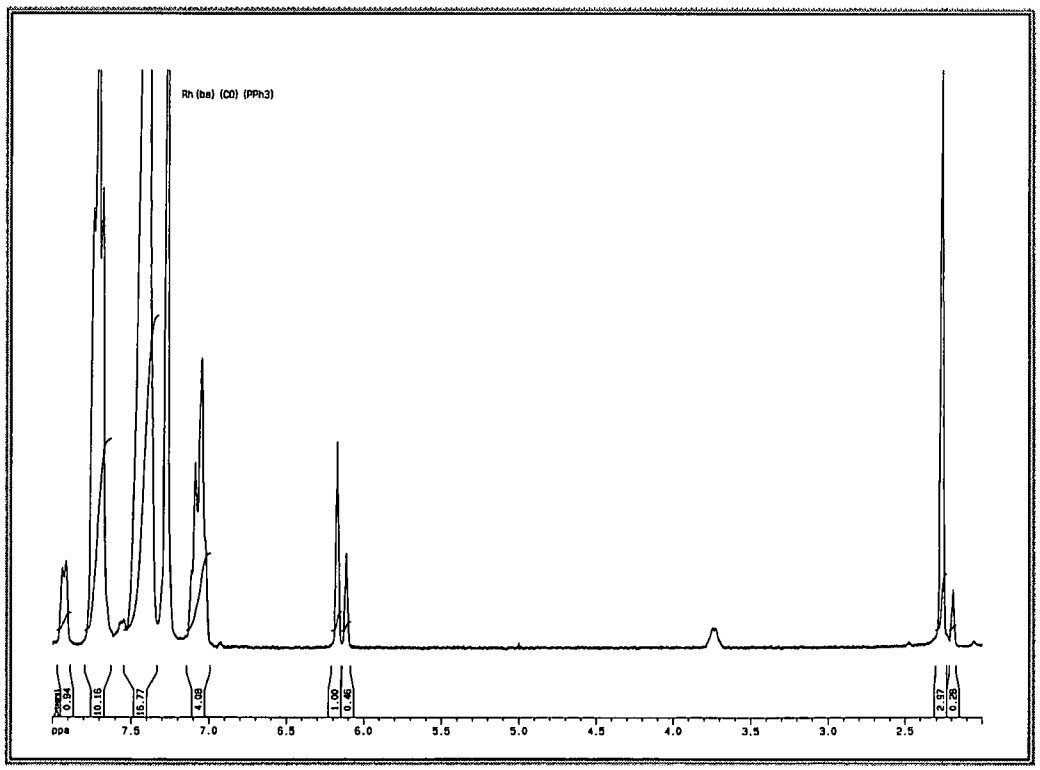

Figure 3.5 (b): NMR Spectrum of Rh(ba)(CO)(PPh_3)

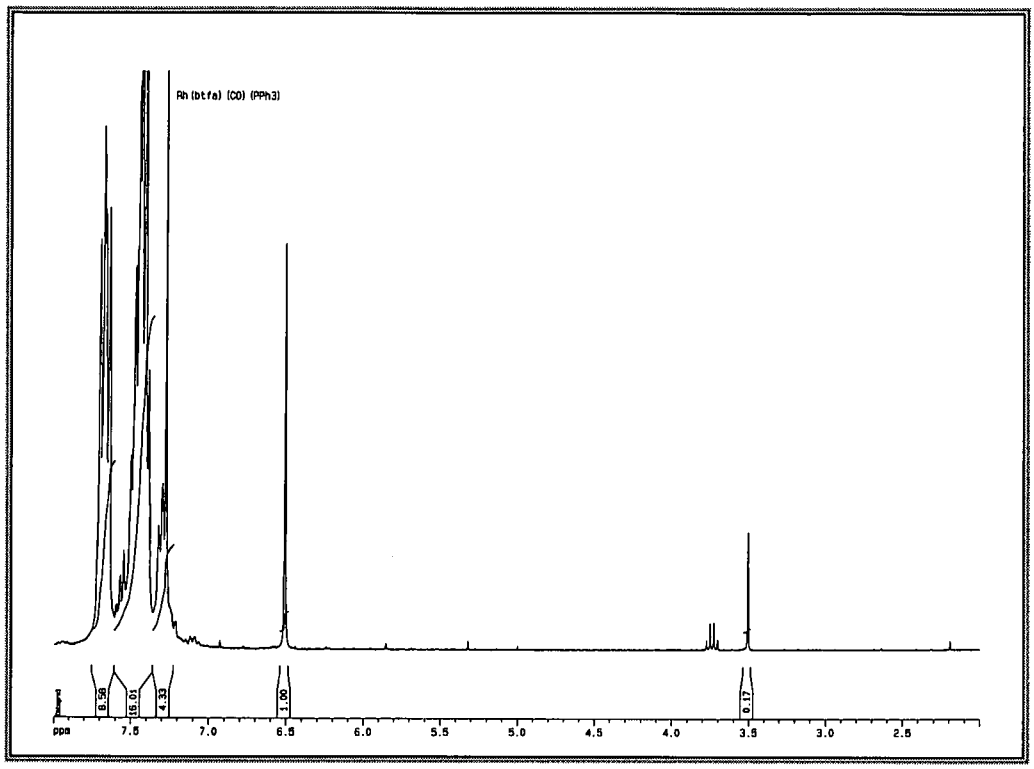

Figure 3.5 (c): NMR Spectrum of Rh(btfa)(CO)(PPh_3)

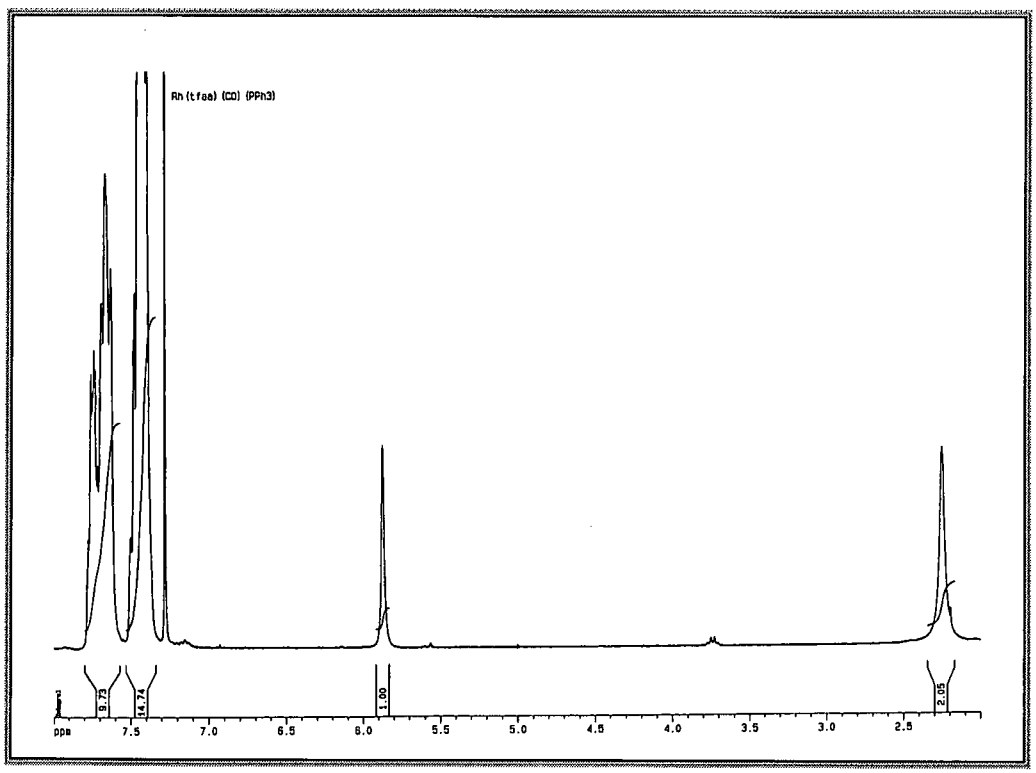

Figure 3.5 (d): NMR Spectrum of Rh(tfaa)(CO)(PPh_3)

3.4 Characterisation of the Rh(I) Dicarbonyl and Rh(I) Carbonyl Phosphine Complexes

3.4.1 Infrared Spectrophotometry characterisation:

The carbonyl stretching frequencies of the Rh(I) Dicarbonyl and Rh(I) Carbonyl Phosphine complexes were determined in a Potassium Bromide (KBr) matrix on a Hitachi 270-50 spectrophotometer (Table 3.4).

Rh(β-diketonato)$(CO)_2$	λ^{-1} (cm^{-1})	
dbm	2000	2100
ba	2000	2080
btfa	2505	2100
tfaa	2050	2125

Rh(β-diketonato)(CO)(PPh_3)	λ^{-1} (cm^{-1})
dbm	1980
ba	1980
btfa	1990
tfaa	2000

Table 3.4: Carbonyl stretching frequencies of Rh(I) Dicarbonyl and Rh(I) Carbonyl Phosphine complexes.

The greater the electron density on the metal ion, the greater the back donation into the π*-orbital of CO. The CO bond order will be lowered, causing the stretching frequency of the co-ordinated CO to decline.

In general, the more electronegative the other ligands attached to the metal ion, the less electron density will be available for back donation and the higher the CO stretching frequency (Table 3.4).

3.4.2 Nuclear Magnetic Resonance (NMR) characterisation

^{1}H-NMR spectra of Rh(I) Carbonyl Phosphine complexes were taken by means of a Bruker 300 MHz AM 300 NMR spectrometer using $CDCl_3$ as a solvent (Figure 3.5 (a) – Figure 3.5 (d)). All the chemical shifts (δ) were reported relative to TMS in ppm.

^{1}H NMR (Rh(dbm)(CO)(PPh$_3$) (Figure 3.5 (a))**):**	δ 6.83 (s, 1H, CH)
^{1}H NMR (Rh(ba)(CO)(PPh$_3$) (Figure 3.5 (b))**):**	δ 6.11 & δ 6.18 (m, 1H, CH)
^{1}H NMR (Rh(btfa)(CO)(PPh$_3$) (Figure 3.5 (c))**):**	δ 6.52 (s, 1H, CH)
^{1}H NMR (Rh(tfaa)(CO)(PPh$_3$), (Figure 3.5 (d))**):**	δ 5.88 (s, 1H, CH)

3.4.3 Molecular Structure of Rh(dbm)(CO)(PPh$_3$) determined by means of X-ray Crystallography

The crystal structure of (1,3-Diphenyl-1,3-propanedionato-κO, κO) Triphenyl Phosphine Rhodium(I) was solved by means of X-ray crystallography and published in Acta Crystallographica[6].

Rh(dbm)(CO)(PPh$_3$) was prepared as previously described (Section 3.2) and re-crystallised from acetone.

The systematic absences *(hkl, h + k = 2n + 1; h0l, l = 2n + 1)* agree with both *C2/c* and *Cc* space groups. The absence of Patterson vectors relates to twofold rotation and screw axes. The successful structural refinement indicates that the correct space group is *Cc* (Figure 3.6).

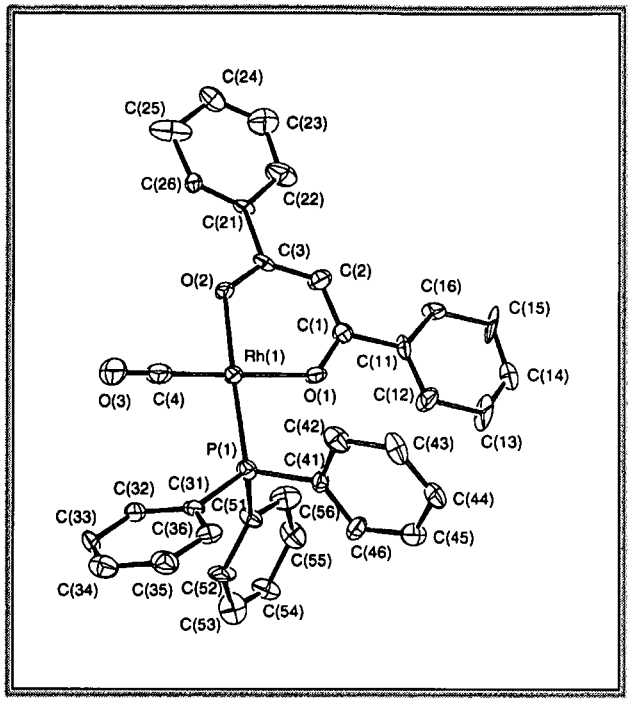

Figure 3.6: The structure of one of the two independent molecules of Rh(dbm)(CO)(PPh_3) with the atomic numbering scheme.

The crystal structure was solved by direct methods.

Crystal Data:	***Data Collection***
$[Rh(C_{15}H_{11}O_2)(C_{18}H_{15}P)(CO)]$	Mac Science MXC18 diffractometer
M_r = 616.46 g.mol^{-1}	$\omega/2\theta$ scans
Monoclinic	Absorption correction:
Cc	ψ scans (North, Phillips & Matthews, 1968)
a = 30.404 (4) Å	T_{min} = 0.781
b = 10.276 (1) Å	T_{max} = 0.870
c = 18.742 (3) Å	7056 measured reflections
β = 108.92 (1)°	6231 independent reflections
V = 5539 (1) Å^3	5972 reflections with I > 2σ(I)
Z = 8	R_{int} = 0.015
D_x = 1.478 mg.m^{-3}	θ_{max} = 26.43°
D_m not measured	h = -39 → 37
Mo Kα radiation	k = -13 → 0
λ = 0.71073 Å	l = 0 → 24
Cell parameters from 26 reflections	3 standard reflections every 150 reflections
θ = 15.5 – 17.5°	Intensity decay: 9.5 %
μ = 0.695 mm^{-1}	
T = 163 K	
Rhombic	
0.78 x 0.45 x 0.20 mm	
Yellow	

Refinement

Refinement on F
$R = 0.035$
$wR = 0.043$
$S = 2.564$
701 parameters
H atoms riding with $U(H) = 1.3\ U_{eq}(C)$
$w = 1/[\sigma^2(F) + 0.001F^2$
$(\Delta/\sigma)_{max} = 0.023$
$\Delta\rho_{max} = 0.55$ e Å^{-3}
$\Delta\rho_{min} = -0.84$ e Å^{-3}
Extinction correction: none
Scattering factors from *International Tables for X-ray Crystallography* (Vol. IV)

The asymmetric unit consists of two crystallographically independent molecules. These molecules form a very close centrosymmetric pair, but not a crystallographic inversion centre (Figure 3.7).

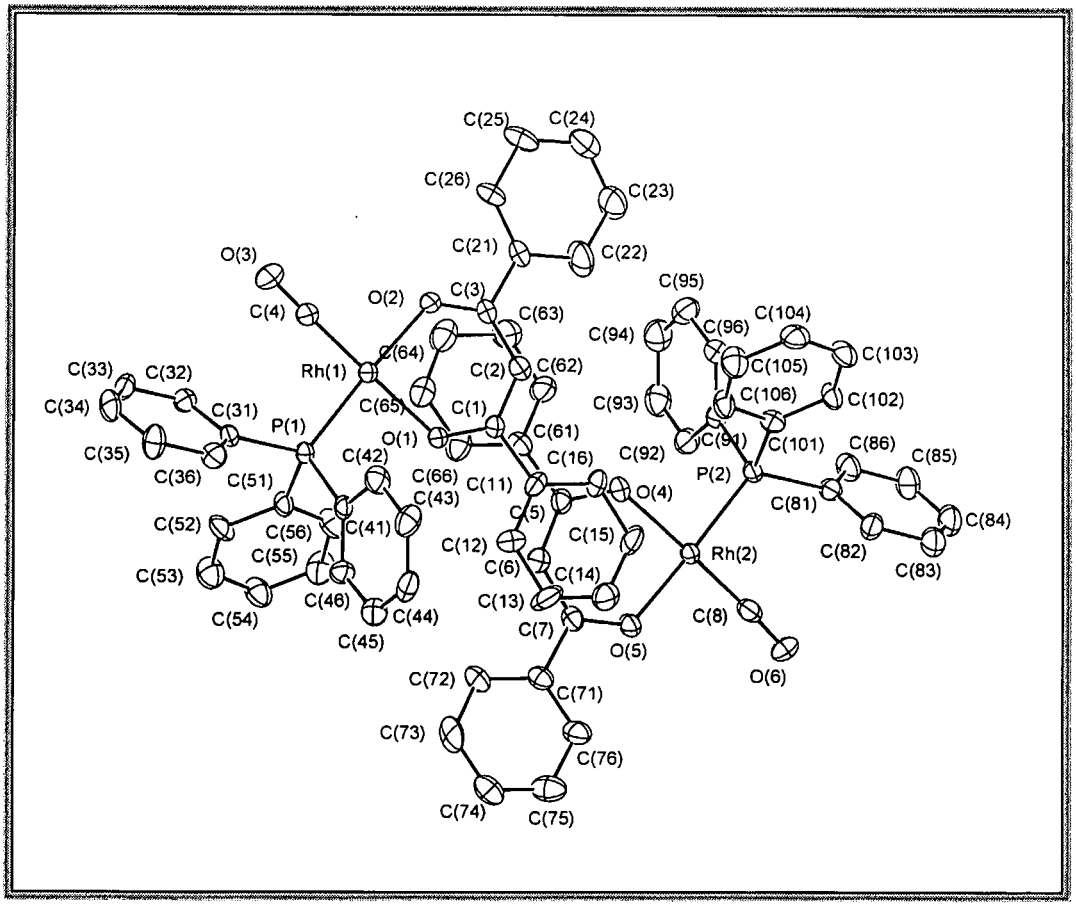

Figure 3.7: The partial overlapping of the two molecules in the unit cell.

The partial overlapping of the chelate ring of the one molecule with the phenyl ring of the other molecule can be attributed to π-π interactions between atoms of the two molecules, which are less than 3.57 Å (Table 3.5).

O1 - C65	3.72(2)	no
O1 - C66	3.53(2)	yes
O2 - C64	3.78(2)	no
O2 - C65	3.71(2)	no
C1 - C65	3.68(2)	no
C1 - C66	3.34(2)	yes
C2 - C65	3.57(2)	no
C2 - C66	3.54(2)	yes
C3 - C64	3.53(2)	yes
C3 - C65	3.55(2)	yes
O4 - C15	3.77(2)	no
O4 - C16	3.67(2)	no
O5 - C14	3.80(2)	no
O5 - C15	3.64(2)	no
C5 - C15	3.72(2)	no
C5 - C16	3.40(2)	yes
C6 - C11	3.77(2)	no
C6 - C14	3.74(2)	no
C6 - C15	3.57(2)	yes
C6 - C16	3.56(2)	yes
C7 - C14	3.46(2)	yes
C7 - C15	3.53(2)	yes

Shortest distances = 3.34(2)

Table 3.5: Contacting atom distances between molecule 1 and molecule 2. "yes" denotes π-π interactions

The Rhodium atom has a square planar co-ordination. The calculation of the best plane through the atoms of the co-ordination polyhedron, *i.e.* P(1), O(1), O(2), C(4) and P(2), O(4), O(5), C(8), showed no significant deviation from a planar conformation.

The calculation of the best plane through the atoms of the chelate ring showed that the ring is nearly planar (Table 3.6).

Plane 1: P(1), O(1), O(2), C(4)
Plane 2: P(2), O(4), O(5) C(8)

PL1	Rh(1) - 0.008	P(1) - 0.058	O(1) - -0.059	O(2) - 0.061	C(4) - -0.060
PL2	Rh(2) - -0.025	P(2) - -0.112	O(4) - 0.114	O(5) - -0.120	C(8) - 0.119

The Rhodium was omitted in the calculation of the best plane of the co-ordination polyhedron
The planarity of plane 1 is better than that of plane 2

Plane3: O(1), O(2), C(1), C(2), C(3)
Plane4: O(4), O(5), C(5), C(6), C(7)

PL3	Rh(1) - -0.065	O(1) - 0.029	O(2) - -0.032	C(1) - -0.031	C(2) - -0.006	C(3) - 0.040
PL4	Rh(2) - 0.080	O(4) - -0.017	O(5) - 0.019	C(5) - 0.018	C(6) - 0.003	C(7) - -0.023

Dihedral angles between planes

The two co-ordination planes are co-planar

PL3-PL4	0.6(6)
PL3-py1	6.6(5)
PL3-py2	10.3(9)
PL4-py6	11.4(5)
PL4-py7	7.1(7)

Table 3.6: Planarity and dihedral angles of the two molecules in the unit cell.

The bond distances Rh(1) - O(2) [2.081 (9) Å] and Rh(2) - O(5) [2.072 (7) Å], when compared to Rh(1) - O(1) [2.038 (10) Å] and Rh(2) - O(4) [2.040 (7) Å] illustrate clearly the larger *trans* influence of the PPh_3 group compared to that of the CO group (Table 3.7).

Rh(1) - P(1)	2.235(3)	Rh(1) - O(1)	2.030(7)
Rh(1) - O(2)	2.089(8)	Rh(1) - C(4)	1.849(13)
Rh(2) - P(2)	2.249(3)	Rh(2) - O(4)	2.039(7)
Rh(2) - O(5)	2.068(8)	Rh(2) - C(8)	1.809(12)
P(1) - C(31)	1.833(10)	P(1) - C(41)	1.846(13)
P(1) - C(51)	1.833(11)	P(2) - C(81)	1.852(11)
P(2) - C(91)	1.824(13)	P(2) - C(101)	1.829(11)
O(1) - C(1)	1.284(12)	O(2) - C(3)	1.293(13)
O(3) - C(4)	1.128(15)	O(4) - C(5)	1.300(13)
O(5) - C(7)	1.262(13)	O(6) - C(8)	1.152(14)
C(1) - C(2)	1.397(16)	C(1) - C(11)	1.525(17)
C(2) - C(3)	1.384(16)	C(3) - C(21)	1.466(16)
C(5) - C(6)	1.375(16)	C(5) - C(61)	1.526(18)
C(6) - C(7)	1.420(16)	C(7) - C(71)	1.604(18)

P(1) - Rh(1) - O(1)	87.9(3)	P(1) - Rh(1) - O(2)	175.5(3)
P(1) - Rh(1) - C(4)	91.7(4)	O(1) - Rh(1) - O(2)	88.6(3)
O(1) - Rh(1) - C(4)	176.0(5)	O(2) - Rh(1) - C(4)	91.9(5)
P(2) - Rh(2) - O(4)	88.1(3)	P(2) - Rh(2) - O(5)	173.8(3)
P(2) - Rh(2) - C(8)	91.0(4)	O(4) - Rh(2) - O(5)	88.4(3)
O(4) - Rh(2) - C(8)	171.4(5)	O(5) - Rh(2) - C(8)	93.2(5)
Rh(1) - P(1) - C(31)	119.8(4)	Rh(1) - P(1) - C(41)	110.7(4)
Rh(1) - P(1) - C(51)	113.4(4)	C(31) - P(1) - C(41)	104.8(6)
C(31) - P(1) - C(51)	104.2(5)	C(41) - P(1) - C(51)	102.1(6)
Rh(2) - P(2) - C(81)	117.6(4)	Rh(2) - P(2) - C(91)	113.8(5)
Rh(2) - P(2) - C(101)	114.0(4)	C(81) - P(2) - C(91)	105.0(5)
C(81) - P(2) - C(101)	102.2(5)	C(91) - P(2) - C(101)	102.4(6)
Rh(1) - O(1) - C(1)	127.5(7)	Rh(1) - O(2) - C(3)	125.1(7)
Rh(2) - O(4) - C(5)	127.7(7)	Rh(2) - O(5) - C(7)	127.3(7)
O(1) - C(1) - C(2)	126.3(10)	O(1) - C(1) - C(11)	114.0(10)
C(2) - C(1) - C(11)	119.6(10)	C(1) - C(2) - C(3)	124.8(10)
O(2) - C(3) - C(2)	127.1(10)	O(2) - C(3) - C(21)	112.4(10)
C(2) - C(3) - C(21)	120.4(10)	Rh(1) - C(4) - O(3)	177.4(12)
O(4) - C(5) - C(6)	124.5(10)	O(4) - C(5) - C(61)	113.2(10)
C(6) - C(5) - C(61)	122.3(10)	C(5) - C(6) - C(7)	126.8(10)
O(5) - C(7) - C(6)	124.9(10)	O(5) - C(7) - C(71)	116.8(10)
C(6) - C(7) - C(71)	118.2(10)	Rh(2) - C(8) - O(6)	176.0(11)

Table 3.7: Selected intramolecular bond lengths (Å) and bond angles (°) (H omitted).

CHAPTER 4:

CHEMICAL OXIDATION AND REACTION MECHANISM

4.1 Introduction

A kinetic study is required to determine the reaction mechanism of the oxidative addition of an alkyl halide to Rh(I)(β-diketonato)(CO)(PPh_3) complexes.

The reaction rate of any chemical change depends primarily on the properties of the reacting molecules. The most important factor that determines the reaction rate is concentration. The rate law, the relationship between the reaction rate and concentration, is the corner-stone of reaction mechanisms and alone allows much insight into the mechanism. However, by carrying out measurements at a number of temperatures and pressures, or even in different mediums, more useful information about the reaction mechanism can be obtained, even though the form of the rate law itself rarely changes.

Visible, infrared and NMR spectroscopy were used to study the reaction rates of the oxidative addition reactions.

4.2 Visible Spectroscopy

The visible spectral region was chosen because reactions of transition metal complexes are accompanied by spectral absorption changes in this region. The alkyl halide (methyl iodide) as well as the solvents used is transparent in this region.

Optical absorption can be a substitution for the concentration changes required in deriving the rate law. All four Rh(I)(β-diketonato)(CO)(PPh_3) complexes used follow the Beer-Lambert law [(Appendix 3)], where plots of absorption *versus* concentration are linear with zero intercepts. Concentration values for testing the Beer-Lambert law are 10% above and below the concentration values used in this study.

All visible kinetics measurements were carried out with a GBC-916 UV/Visible Spectrophotometer equipped with a multi-cell thermostat cell holder (±0.2 °C).

4.2.1 The dependence of Reaction Rate on Reactant Concentration

$$Rh(I)(\beta\text{-diketonato})(CO)(PPh_3) + CH_3I \xrightarrow{k_2} \text{PRODUCTS} \quad ①$$

$$\frac{-\partial[Rh(\beta-\text{Diketonato})(CO)(PPh_3)]}{\partial t} = k_2[Rh(\beta-\text{Diketonato})(CO)(PPh_3)][CH_3I] \quad ②$$

If the $[CH_3I]$ is at least ten-time in excess over the [Rh(I)(β-diketonato)(CO)(PPh_3)], the overall order of the reaction is reduced to a pseudo first order reaction,

$$\frac{-\partial[Rh(\beta-\text{Diketonato})(CO)(PPh_3)]}{\partial t} = k_{obs}[Rh(\beta-\text{Diketonato})(CO)(PPh_3)] \quad ③$$

$$k_{obs} = k_2[CH_3I] \quad ④$$

k_{obs} = observed rate constant.

The observed rate constant (k_{obs}) can be either dependent on or independent of the concentration[1] of CH_3I (Figure 4.1).

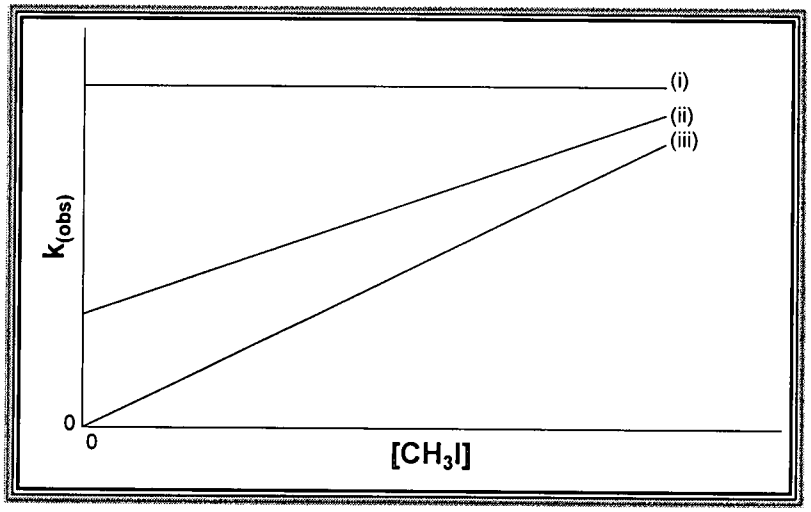

Figure 4.1: *Various types of dependencies of k_{obs} on the $[CH_3I]$*

(i) *k_{obs} is independent of $[CH_3I]$,*

(ii) *k_{obs} is dependent on $[CH_3I]$ with a positive intercept*

(iii) *k_{obs} is dependent on $[CH_3I]$ with a zero intercept*

Type (ii) (Figure 4.1) indicates a possible equilibrium condition between reagents and products and/or a possible interaction between solvent and reagents. In

[1] Wilkins R.G., Kinetics and Mechanisms of reactions of Transition Metal Complexes, Chapter 1, Second Edition, VCA, (1991)

this study all complexes followed the relation as in type (iii) (Figure 4.1) for a first reaction and type (i) (Figure 4.1) for a second reaction where isomerisation of the products is postulated.

a) Overlay Spectra

Overlay scans of the four Rh(β-diketonato)(CO)(PPh_3) complexes, where the β-diketone is dbm, ba, btfa and tfaa, were recorded in the visible region from 350nm – 600nm. Overlay scans for Rh(dbm)(CO)(PPh_3) are reported (Figure 4.2 (a) and (b)). Overlay scans for the other three Rh(β-diketonato)(CO)(PPh_3) complexes gave similar results and the overlay scans were used to select optimum wavelengths for the study of the change in absorption as a function of time.

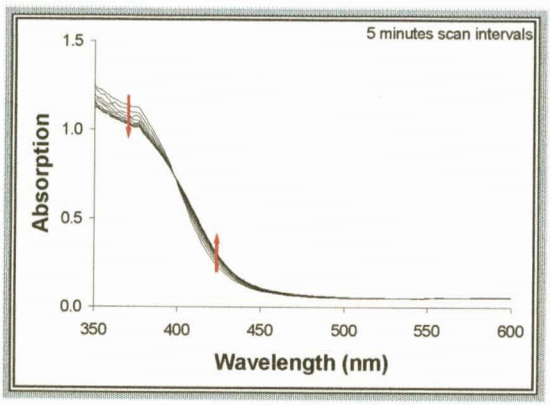

Figure 4.2 (a): *Overlay scans of the first reaction between Rh(dbm)(CO)(PPh_3) and CH_3I at 25 °C.*

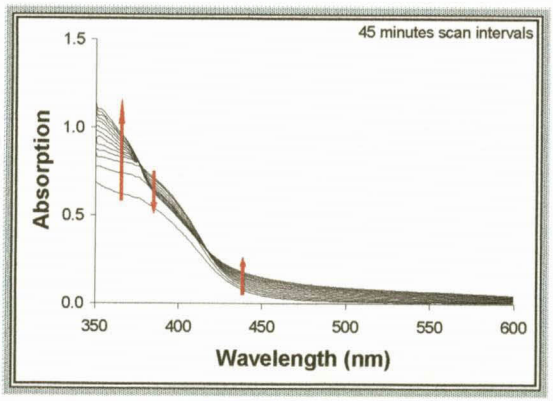

Figure 4.2 (b): *Overlay scans of the second reaction between Rh(dbm)(CO)(PPh_3) and CH_3I at 25 °C.*

The isosbestic points observed were at 400nm for the first reaction (Figure 4.2 (a)) and at 380nm for the second reaction (Figure 4.2 (b)). The first reaction was therefore studied at 380nm while the second reaction was studied at 400nm. The advantage of studying the second reaction at the isosbestic point of the first reaction is that the second reaction can be completely separated from the first reaction.

From the above (Figure 4.2 (a) and (b)) it is clear that there are two different reactions. This fact is more clearly demonstrated (Figure 4.3) where the reaction rates of both reactions were studied at 360nm as a function of time. The first reaction, represented by the decrease in absorption is an oxidative addition step, while the slower second reaction, represented by the increase in absorption is an isomerisation step (Figure 4.21).

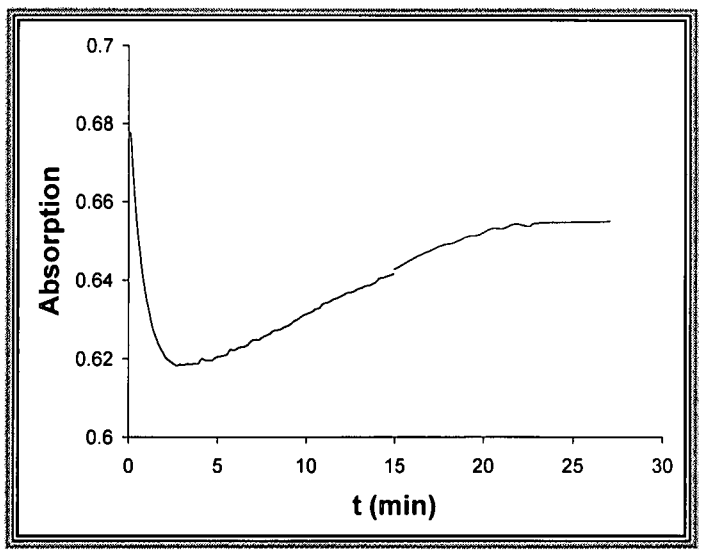

Figure 4.3: *Absorption versus time scan obtained during the reaction of Rh(dbm)(CO)(PPh_3) with 0.5 mol.dm^{-3} CH_3I at 35 °C in acetone.*

b) The dependence of the observed pseudo first order rate constant on the [Rh(β-diketonato)(CO)(PPh_3)]

All plots of $\ln\left\{\frac{(A_\infty - A_t)}{(A_\infty - A_o)}\right\}$ *versus* time were linear up to ~90% conversion, as expected for first order reactions (Figure 4.4).

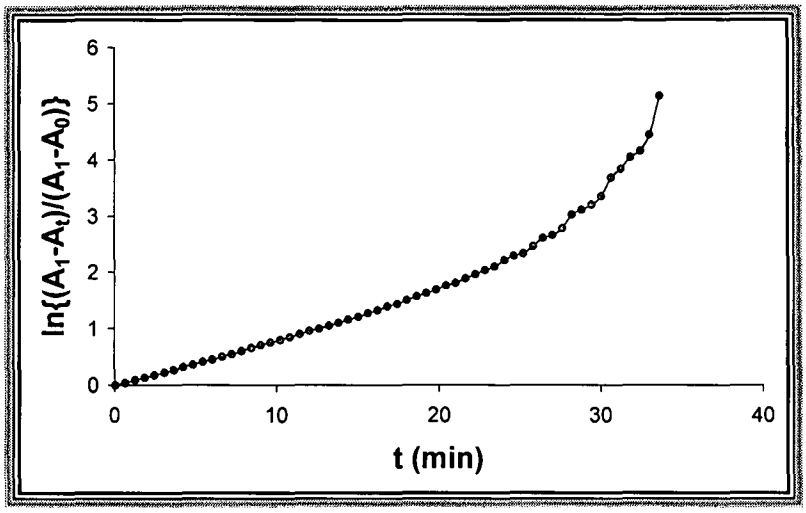

Figure 4.4: *An example of a plot of* $ln\left\{\frac{(A_\infty - A_t)}{(A_\infty - A_0)}\right\}$ *versus time for the oxidative addition of 0.25 mol.dm^{-3} CH_3I to Rh(dbm)(CO)(PPh_3) at 15 °C in acetone.*

(A_∞ is denoted as A_1 in figure)

To further prove that the reactions were in fact first order in the Rh(I)-complex, the observed rate constant was plotted *versus* [Rh(β-diketonato)(CO)(PPh_3)] (Table 4.1). The results (Figure 4.5) were in agreement with equation ③ where the observed rate constant is independent of [Rh(β-diketonato)(CO)(PPh_3)]. The concentrations of the Rh(β-diketonato)(CO)(PPh_3) complexes employed in this study were therefore not stipulated in graphs and tables and were all within the given limits (Table 4.1).

[Rh(dbm)(CO)(PPh_3)] x 10^4 (mol.dm^{-3})	k_{obs} x 10^3 (s^{-1})
0.568	2.44
1.136	2.45
1.622	2.45
2.028	2.45

Table 4.1: *Observed pseudo first order rate constants obtained for [Rh(dbm)(CO)(PPh_3)] during oxidative addition at 25 °C in acetone.*
[CH_3I] = 0.25 mol.dm^{-3}

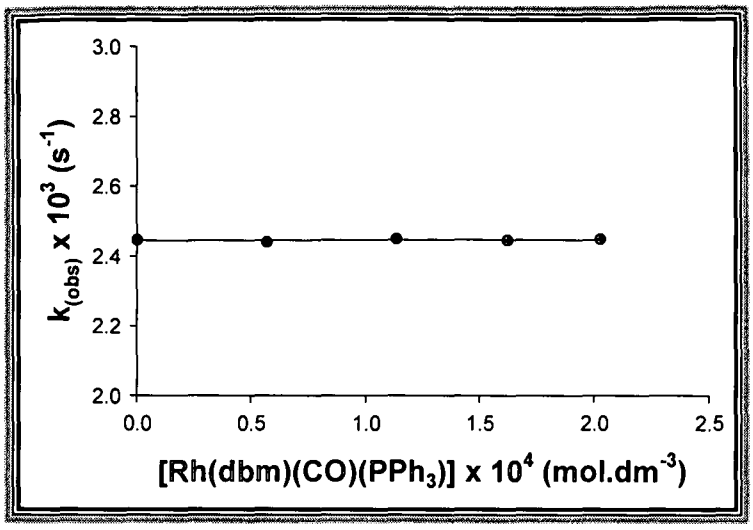

Figure 4.5: Independent relationship between the k_{obs} and [Rh(dbm)(CO)(PPh_3)].

c) The dependence of the observed pseudo first order rate constant on the concentration of CH_3I

The dependence of the pseudo first order rate constant, k_{obs}, on the [CH_3I] is given below (Table 4.2), where the second order rate constants, k_2, were calculated from the slopes of k_{obs} *versus* [CH_3I] (Figure 4.6). The relation between pKa and k_2 is tabulated (Table 4.2) and graphed (Figure 4.7).

β-diketone	[CH_3I] (mol.dm^{-3})	k_{obs} x 10^3 (s^{-1})
dbm	0.126	1.27
	0.249	2.47
	0.376	3.65
	0.501	4.73
ba	0.127	1.13
	0.249	2.24
	0.374	3.45
	0.499	4.80
btfa	0.125	0.15
	0.249	0.29
	0.375	0.43
	0.497	0.55
tfaa	0.126	0.20
	0.249	0.38
	0.376	0.55
	0.501	0.72

β-diketone	pKa	$k_2 \times 10^3$ ($mol^{-1}.dm^3.s^{-1}$)
dbm	9.4	9.61
ba	8.7	9.30
btfa	6.3	1.12
tfaa	6.3	1.46

Table 4.2: $[CH_3I]$ dependence of the observed pseudo first order rate constant and pKa dependence of the second order rate constant for the oxidative addition of CH_3I to Rh(β-diketonato)(CO)(PPh_3) at 25 °C in acetone.

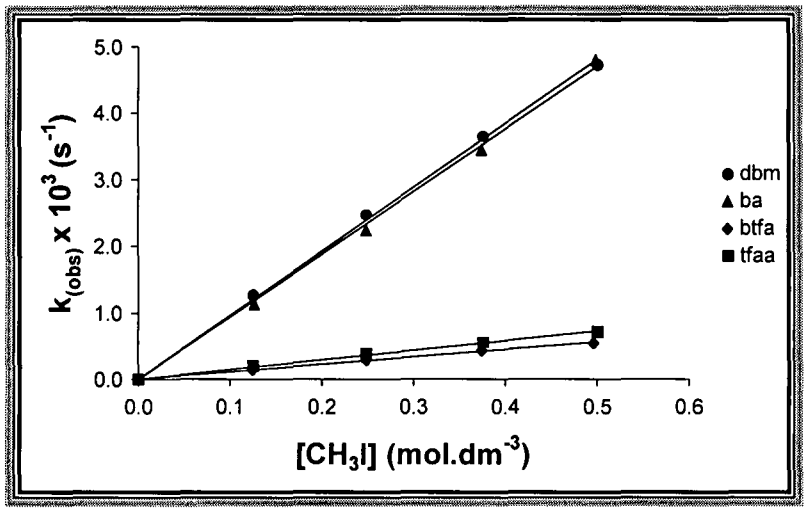

Figure 4.6: The linear relationships between the observed pseudo first order rate constant and $[CH_3I]$ at 25 °C in acetone.

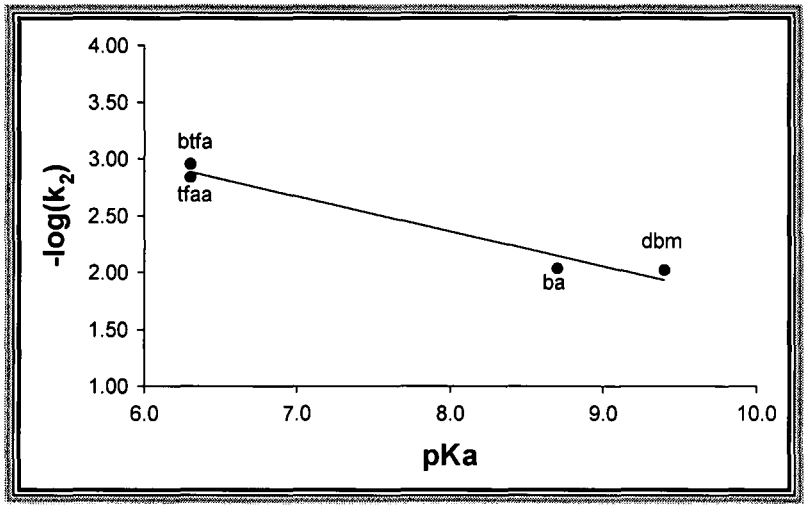

Figure 4.7: Plot of –log(k_2) versus pKa at 25 °C in acetone

The results of a similar study using dichloromethane as solvent (Table 4.3) showed that the relation between pKa and k_2 obtained in dichloromethane

(Figure 4.8) was identical to the relation between pKa and k_2 obtained in acetone (Figure 4.7).

β-diketone	$[CH_3I]$ (mol.dm^{-3})	k_{obs} x 10^3 (s^{-1})
dbm	0.125	2.83
	0.249	5.63
	0.375	8.29
	0.499	11.47
ba	0.126	1.28
	0.249	2.53
	0.376	3.72
	0.500	4.91
btfa	0.126	0.202
	0.249	0.368
	0.376	0.531
	0.500	0.667
tfaa	0.126	0.28
	0.249	0.50
	0.376	0.73
	0.500	0.88
β-diketone	**pKa**	**k_2 x 10^3 (mol^{-1}.dm^3.s^{-1})**
dbm	9.4	22.70
ba	8.7	9.91
btfa	6.3	1.39
tfaa	6.3	1.92

Table 4.3: $[CH_3I]$ dependence of the observed pseudo first order rate constant and pKa dependence of the second order rate constant for the oxidative addition of CH_3I to Rh(β-diketonato)(CO)(PPh_3) at 25 °C in dichloromethane.

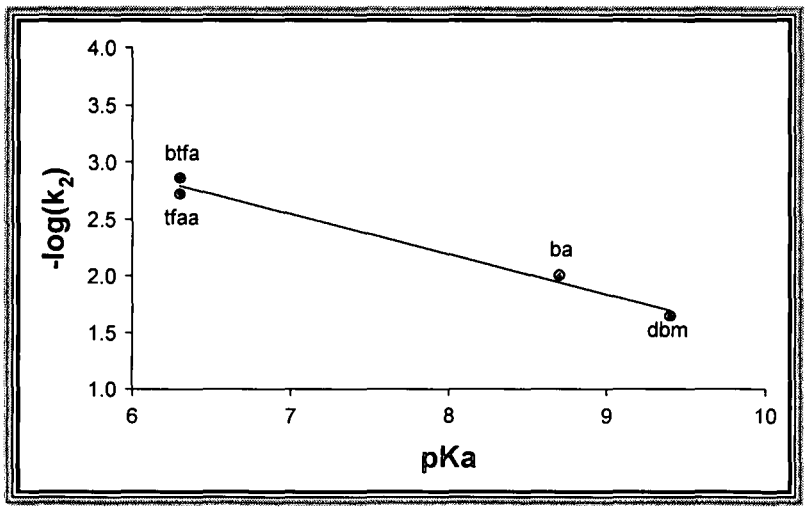

Figure 4.8: Plot of –log(k_2) versus pKa at 25 °C in dichloromethane.

More polar solvents (Section 4.2.4) enhanced the reaction rates obtained during oxidative addition. An increase in $[CH_3I]$ also increases the reaction rates (Figure 4.6). Care should be taken that the $[CH_3I]$ is not increased, for the mere sake of a convenient reaction time, to the point where it begins to play the role of a solvent. CH_3I, being a highly polar solvent, will increase the reaction rate not only because of increased concentration, but also as a result of an increased polarity of the solvent media. This effect is clearly demonstrated (Figure 4.9) and it was ensured in this study that employed CH_3I concentrations did not exceed the point of a linear relationship, namely ~ 0.5 mol.dm^{-3} CH_3I. Benzene, as solvent, was chosen as an example to illustrate this point (Figure 4.9) since the reactions were relatively slower in the non-polar benzene medium.

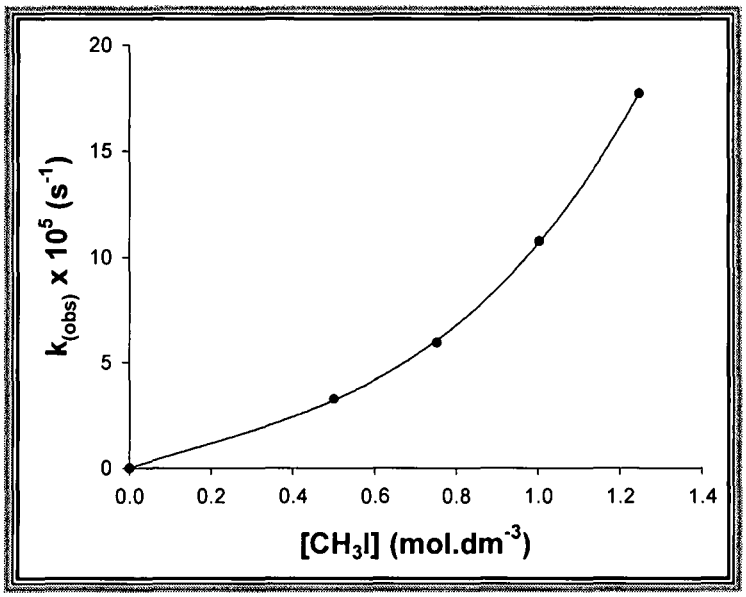

Figure 4.9: Relationship between the observed pseudo first order rate constant and $[CH_3I]$. Oxidative addition of CH_3I to Rh(dbm)(CO)(PPh_3) at 25 °C in benzene.

All Rh(β-diketonato)(CO)(PPh_3) complexes were tested for stability in various solvents by means of overlay spectra for at least 24 hours. Possible reactions between solvent and Rh(I) complexes were further ruled out by performing oxidative addition kinetics on freshly prepared solutions and solutions that had been standing for up to 24 hours (Table 4.4).

Standing period (hour)	$k_2 \times 10^2$ ($mol^{-1}.dm^3.s^{-1}$)
0	2.27(2)
24	2.38(4)

Table 4.4: Second order rate constant obtained during oxidative addition of CH_3I to $Rh(dbm)(CO)(PPh_3)$ with different standing periods.

The second reaction (Figure 4.3) observed during the oxidative addition of CH_3I to Rh(β-diketonato)(CO)(PPh_3) was independent of the [CH_3I] (Table 4.5 and Figure 4.10).

$[CH_3I]$ ($mol.dm^{-3}$)	$k_{obs} \times 10^5$ (s^{-1})	$k_1 \times 10^5$ ($mol^{-1}.dm^3.s^{-1}$)
0.124	7.26	7.30
0.248	7.28	
0.375	7.32	
0.499	7.32	

Table 4.5: The first order rate constant of the second reaction obtained during oxidative addition of CH_3I to $Rh(dbm)(CO)(PPh_3)$ at 25 °C in dichloromethane.

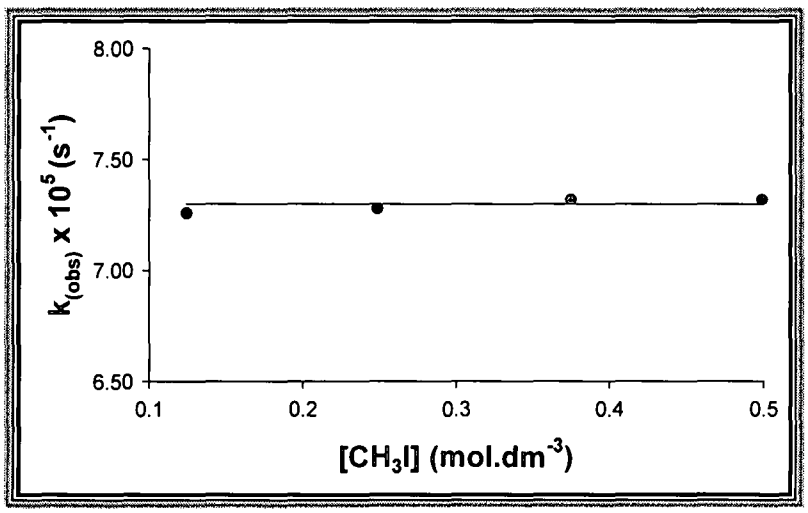

Figure 4.10: The independent relationship between the k_{obs} and $[CH_3I]$ for the second reaction obtained during oxidative addition of CH_3I to $Rh(dbm)(CO)(PPh_3)$ at 25 °C in dichloromethane.

4.2.2 The variation of reaction rate with temperature

The rate of most chemical reactions increases with temperature. The rate constant is the only temperature dependent term of the rate expression since the reactant concentration is unaffected by temperature and an increase in temperature will seldom have an effect on the reaction order.

Arrhenius (1889) found that the experimentally observed variation of the rate constant with temperature can be expressed by the following equation[2]:

$$\ln k = B - \frac{C}{T} \text{ or } \frac{\partial \ln k}{\partial T} = \frac{C}{T^2} \text{ where} \qquad ⑤$$

B and C are constants for a particular reaction.

Every collision between two atoms does not necessarily lead to a reaction. Two atoms colliding must overcome the activation energy before a reaction can take place. The Arrhenius equation can be rewritten as:

$k = Ae^{\frac{-E^*}{RT}}$, where E* represents the activation energy ⑥

A similar relationship is also postulated by the absolute reaction rate theory, which is used almost exclusively in considering the kinetics of reactions in solution. During a chemical reaction, an activated complex is formed in equilibrium with the reagents:

$$A + B \overset{K^*}{\rightleftharpoons} (A,B)^* \xrightarrow{k_2} AB$$

The reaction rate is given by the decomposition of the activated complex and the second order rate constant is given by:

$$k_2 = \frac{RT}{Nh} \times K^* \text{ (Appendix 4)} \qquad ⑦$$

R is the gas constant, N is Avogradro's constant and h is Planck's constant. From basic thermodynamics it can be shown that:

$$k_2 = \frac{RT}{Nh} e^{\frac{-\Delta H^*}{RT}} \cdot e^{\frac{\Delta S}{R}}, \text{ and} \qquad ⑧$$

$$\ln \frac{k_2}{T} = \left(\ln \frac{R}{Nh} + \frac{\Delta S^{o^*}}{R} \right) - \frac{\Delta H^{o^*}}{RT} \qquad ⑨$$

[2] Stevens B, Physical Chemistry Textbooks, Chemical Kinetics, Chapman and Hall Ltd, London, (1965)

A plot of $\ln\frac{k_2}{T}$ *versus* T^{-1} is linear with a slope of $-\frac{\Delta H^{o*}}{RT}$ and an intercept of $\ln\frac{R}{Nh}+\frac{\Delta S^{o*}}{R}$.

The above equation is referred to as the Eyring relationship. The agreement of the values of the enthalpy and entropy of activation is not always very good. This arises from the inaccuracy in obtaining $\Delta S°*$ values by long extrapolations of the Eyring plots to T^{-1} at 0 K^{-1}. Values of volume of activation, $\Delta V*$, are more accurate, but not easily measured.

Large positive $\Delta H°*$ and $\Delta S°*$ values are an indication of a dissociative activity, whereas small positive $\Delta H°*$ values and negative $\Delta S°*$ values indicate an associative mechanism.

a) The determination of the enthalpy and entropy of activation during oxidative addition

The oxidative addition of CH_3I to the Rh(β-diketonato)(CO)(PPh_3) complexes was investigated at 15 °C, 25 °C and 35 °C in acetone. The results are tabulated (Table 4.6) and graphed (Figure 4.11 (a) and (b)).

β-diketone	[CH_3I] ($mol.dm^{-3}$)	k_{obs} x 10^3 (s^{-1}) 15 °C	k_{obs} x 10^3 (s^{-1}) 25 °C	k_{obs} x 10^3 (s^{-1}) 35 °C
dbm	0.126	0.53	1.27	2.75
	0.249	1.11	2.47	4.94
	0.376	1.85	3.65	7.04
	0.501	2.17	4.73	8.97
ba	0.127	0.73	1.13	3.23
	0.249	1.29	2.24	5.10
	0.374	1.94	3.45	7.40
	0.499	2.40	4.80	9.60
btfa	0.125	0.003	0.15	0.26
	0.249	0.13	0.29	0.53
	0.375	0.20	0.43	0.77
	0.497	0.26	0.55	0.98
tfaa	0.126	0.08	0.20	0.39
	0.249	0.14	0.38	0.73
	0.376	0.20	0.55	1.09
	0.501	0.27	0.72	1.31

β-diketone	T (°C)	T (K)	$k_2 \times 10^3$ ($mol^{-1}.dm^3.s^{-1}$)	ΔH (kJ)	ΔS ($J.K^{-1}$)
dbm	15.5	288.7	4.52	49,9	-116
	24.9	298.1	9.61		
	34.8	308.0	18.50		
ba	15.9	289.1	5.00	55,7	-97
	25.1	298.3	9.30		
	34.4	307.6	19.80		
btfa	16.1	289.3	0.525	49,6	-135
	25.2	298.4	1.120		
	34.4	307.6	2.020		
tfaa	15.4	288.6	0.546	52,3	-124
	25.2	298.4	1.460		
	34.7	307.9	2.670		

Table 4.6: Observed pseudo first order, second order rate constants and activation parameters obtained during oxidative addition of CH_3I to Rh(β-diketonato)(CO)(PPh_3) complexes at 15 °C, 25 °C and 35 °C, in acetone.

The data were processed by means of the software package MINSQ[3] to calculate ΔH°* and ΔS°* from equation ⑧ while equation ⑨ was used for the plots (Figure 4.11 and (b)).

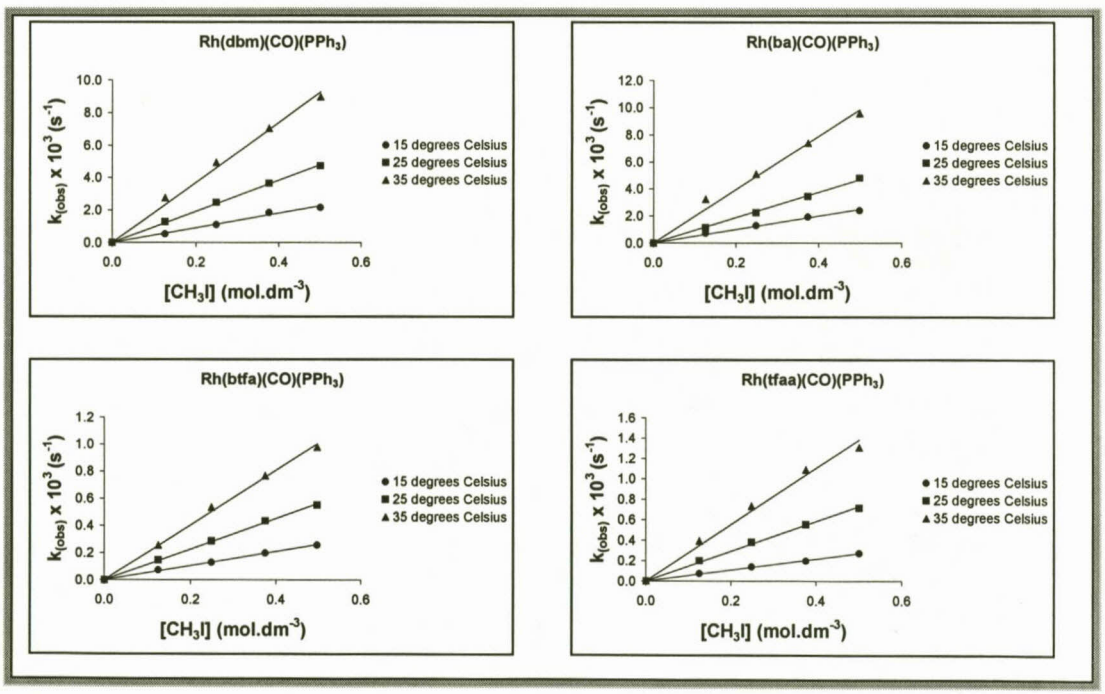

Figure 4.11 (a): Temperature and $[CH_3I]$ dependence of k_{obs} for the oxidative addition of CH_3I to Rh(β-diketonato)(CO)(PPh_3) complexes in acetone.

[3] MINSQ, Least Square Parameter Optimisation V 3.12, MicroMath, (1990)

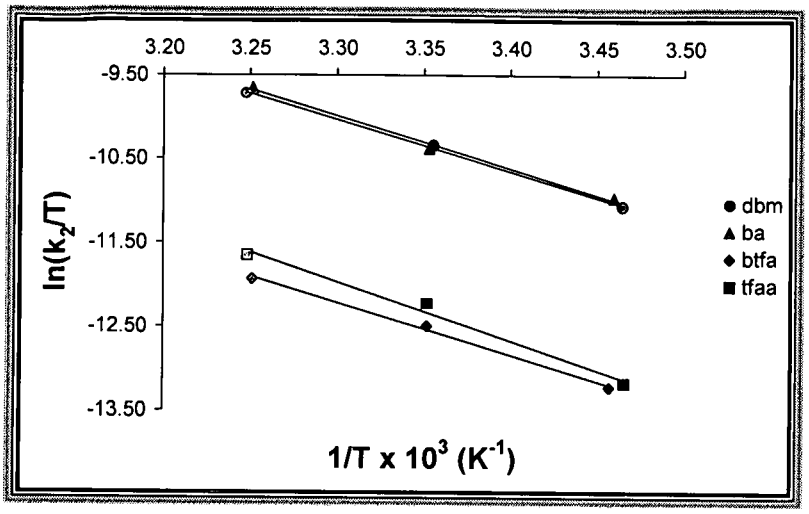

Figure 4.11 (b): Temperature dependence of k_2 values as from Table 4.6.

Small positive $\Delta H^{\circ *}$ and negative $\Delta S^{\circ *}$ values were obtained during the temperature variation investigation of the Rh(β-diketonato)(CO)(PPh_3) complexes.

4.2.3 The effect of pressure on the reaction rate

By considering the following chemical equation,

$$A + B \underset{}{\overset{K^*}{\rightleftharpoons}} (A,B)^* \xrightarrow{k_2} AB$$

the volume of activation, $\Delta \overline{V}^*$, is seen to be equal to the difference in the volume between the transition state and the reactants.

From basic thermodynamics, equation ⑦ (Appendix 4) can be rewritten as:

$$k_2 = \frac{RT}{Nh} e^{\frac{-\Delta G^{\circ *}}{RT}} \qquad ⑩$$

$$\text{Therefore } \ln k_2 = \ln \frac{RT}{Nh} - \frac{\Delta G^{\circ *}}{RT} \qquad ⑪$$

Differentiation of the above equation with respect to pressure, P, leads to:

$$\frac{\partial \ln k_2}{\partial P} = -\frac{\partial (\Delta G^{\circ *})}{RT \partial P} \text{ and } \left(\frac{\partial \ln k_2}{\partial P}\right)_T = -\frac{\Delta \overline{V}^*}{RT}, \qquad ⑫$$

because $\partial\Delta\overline{G}^{\circ *} = \Delta\overline{V}^{\circ *}\partial P$ at constant temperature. Plots of $\ln k_2$ *versus* P, at constant pressure, will consequently leads to a negative slope of $\frac{\Delta\overline{V}^{*}}{RT}$.

Although $\Delta\overline{V}^{*}$ is easy to understand, there is a problem in its interpretation. The observed volume of activation is comprised of two components, $\Delta\overline{V}^{*}_{intrinsic}$ and $\Delta\overline{V}^{*}_{solvating}$. $\Delta\overline{V}^{*}_{Intrinsic}$ is the change in volume due to change in bond lengths and bond angles during the formation of the activated complex. $\Delta\overline{V}^{*}_{solvating}$ is the change in volume due to different interactions of the activated complex formed with the solvent, as well as the interaction of the reactants with the solvent.

In weak polar complexes, the $\Delta\overline{V}^{*}_{solvating}$ contribution to the observed volume of activation is very small and the observed volume of activation will be a good indication of the $\Delta\overline{V}^{*}_{intrinsic}$.

A negative value for the observed volume of activation implies the possibility of an associative mechanism.

a) The determination of the observed volume of activation

A GBC 916 UV/Visible Spectrophotometer equipped with a single high pressure thermostated cell holder (Nova Swiss) was used during all the high pressure kinetic investigations.

Pressures were applied to a high pressure cell containing $Rh(dbm)(CO)(PPh_3)$ with a concentration of 1×10^{-4} mol.dm^{-3} and CH_3I with a concentration of 0.13 mol.dm^{-3}. The observed pseudo first order rate constants at each applied pressure (Table 4.7) were obtained at a constant temperature of 25 °C in acetone.

Pressure (Bar)	Pressure x 10^{-7} (Pa)	k_2 x 10^3 ($mol^{-1}.dm^3.s^{-1}$)	$\Delta\bar{V}^*$ ($mol^{-1}cm^3$)
100	1	9.42	-20.3
300	3	11.43	
500	5	13.12	
700	7	15.54	

Table 4.7: Second order rate constants obtained during oxidative addition of CH_3I to Rh(dbm)(CO)(PPh3) at various pressures and the calculated volume of activation.

The plot of $\ln k_2$ *versus* the applied pressure, P, (Figure 4.12) indicated an associative activity because of the observed negative value of the volume of activation.

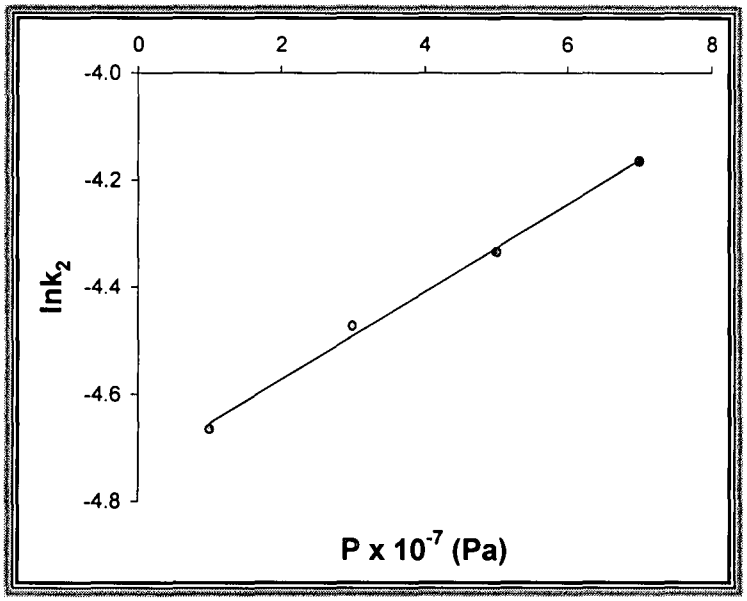

Figure 4.12: Linear relationship between the second order rate constants obtained during oxidative addition of CH_3I to Rh(dbm)(CO)(PPh_3) in acetone and the applied pressure.

4.2.4 The solvent effect

The solvent can be regarded as an "inert" medium or it can act as a nucleophile and an active participant in the reaction.

The dielectric constant of the solvent is the most important parameter with regards to the expression of the solvent as an "inert" medium.

Consider the following equation:

$$A + B \overset{K^*}{\rightleftharpoons} (A,B)^* \xrightarrow{k_2} AB$$

If the transition state, (A,B)* is polar, more polar solvents will stabilise its formation and consequently lead to an increase in the reaction rate.

The dielectric effect can be semi-quantitatively evaluated for ion-ion or ion-dipolar reactant mixtures, where electrostatic considerations dominate. For a reaction between two ions, of charge z_A and z_B, the rate constant, reduced to zero ionic strength, is given by[4]:

$$\ln k = \ln k_o - \frac{e^2}{2\varepsilon kT}\left[\frac{(z_A + z_B)^2}{r^*} - \frac{z^2_A}{r_A} - \frac{z^2_B}{r_B}\right] \qquad (13)$$

k_o is the hypothetical rate constant in a medium of infinite dielectric constant, ε, r_A, r_B and r^* are the radii of the reactant ions A and B and the activated complex respectively.

During a reaction between an ion z_A and a polar molecule, equation (13) becomes:

$$\ln k = \ln k_o + \frac{z^2_A e^2}{2\varepsilon kT}\left[\frac{1}{r_A} - \frac{1}{r^*}\right], \text{ because } z_B = 0$$

A plot of ln k *versus* ε^{-1} should therefore be linear.

The oxidative addition of CH_3I to $Rh(dbm)(CO)(PPh_3)$ was studied in the solvents acetone, benzene, dichloromethane and chlorobenzene. The second order rate constant obtained in the various solvents during the oxidative addition were determined with zero intercept plots of the observed pseudo first order rate constant *versus* $[CH_3I]$ (Table 4.8).

[4] Wilkins R.G., Kinetics and Mechanisms of reactions of Transition Metal Complexes, Chapter 2, Second Edition, VCA, (1991)

Solvent	ε	k_2 ($mol^{-1}.dm^3.s^{-1}$)
benzene	2.8	7.30E-05
chlorobenzene	5.6	1.81E-03
dichloromethane	9.1	2.27E-02
acetone	20.7	9.61E-03

Table 4.8: Second order rate constants at 25°C obtained during oxidative addition of CH_3I to $Rh(dbm)(CO)(PPh_3)$ in solvents with different dielectric constants.

The more polar the solvents, or the higher their dielectric constant, the larger the second order rate constant obtained during oxidative addition (Figure 4.13).

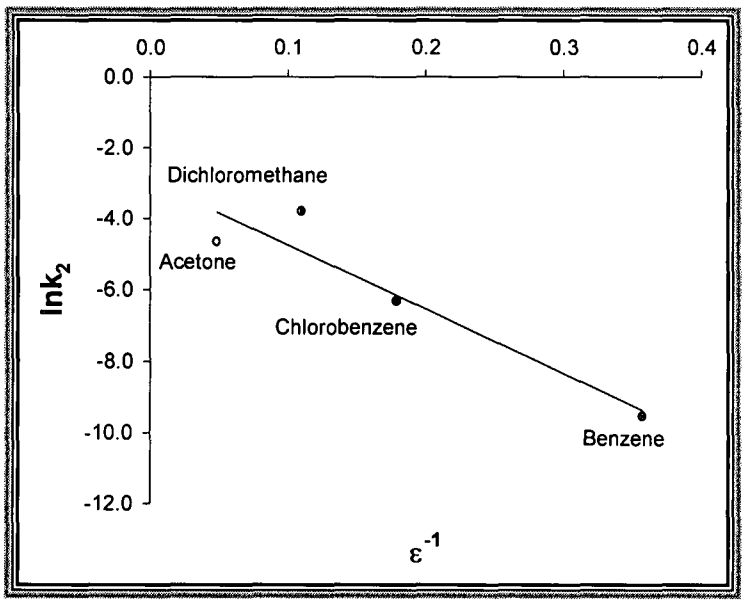

Figure 4.13: Linear relationship between the second order rate constant and the dielectric constant of the solvent used during oxidative addition of CH_3I to $Rh(dbm)(CO)(PPh_3)$ at 25°C.

4.3 Infrared Spectroscopy

Infrared monitoring provides structural information not obtainable using visible spectroscopy. The CO stretching frequencies are very sensitive to the metal environment and substitution reactions, including CO exchange and geometrical isomerisations.

Infrared kinetic investigations were carried out on a Hitachi 270 – 50 Infrared absorption Spectrophotometer.

4.3.1 The dependence of the final oxidative addition product on the nucleophilic character of the Rhodium(I) centre

Infrared kinetic investigations of Rh(dbm)(CO)(PPh_3) complexes were studied at 25 °C in dichloromethane as solvent. The reactant concentrations were 1 x 10^{-2} mol.dm^{-3} and 0.25 mol.dm^{-3} for the Rh(β-diketonato)(CO)(PPh_3) and CH_3I respectively.

The depletion of the Rh(I) carbonyl peak (2056 cm^{-1}) and the simultaneous formation of the Rh(III) carbonyl peak (2124 cm^{-1}) and the Rh(III) acyl peak (1740 cm^{-1}) for the first reaction of Rh(dbm)(CO)(PPh_3) are tabulated (Table 4.9) and the spectral information is also given (Figure 4.17 (a) (i)).

Disappearance of Rh(I)(dbm)(CO)(PPh_3)			
t (min)	**Absorption (λ = 2056 cm^{-1})**	**k_{obs} x 10^3 (s^{-1})**	**k_2 x 10^2 ($mol^{-1}.dm^3.s^{-1}$)**
0.0	0.36	3.5(2)	1.4(2)
2.5	0.22		
5.0	0.12		
7.5	0.07		
10.0	0.05		
12.5	0.03		
15.0	0.02		
Formation of *trans*-Rh(III)(dbm)(CO)(I)(CH_3)(PPh_3)			
t (min)	**Absorption (λ = 2124 cm^{-1})**	**k_{obs} x 10^3 (s^{-1})**	**k_2 x 10^2 ($mol^{-1}.dm^3.s^{-1}$)**
0.0	0.03	8.8(3)	3.5(3)
2.5	0.07		
5.0	0.07		
7.5	0.08		
10.0	0.08		
12.5	0.08		
15.0	0.08		

Formation of Rh(III)(dbm)($COCH_3$)(I)(PPh_3)			
t (min)	Absorption (λ = 1740 cm^{-1})	k_{obs} x 10^3 (s^{-1})	k_2 x 10^2 ($mol^{-1}.dm^3.s^{-1}$)
0.0	0.02	3.4(3)	1.4(3)
2.5	0.06		
5.0	0.10		
7.5	0.12		
10.0	0.13		
12.5	0.13		
15.0	0.14		

Table 4.9: Second order rate constants obtained during the first oxidative addition reaction of CH_3I to Rh(dbm)(CO)(PPh_3) at 25 °C in dichloromethane

The second order rate constants of the first reaction obtained for the simultaneous depletion of the Rh(I) carbonyl peak (1.4 x 10^{-2} $mol^{-1}.dm^3.s^{-1}$) and the formation of the Rh(III) carbonyl peak as well as the formation of the Rh(III) acyl peak observed during infrared spectroscopy, (Figure 4.14) compare well, within the experimental error, with the second order rate constant, k_2 = 2.27 x 10^{-2}, obtained using Visible Spectroscopy (Table 4.3).

The [CH_3I] was not varied since it was proved repeatedly that the graph of k_{obs} *versus* [CH_3I] was linear with zero intercepts. The k_2-values obtained from IR kinetics must be expected to be less accurate than the k_2-values obtained from visible kinetics because it was not possible to study absorption as a function of time at a constant wavelength with the IR apparatus used. Absorption data could only be calculated manually from the overlay spectra.

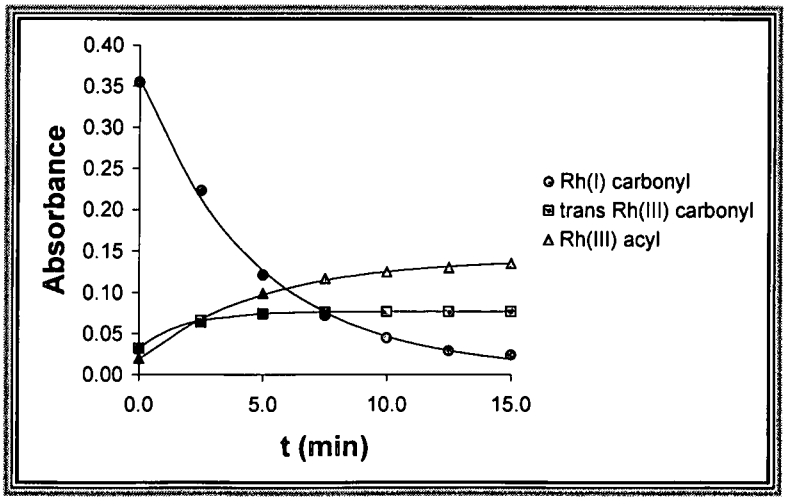

Figure 4.14: The simultaneous depletion of the Rh(I) carbonyl peak and the formation of the expected trans Rh(III) carbonyl peak and the Rh(III) acyl peak.

A second reaction was observed with the simultaneous depletion of the expected *trans* Rh(III) carbonyl peak (2124 cm^{-1}) and the Rh(III) acyl peak (1740 cm^{-1}) with the formation of an expected *cis* Rh(III) carbonyl peak (2115 cm^{-1}). The results are tabulated (Table 4.10) and the spectral data are given (Figure 4.17 (a) (ii)).

Formation of *cis*-Rh(III)(dbm)(CO)(I)(CH_3)(PPh_3)		
t (min)	**Absorption (λ = 2115 cm^{-1})**	**k_{obs} x 10^5 (s^{-1})**
60	0.05	4.5(2)
120	0.08	
180	0.09	
242	0.11	
300	0.12	
360	0.13	
420	0.14	
480	0.15	
540	0.16	
1440	0.20	
Disappearance of Rh(III)(dbm)($COCH_3$)(I)(PPh_3)		
t (min)	**Absorption (λ = 1740 cm^{-1})**	**k_{obs} x 10^5 (s^{-1})**
60	0.12	5.2(2)
120	0.11	
180	0.10	
242	0.09	
300	0.08	
360	0.08	
420	0.07	
480	0.07	
540	0.06	
600	0.06	
1440	0.05	

Table 4.10: The second order rate constant of the isomerisation reaction obtained during the simultaneous depletion of the Rh(III) acyl peak and formation of an expected cis Rh(III) carbonyl peak.

The first order rate constant of the second reaction (5.2 x 10^{-5} $mol^{-1}.dm^3.s^{-1}$), which comprised the simultaneous depletion of the Rh(III) acyl peak and formation of the expected *cis* Rh(III) carbonyl peak (Figure 4.15), compared well,

within experimental error, with the first order rate constant (k_1 = 7.30 x 10^{-5} $mol^{-1}.dm^3.s^{-1}$) obtained during Visible Spectroscopy (Table 4.5).

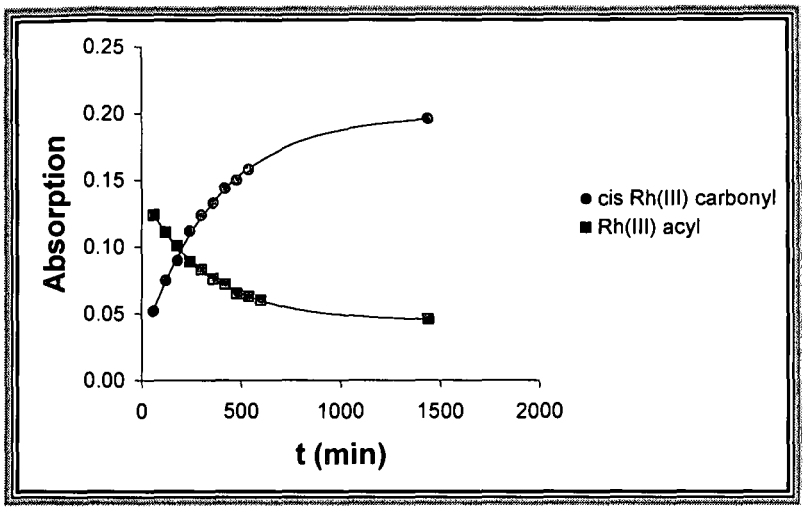

Figure 4.15: *The simultaneous depletion of the Rh(III) acyl peak and formation of an expected cis Rh(III) carbonyl peak.*

The solvent effect on the rate of disappearance of the Rh(I) carbonyl peak during oxidative addition was investigated in acetone, dichloromethane, dichloroethane, chlorobenzene and benzene at 25 °C (Table 4.11).

Solvent	ε	k_2 ($mol^{-1}.dm^3.s^{-1}$)
benzene	2.8	6.5E-05
chlorobenzene	5.6	1.4E-03
dichloromethane	9.1	1.4E-02
dichloroethane	10.6	1.2E-02
acetone	20.7	7.3E-03

Table 4.11: *Second order rate constants obtained during the disappearance of the Rh(I) carbonyl peak in various solvents.*

A plot of $\ln k_2$ *versus* ε^{-1} was linear (Figure 4.16) and correlated well with the results obtained during Visible Spectroscopy (Figure 4.13).

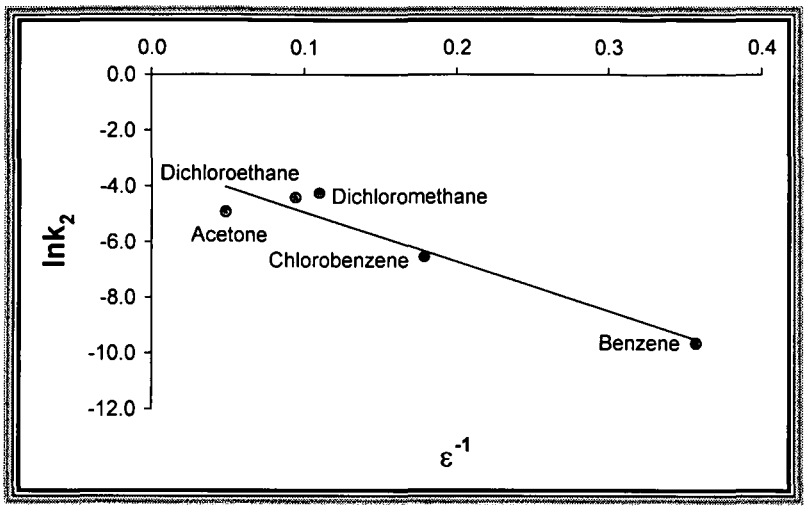

Figure 4.16: *Linear relationship between the second order rate constants and the dielectric constant of the solvent used during oxidative addition studied in the IR region at 25°C.*

The second order rate constants of the depletion of the Rh(I) carbonyl peak obtained during Infrared Spectroscopy and the second order rate constants for the oxidative addition obtained during Visible Spectroscopy are summarised (Table 4.12).

		INFRARED	VISIBLE
Solvent	ε	**k_2 ($mol^{-1}.dm^3.s^{-1}$)**	**k_2 ($mol^{-1}.dm^3.s^{-1}$)**
benzene	2.8	6.5E-05	7.3E-05
chlorobenzene	5.6	1.4E-03	1.8E-03
dichloromethane	9.1	1.4E-02	2.3E-02
acetone	20.7	7.3E-03	9.6E-03

Table 4.12: *Correlation between the second order rate constant obtained during Infrared Spectroscopy and Visible Spectroscopy.*

The IR spectra revealed that Rh(ba)(CO)(PPh_3) and Rh(dbm)(CO)(PPh_3) form the same final isomers. The oxidative addition reaction of CH_3I to Rh(btfa)(CO)(PPh_3) and to Rh(tfaa)(CO)(PPh_3) was different from that of Rh(ba)(CO)(PPh_3) and Rh(dbm)(CO)(PPh_3) in the following respects (Figure 4.17).

- The first reaction involved the disappearance of the Rh(I) carbonyl peak and the simultaneous formation of the Rh(III) carbonyl peak.
- The second reaction involved the disappearance of the Rh(III) carbonyl peak to form the Rh(III) acyl peak.

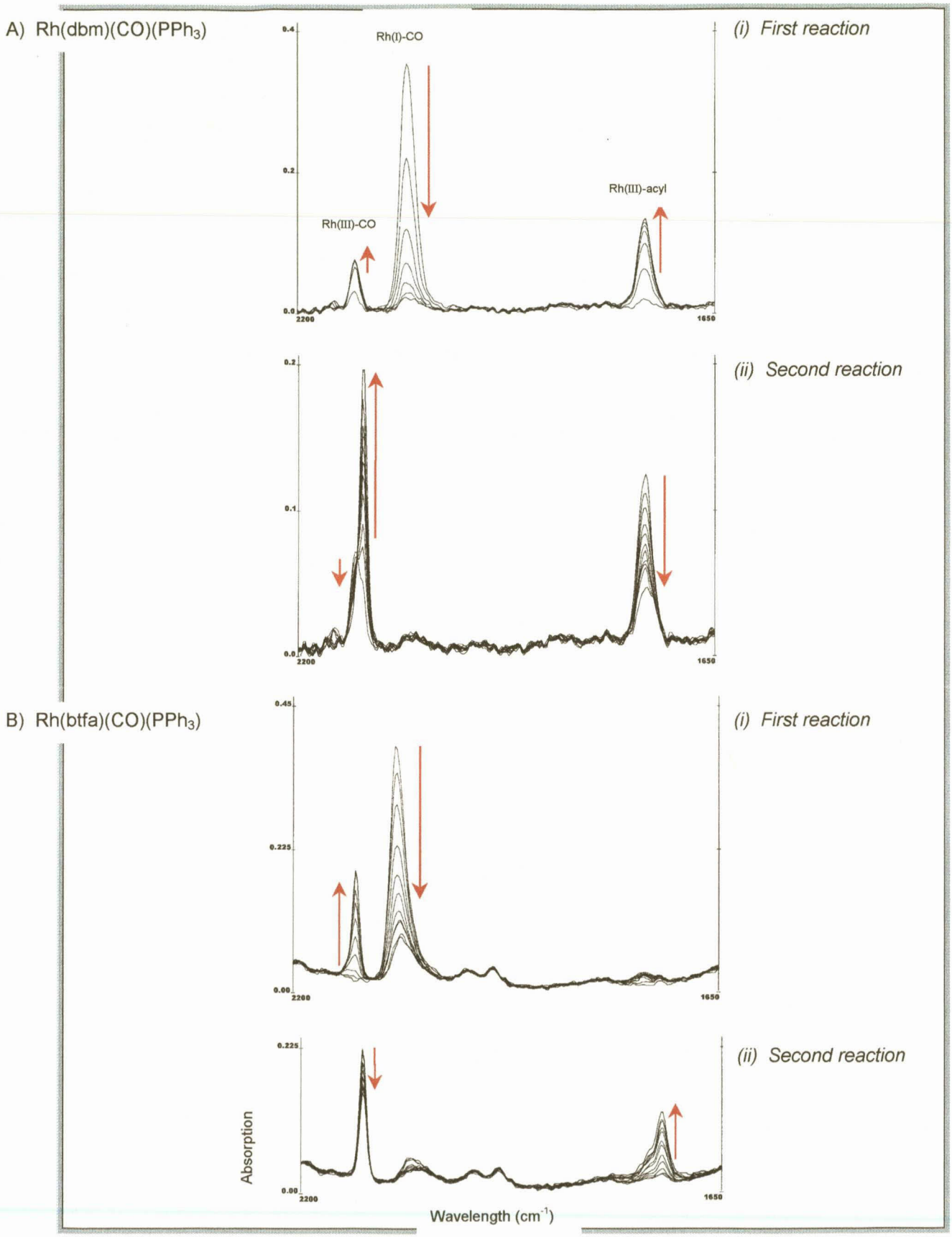

Figure 4.17: Overlay scans obtained during oxidative addition of CH_3I to $Rh(dbm)(CO)(PPh_3)$ and $Rh(btfa)(CO)(PPh_3)$ to demonstrate the different final isomers formed.

4.4 NMR Spectroscopy

NMR can be used simply as an analytical tool in which the strength of the signal is a measurement of the concentration of a particular complex. One disadvantage of NMR Spectroscopy is the relatively high concentrations of solute required for a spectrum.

Proton NMR spectroscopy was used to investigate the oxidative addition of CH_3I to $Rh(dbm)(CO)(PPh_3)$ at 25°C in $CDCl_3$ (Figure 4.18). The reactant concentrations were 1.5×10^{-2} mol.dm^{-3} and 0.15 mol.dm^{-3} for $Rh(dbm)(CO)(PPh_3)$ and CH_3I respectively.

The formation and strength of the newly formed methyl signal at ν = 3.05 was investigated for an hour with non-sequential time intervals (Table 4.13).

t (min)	Methyl peak formation (3.05 ppm)	$k_{obs} \times 10^3$ (s^{-1})	$k_2 \times 10^2$ ($mol^{-1}.dm^3.s^{-1}$)
0	0	2.30	2(1)
2	0.138		
4	0.216		
8	0.375		
16	0.496		
32	0.545		
64	0.550		

Table 4.13: Second order rate constant obtained during oxidative addition by means of NMR spectroscopy.

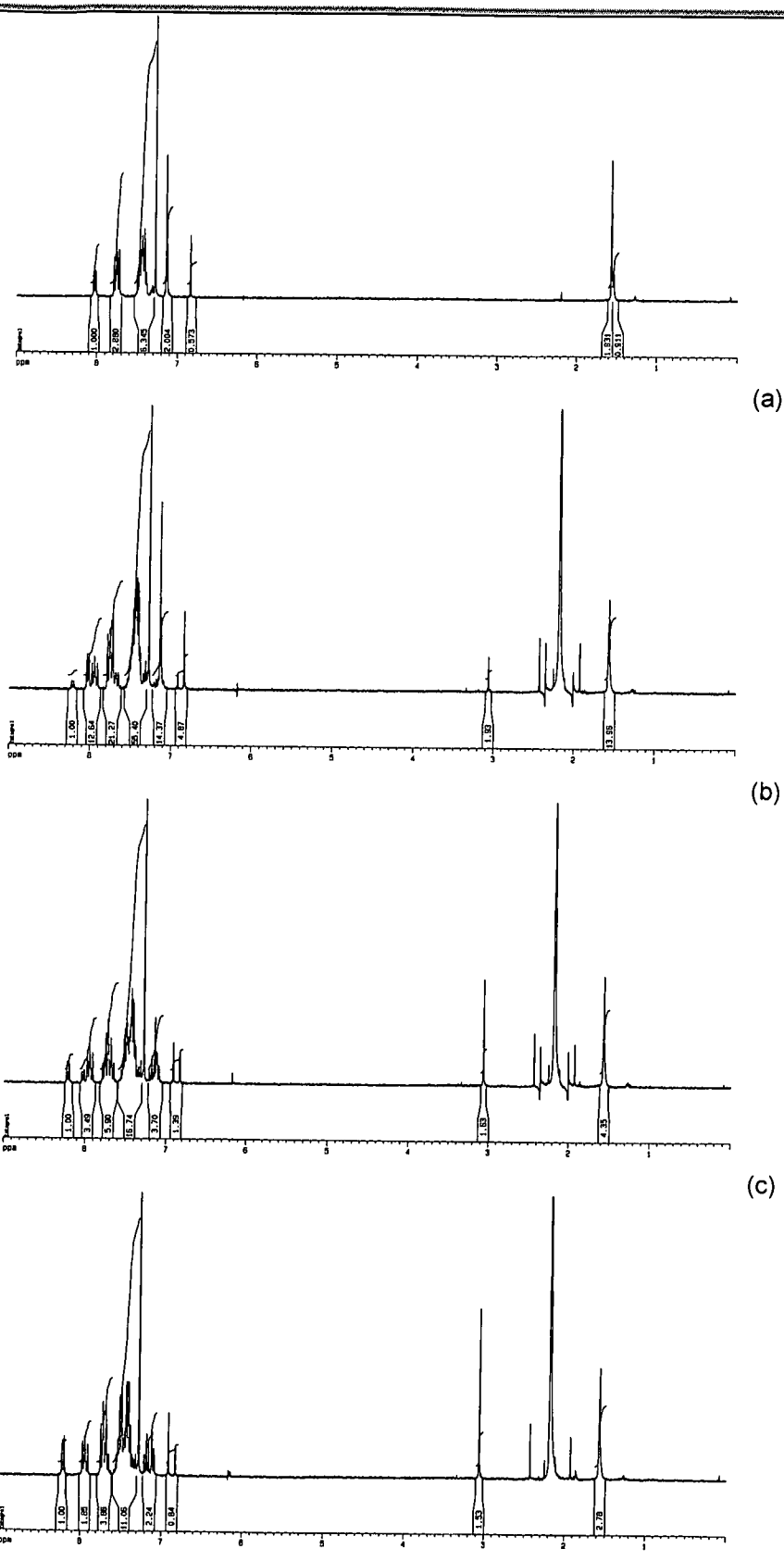

Figure 4.18: *^1H NMR of oxidative addition of CH_3I to $Rh(dbm)(CO)(PPh_3)$ at 25°C in $CDCl_3$. t = (a) 0 min, (b) 2 min, (c) 8 min, (d) 64 min*

The second order rate constant for the oxidative addition of CH_3I to $Rh(dbm)(CO)(PPh_3)$ by means of proton NMR Spectroscopy (Figure 4.19), correlated very well, within experimental error, with the second order rate constants obtained during Visible and Infrared Spectroscopy (Table 4.14).

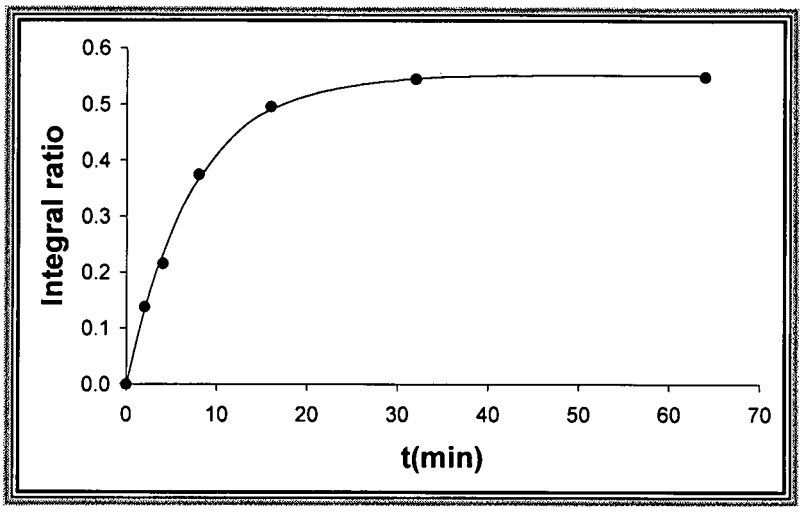

Figure 4.19: Plot of the integral ratio of the methyl signal obtained during oxidative addition of CH_3I to $Rh(dbm)(CO)(PPh_3)$ at 25°C in $CDCl_3$ versus time.

	VISIBLE	INFRARED	NMR
Solvent	**$k_2 \times 10^2$ ($mol^{-1}.dm^3.s^{-1}$)**	**$k_2 \times 10^2$ ($mol^{-1}.dm^3.s^{-1}$)**	**$k_2 \times 10^2$ ($mol^{-1}.dm^3.s^{-1}$)**
Chloroform	3.85(2)	2.3(5)	2(1)

Table 4.14: Second order rate constants obtained during oxidative addition of CH_3I to $Rh(dbm)(CO)(PPh_3)$ at 25 °C.

4.5 The kinetics in perspective

4.5.1 Catalytic Activity

In almost every publication on Rhodium chemistry, the following statement is found in the introduction: "Rhodium compounds are used in many homogenous catalytic cycles, such as alkane activation, olefin hydrogenation and carbonylation, for example, the industrial conversion of methanol into

acetic acid." It appears that, after having said the above, researchers tend to forget the possibility of catalysis.

It was mentioned (Section 3.2) that the same reaction vessel must be used repeatedly in order to obtain consistent reaction rates and yields during the reduction of $RhCl_3.3H_2O$ with DMF to form the dimer $[RhCl(CO)_2]_2$. The only possible explanation is that Rhodium and/or its complexes, absorbed on the glass surface, was engaged in some catalytic activity in decomposing DMF to yield free CO gas (Figure 3.1). DMF is a stable molecule which does not decompose upon refluxing under normal conditions.

The above possible catalytic involvement was not important within the boundaries of this investigation because pure Rh(I) Dicarbonyl complexes could be obtained. It could, however, have serious consequences for the kinetic investigations, as discussed below.

A part of this study was originally used for the purpose of obtaining a M.Sc. degree. The M.Sc. was upgraded to a Ph.D. and one of the motivations for upgrading is quoted: "In previous publications (and references therein) it was postulated that the reaction rate is enhanced by more polar solvents during oxidative addition. The solvent effect is indicative of a mechanism in which a polar transition state is stabilised by more polar solvents. In this study the exact opposite trend was observed. Before jumping to conclusions a more detailed study is now required."

In the follow-up investigations, a whole range of solvents were studied as reaction media during the oxidative addition of CH_3I to the Rh(β-diketonato)(CO)(PPh_3) complexes. The results revealed a complete inconsistency regarding the effect of the solvents on the reaction rate, as well as irreproducible results, especially in chlorinated and polar solvents.

The original studies on the oxidative addition of CH_3I to the Rh(β-diketonato)(CO)(PPh_3) complexes done in chloroform as reaction medium in

the IR region are given as an example of the irreproducible and inconsistent results (Figure 4.20). The Rh(I) peak at 2061cm^{-1} decreases with a simultaneous increase of the Rh(III) carbonyl peak at 2124cm^{-1} and the Rh(III) acyl peak at 1740cm^{-1}.

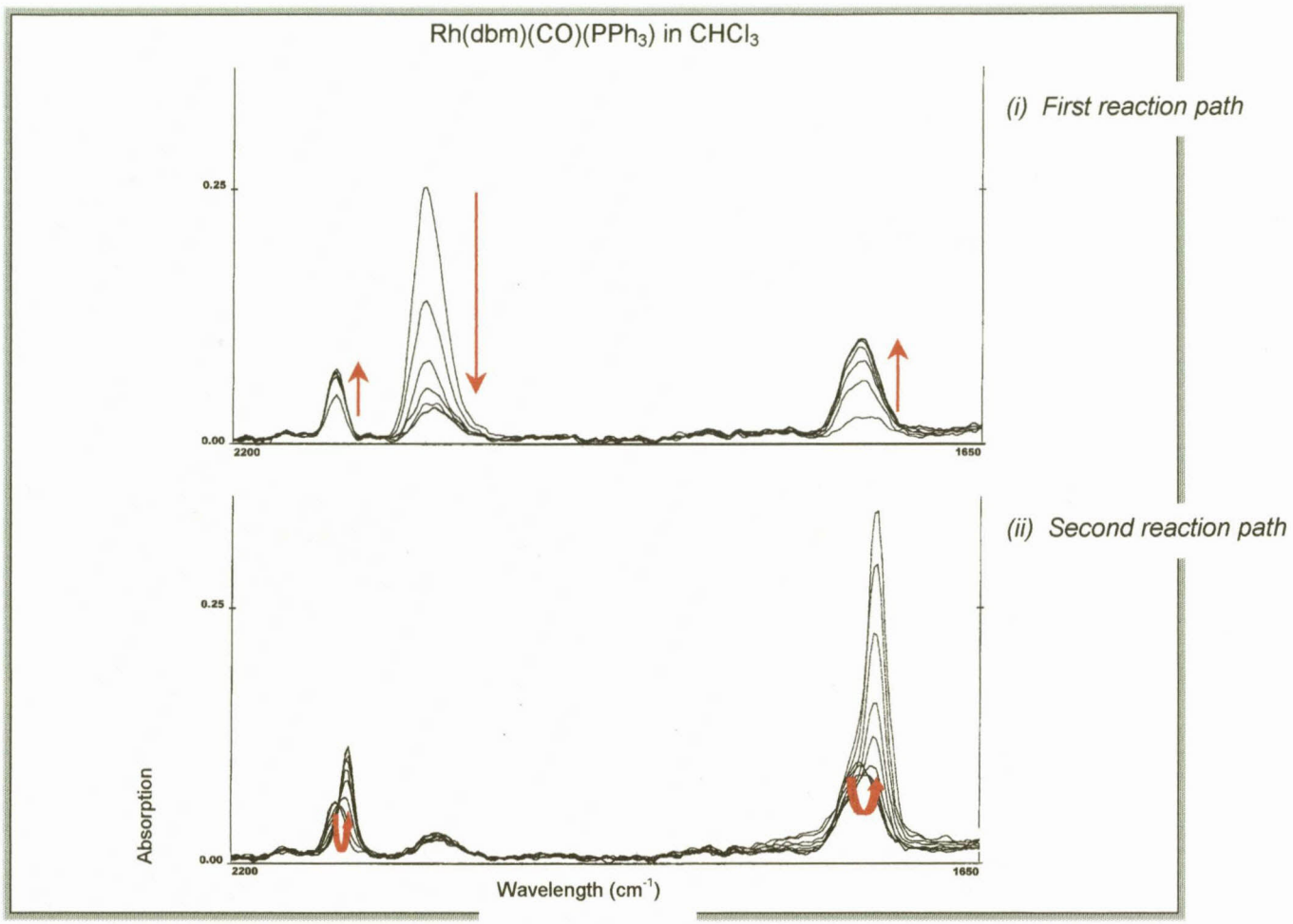

Figure 4.20: Infrared spectra of the formation of a second peak in the region of the Rh(III) acyl peak at 1727 cm^{-1} which occurred during the oxidative addition of CH_3I to Rh(dbm)(CO)(PPh_3) in chloroform.

The reaction sequence of the oxidative addition of CH_3I to Rh(dbm)(CO)(PPh_3) in chloroform as reaction medium was therefore the same as the oxidative addition of CH_3I to Rh(dbm)(CO)(PPh_3) in dichloromethane as reaction medium (Figure 4.17), except for the inconsistent formation of a peak at 1727 cm^{-1} (Figure 4.20). This peak at 1727 cm^{-1} was observed in almost all solvents except non-polar benzene. Infrared spectra of Rh(dbm)(CO)(PPh_3), in the absence of CH_3I, gave the same peak formation

at 1727 cm^{-1} and even infrared spectra of only the pure polar solvents, without the addition of $Rh(dbm)(CO)(PPh_3)$ and without the addition of CH_3I gave the same peak at 1727cm^{-1}! When the infrared cells were polished and the oxidative addition of CH_3I to $Rh(dbm)(CO)(PPh_3)$ was repeated under the same experimental conditions the peak formation at 1727cm^{-1} did not occur at all. The irregular peak formation at 1727 cm^{-1} could once again only be attributed to some form of catalytic activity by the Rhodium and/or its complexes absorbed on the infrared cells. A possible explanation in the case of chloroform used as reaction medium is that the known decomposition upon radiation of chloroform to form phosgene, $COCl_2$, is catalysed by the Rhodium and/or its compounds absorbed on the infrared cells.

The problem, however, was not solved yet since the same abnormal behaviour with inconsistent results was also observed in the visible region. Once the quartz cells were cleaned, for their use in the visible region, with concentrated nitric acid in an ultrasonic bath, the reproducible results reported in this chapter were obtained.

It is important to note that the results of the oxidative addition of CH_3I to $Rh(tfaa)(CO)(PPh_3)$ have already been published[5]. Biphasic kinetics, Phosphine dissociation and saturation kinetic results were obtained, none of which could be reproduced in this kinetic study. Consistent and reproducible second order rate constants were obtained under pseudo first order conditions during the kinetic study after the above mentioned cell treatment, resulting in zero intercepts of the plots of the observed pseudo first order rate constants *versus* $[CH_3I]$ (Figure 4.11 (a)).

4.5.2 Chemical oxidation mechanism

Based upon the kinetic results, the following reaction mechanism is postulated for the oxidative addition of CH_3I to the Rh(β-diketonato)$(CO)(PPh_3)$ complexes (Figure 4.21 (a),(b) and (c)).

[5] Basson S.S., Leipoldt J.G., Nel J.T., *Inorg. Chim. Acta*, **84**, 167, (1984)

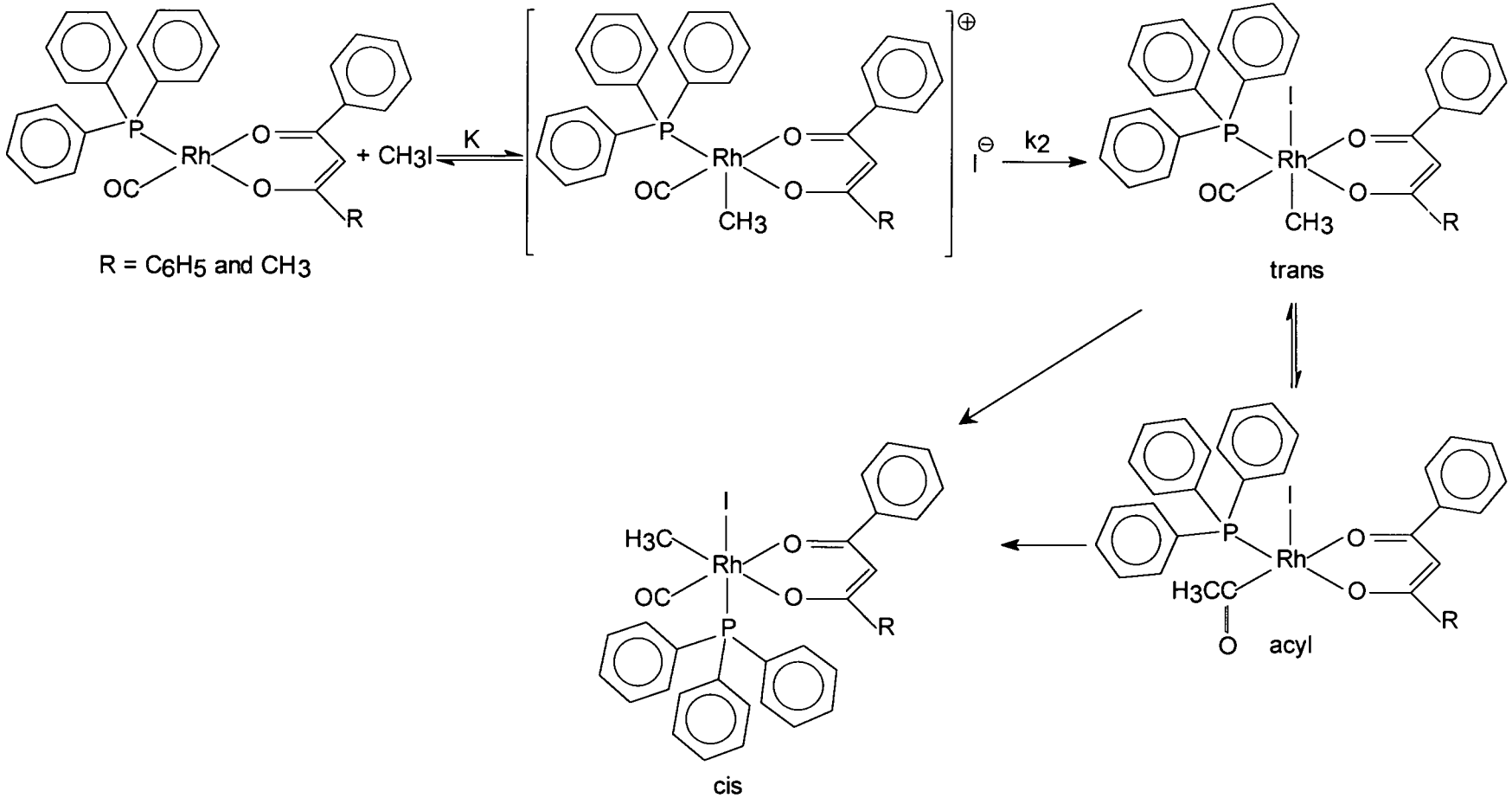

Figure 4.21 (b): Mechanism for the oxidative addition of CH_3I to Rh(dbm)(CO)(PPh_3) and Rh(ba)(CO)(PPh_3)

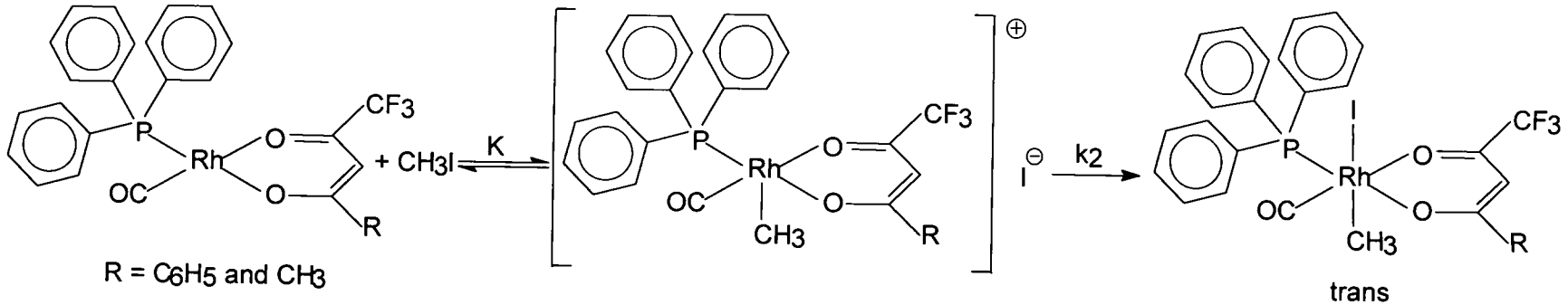

Figure 4.21 (c): Mechanism for the oxidative addition of CH_3I to Rh(btfa)(CO)(PPh_3) and Rh(tfaa)(CO)(PPh_3)

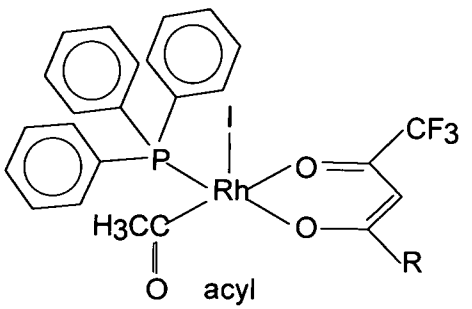

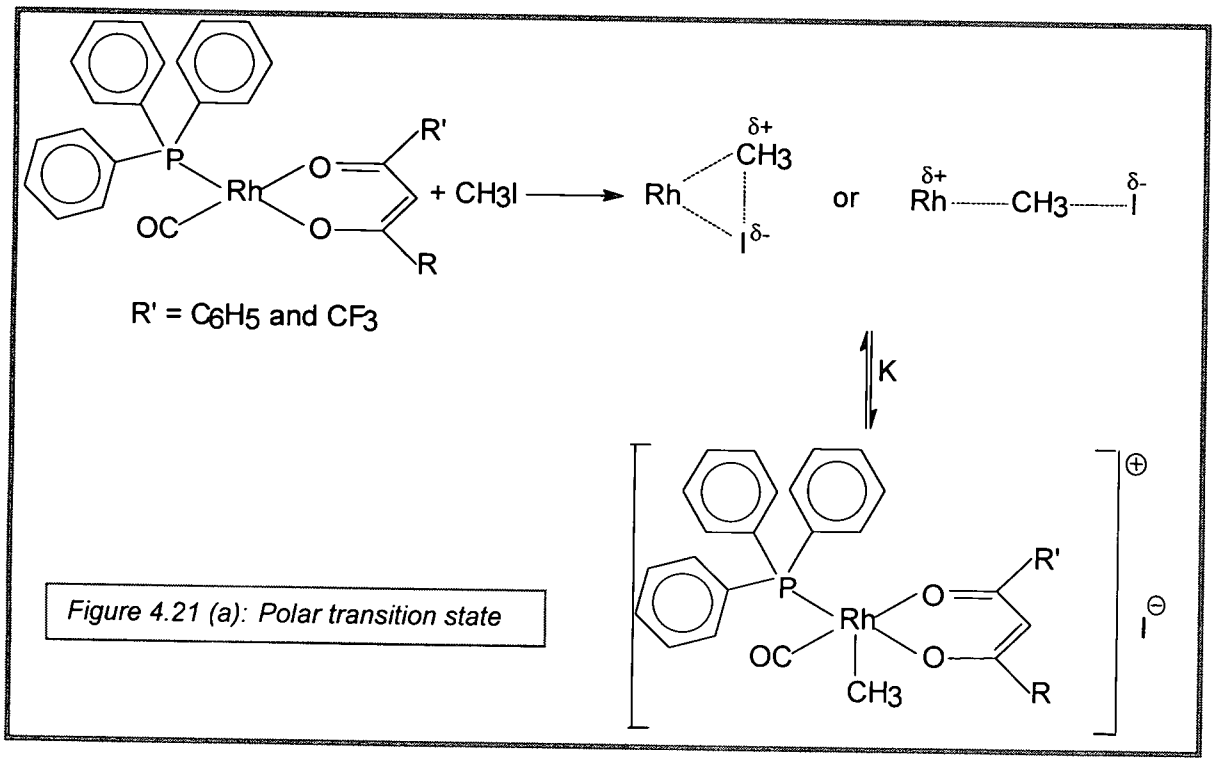

Figure 4.21 (a): Polar transition state

4.5.3 The transition state

Based on the present as well as other kinetic studies[6,7,8,9], the proposed mechanism is a nucleophilic attack by the Rhodium atom on the Carbon atom of the methyl iodide where a linear polar transition state (Figure 4. 21(a)) is formed which leads to *trans* addition. The possibility of a three-centred polar transition state (Figure 4.22), which normally leads to *cis* addition, cannot be ruled out[10].

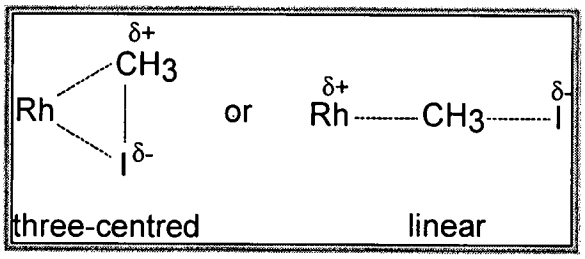

Figure 4.22: The two possible intermediates that can occur during oxidative addition.

The question of the two possible intermediates will also be addressed in PART 3 with the aid of molecular mechanics.

The temperature effect (Section 4.2.2), pressure effect (Section 4.2.3) and solvent effect (Section 4.2.4) suggest a five co-ordinated charged intermediate (Figure 4. 21(a)).

If there is an increase in the co-ordination number during the formation of the transition state, large negative values for the entropy are expected. The large negative values of ΔS^* (Table 4.6) therefore point towards an associative mechanism where, in the present case, a five co-ordinated intermediate is postulated (Figure 4. 21(a)). The values of the enthalpy of activation, ΔH^*, are small and virtually constant with no real relation to the properties of the respective β-diketones.

[6] Lamprecht G.J., Beetge J.H., *S. Afr. J. Chem.*, **40(2)**, 131, (1987)
[7] van Zyl G.J., Lamprecht G.J., Leipoldt J.G., *Inorg. Chim. Acta*, **122**, 75, (1986)
[8] Leipoldt J.G., Basson S.S., Botha L.J., *Inorg. Chim. Acta*, **168**, 215, (1990)
[9] Venter J.A., Leipoldt J.G., van Eldik R, *Inorg. Chem.*, **30(9)**, 2207, (1991)
[10] van Zyl G.J., Lamprecht G.J., Leipoldt J.G., Swaddle T.W., *Inorg. Chim. Acta*, **143**, 223, (1988)

The results obtained by increasing the pressure (Table 4.7) also point towards an associative mechanism where a negative experimental volume of activation (-20.3 $cm^3.mol^{-1}$) was observed. Both $\Delta\overline{V}^*_{intrinsic}$ and $\Delta\overline{V}^*_{solvating}$ must be taken into account before final conclusions about the mechanism are made, but since a charged intermediate is postulated, it is expected that $\Delta\overline{V}^*_{solvating}$ would make a significant contribution to the experimental volume of activation[10]. The present value of -20.3 $cm^3.mol^{-1}$ for $\Delta\overline{V}^*_{experimental}$ agrees well with published data[11], where in spite of the large $\Delta\overline{V}^*_{solvating}$ contribution, an associative mechanism is proposed.

An increase in solvent polarity leads to an increase in the second order rate constant during oxidative addition (Figure 4.13). The above results were also obtained in the IR region (Figure 4.16). These results are indicative of a mechanism where a polar transition state is formed and can be taken as evidence that the function of the solvent is to ease the charge separation during the formation of the transition state.

4.5.4 Molecular structure of reactants and products

Based on the molecular structure of $Rh(dbm)(CO)(PPh_3)$ (Section 3.4.3) and publications on similar structures[12,13,14,15], the structures of the reagents in this study can be taken as presented (Figure 3.3). In the case of $Rh(dbm)(CO)(PPh_3)$ and $Rh(ba)(CO)(PPh_3)$, the final oxidation product is the *cis* Rh(III) Carbonyl Phosphine complex (Figure 4.21 (b)). From IR spectroscopy (Figure 4.17 (A) (ii)) it was clear that only one isomer formed as final product during oxidative addition. The formation of the final product must have been through isomerisation since the final reaction path was independent of $[CH_3I]$ (Figure 4.10). The oxidative addition of CH_3I to Rh(ferrocenyltrifluoroacetonato)$(CO)(PPh_3)$ followed the same IR pattern and the molecular structure of the final oxidative addition product was determined as the *cis* configuration[16]. The molecular structure of

[11] Leipoldt J.G., Steynberg E.C., van Eldik R., *Inorg. Chem.*, **26**, 3068, (1987)
[12] Steynberg E.C., Lamprecht G.J., Leipoldt J.G., *Inorg. Chim. Acta.*,**133**, 33, (1981)
[13] Leipoldt J.G., Lamprecht G.J., Graham D.E., *Inorg. Chim. Acta.*,**101**, 123, (1985)
[14] Lamprecht G.J.,Swarts J.C., Conradie J., Leipoldt J.G., *Acta Cryst.*, **149**, 82, (1993)
[15] Graham D.E., Lamprecht G.J., Potgieter I.M., Roodt A., Leipoldt J.G., *Trans. Met., Chem.*, 193, (1991)
[16] Conradie J., Lamprecht G.J., Swarts J.C., *to be published*

$Rh(cupferrate)(CO)(CH_3)(I)(PPh_3)$[17] also exhibited a *cis* configuration for the final isomer formed via the formation of the Rh(III) acyl during oxidative addition.

In the case of $Rh(btfa)(CO)(PPh_3)$ and $Rh(tfaa)(CO)(PPh_3)$ the final oxidative addition product is the Rh(III) acyl complex (Figure 4.21 (c)). From IR spectroscopy (Figure 4.17 (B) (ii)) it is apparent that only one final product formed, also via isomerisation, during oxidative addition. The Rh(III) acyl complex was also the final product of oxidative addition of CH_3I to $Rh(thioacetylacetonato)(CO)(PPh_3)$ complexes[18].

These results indicate that the final isomer formed during oxidative addition of CH_3I depends on the nature and nucleophilicity of the ligands. The final isomer can, however, also be a function of steric properties, since the final isomer formed during oxidative addition of I_2 to $Rh(tfaa)(P(OPh)_3)$ exhibited the *trans* diiodo complex[19].

4.5.5 Electronic and Steric effect

Plots of k_{obs} *versus* $[CH_3I]$ were linear with zero intercepts (Figure 4.6 and 4.11 (a)). The electronic effect of the substituents on the β-diketones showed that the reaction rate decreases with the lowering of the pKa-values of the free β-diketones (Figure 4.7 and 4.8). The effect of more electronegative substituents on the reactivity of the Rh(I) centre is explained by the fact that electron density is removed from the Rhodium metal, making the complex a stronger Lewis acid and less reactive towards oxidative addition[20,21,22]. The Rhodium atom thus becomes a weaker nucleophile.

---

[17] Basson S.S., Leipoldt J.G., Roodt A., Venter J.A., *Inorg. Chim. Acta*, **128**, 31, (1987)
[18] Leipoldt J.G., Basson S.S., Botha L.T., *Inorg. Chim. Acta*, **168**, 215, (1990)
[19] van Zyl G.J., Lamprecht G.J., Leipoldt J.G., *Inorg. Chim. Acta*, **122**, 75, (1986)
[20] Basson S.S., Leipoldt J.G., Nel J.T., *Inorg. Chim. Acta*, **84**, 167, (1984)
[21] Thompos W.H., Sears C.T., *Inorg. Chem.*, **16**, 769, (1977)
[22] Hart-Davis A.J., Graham W.A.G., *Inorg. Chem.*, **9**, 2658, (1970)

Steric effects, however, can also be important factors in controlling the rates of oxidation addition reactions[23]. These effects are also perceptible in the present study where the β-diketones, btfa and tfaa, have the same pKa-values. The reaction rate of the more bulkier btfa was slower than that of tfaa (Table 4.2, Figure 4.7 and Table 4.3, Figure 4.8)

[23] Ugo R., Pasini A., Fusi A., Cerini S., *J. Am. Chem. Soc.*, **94**, 7364, (1972)

PART 2
ELECTROCHEMISTRY

ELECTROCHEMICAL OXIDATION OF RHODIUM(I) β-DIKETONATO CARBONYL PHOSPHINE COMPLEXES

CHAPTER 5:

STATIONARY-ELECTRODE CYCLIC VOLTAMMETRY

5.1 Introduction

Cyclic Voltammetry (CV) was first reported in 1938 and described theoretically in 1948 by Randles and Sevcik[1]. CV is the electrochemical equivalent of spectroscopy. It is the single most powerful tool for examining the electrochemical properties of a chemical substance or material. Both thermodynamic and kinetic information are available in a single experiment. Thus both reduction potentials and heterogeneous electron transfer rates can be measured and also the rate and nature of chemical reactions coupled to the electron transfer step can be studied. A single CV or a series carried out over a range of scan rates, concentrations, pH and temperatures can provide a wealth of mechanistic information.

Perhaps the most useful aspect of CV is its application to the qualitative diagnosis of electrode reactions that are coupled to homogeneous chemical reactions. The forte of CV is its ability to generate a species during one scan and then probe its fate with subsequent scans.

The weakness of voltammetry is that although it shows that "something is happening", what that might be is often beyond the capability of the technique. A

[1] Christensen P.A., Hamnett A., *Techniques and Mechanism in Electrochemistry*, Chapter 2, Blackie Academic & Professional, (1994)

chemical system should therefore be examined using several carefully chosen electrochemical techniques in combination with spectroscopic information and good chemical intuition.

Dynamic electrochemical methods fall into two convenient categories, large amplitude and small amplitude, related to the magnitude of the excitation signal. Two principal classes may be distinguished within these broad categories, depending on whether current or voltage is the controlled parameter (Figure 5.1)[2].

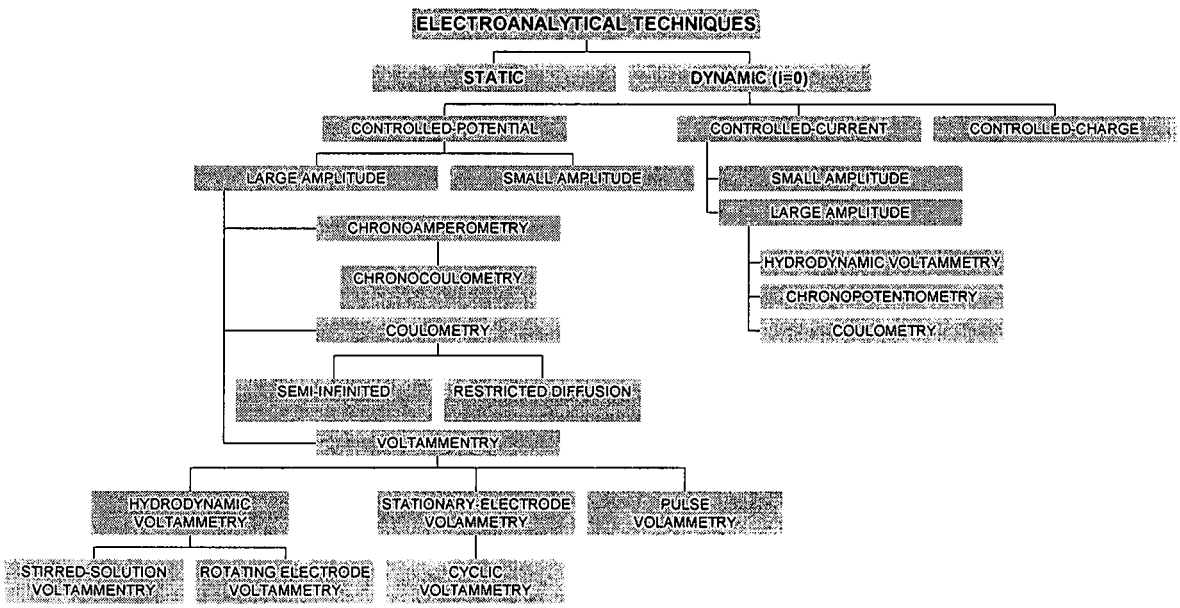

Figure 5.1: A family tree showing the relationships of the most important electroanalytical techniques.

5.2 Reversible processes

CV consists of cycling the potential of an electrode, which is immersed in an unstirred solution, and measuring the resulting current. The potential of this working electrode is controlled *versus* a reference electrode. The controlling potential, which is applied across the two electrodes, can be considered an excitation signal. The excitation signal for a CV is a linear potential scan with a triangular waveform. The current can be considered the response signal to the potential excitation signal. The

[2] Kissinger P.T., Heineman W.R., *Laboratory Techniques in Electroanalytical Chemistry*, Chapter 1, Dekker, (1984)

current depends on the movement of electro-active material to the surface of the electrode and the electron transfer reaction[3].

Mass transfer, the movement of material from one location in solution to another, arises from difference in either electrical or chemical potentials at the two locations. The modes of transfer are[4]:

I. Migration: Movement of a charged body under the influence of an electric field.

II. Diffusion: Movement of a species under the influence of a chemical potential gradient.

III. Convection: Stirring of a solution or hydrodynamic transport.
Example: density gradients

Since the CV experiment is performed at a stationary electrode in an unstirred solution, diffusion is the principal means of moving the reactant to the electrode surface. If, as is normal, the solution is not stirred, then the conditions of laminar (uniform) diffusion characterising the mass transfer during a CV experiment, will hold only for a short time. For longer periods, thermal and concentration gradients induce random convection processes and the resulting currents show sizeable fluctuations.

Most modern equipment uses a three electrode cell in which a counter or auxiliary electrode provides the current that is needed at the working electrode. Therefore, virtually no current flows through the reference electrode and its potential remains constant. A three-electrode system also makes it possible to minimise voltage errors due to ohmic, or IR loss through the solution, by placing the reference electrode close to the working electrode's surface.

5.2.1 The ideal Nernstian reaction

The simplest electrode reactions are those in which the kinetics of all electron transfer and associated chemical reactions are very rapid compared to those of the mass transfer processes. If an electrode process involves only fast

[3] Mabbott G.A., *J. Chem. Ed.*, **60(9)**, 697, (1983)
[4] Bard A.J., Faulkner L.R., *Electrochemical Methods – Fundamentals and Applications*, Chapter 1, Wiley, (1980)

heterogeneous charge transfer kinetics and mobile, reversible, homogeneous reactions it will be found that:

I. The homogeneous reaction can be regarded as being at equilibrium.

II. The surface concentration of species involved in the faradaic process is related to the electrode potential by an equation of the Nernst form.

For an ideal Nernstian reaction, the peak potentials of the cathodic and anodic sweeps will be the same and equal to E° (Figure 5.2).

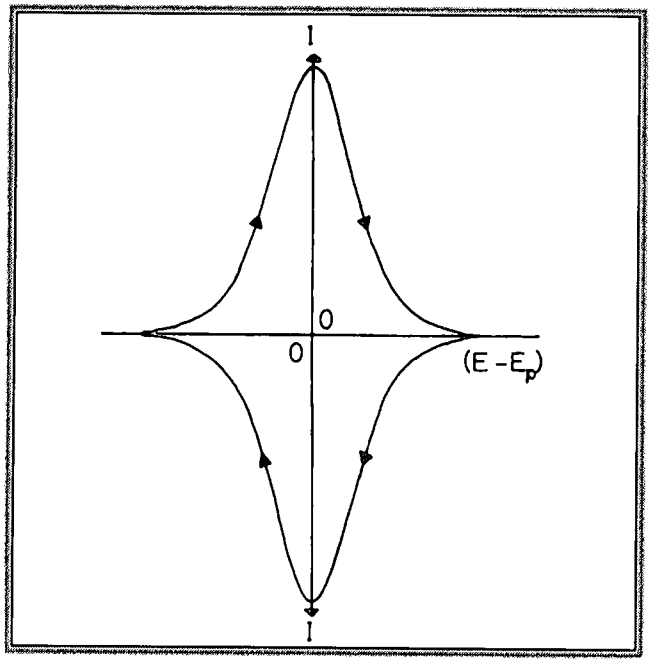

Figure 5.2: The current/potential curve expected from CV studies on the reversible redox reaction: $O + ne^- \rightleftharpoons R$

Figure 5.2 shows the CV that would be expected from an electro-active species assuming that:

(i) At time t = 0, the electrode surface has a maximum coverage of the oxidised form.

(ii) That the electrochemical reaction can be expressed by $O + ne^- \rightleftharpoons R$ and is kinetically fast enough to maintain Nernstian behaviour at each point in the CV scan so that the concentration of O and R near the electrode obey the Nernstian equation.

(iii) That the oxidised and reduced species are both strongly absorbed and have the same enthalpy of absorption.

5.2.2 Important parameters of a Cyclic Voltammogram

It is common practice to report the average of the forward and return peak potentials as the formal reduction potential, E°, for the redox couple in which both species rapidly exchange electrons. This is therefore an approximation that is only at its most accurate when the electron transfer process is reversible, and the separation in the peak potentials, ΔE_p, will then be close to equal $\frac{0.059}{n}$ V at 25°C. The relationship can be used to calculate n. This $\frac{0.059}{n}$ V separation of peak potentials is independent of scan rate for a reversible couple, but is slightly dependent on switching potential and cycle number. E° for a reversible couple is centred between $E_{p,a}$ and $E_{p,c}$ (Figure 5.3):

$$E^\circ = \frac{E_{p,a} + E_{p,c}}{2} \qquad ①$$

E° = formal reduction potential

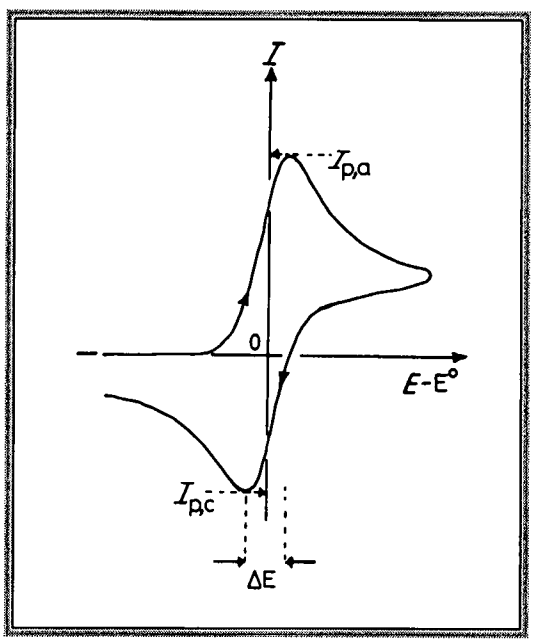

Figure 5.3: *Schematic of the CV expected from a reversible electrochemical redox system: $O + ne^- \rightleftharpoons R$.*

The peak current for a reversible system is described by the Randles-Sevcik equation for the forward sweep of the first cycle[5]:

$I_p = (2.69 \times 10^5)n^{3/2}AD^{1/2}C\nu^{1/2}$ ②

I_p = peak current (A)

n = electron stoichiometry

A = electrode area (cm^2)

D = diffusion coefficient ($cm^2.s^{-1}$)

C = concentration

I_p increases with $\nu^{1/2}$ and is directly proportional to concentration. The relationship of I_p to concentration is particularly important in analytical applications and in electrode mechanistic studies. The values of $I_{p,a}$ and $I_{p,c}$ should be identical for a reversible fast couple: $\frac{I_{p,a}}{I_{p,c}} \approx 1$ ③

Although the peak current increases with scan rate, the potential at which the peak occurs is invariant with scan rate.

5.3 Quasi-Reversible and Irreversible processes

If the electrochemical kinetics is slow, but the redox process still takes place, the system is termed quasi-reversible[1]. The peak current for a quasi-reversible system is not proportional to $\nu^{1/2}$ except when the peaks are so widely separated that the system is more appropriately seen as totally irreversible[3].

A quasi-reversible or irreversible reaction will give as much as 50% less current formation. Irreversibility manifests itself through $\Delta E_p > \frac{0.059}{n}$ V. Slow electron transfer at the working electrode surface, "irreversibility", causes the peak separation to increase (Figure 5.4).

[5] Kissinger T.P., Heineman W.R., *J. Chem. Ed.*, **60(9)**, 702, (1983)

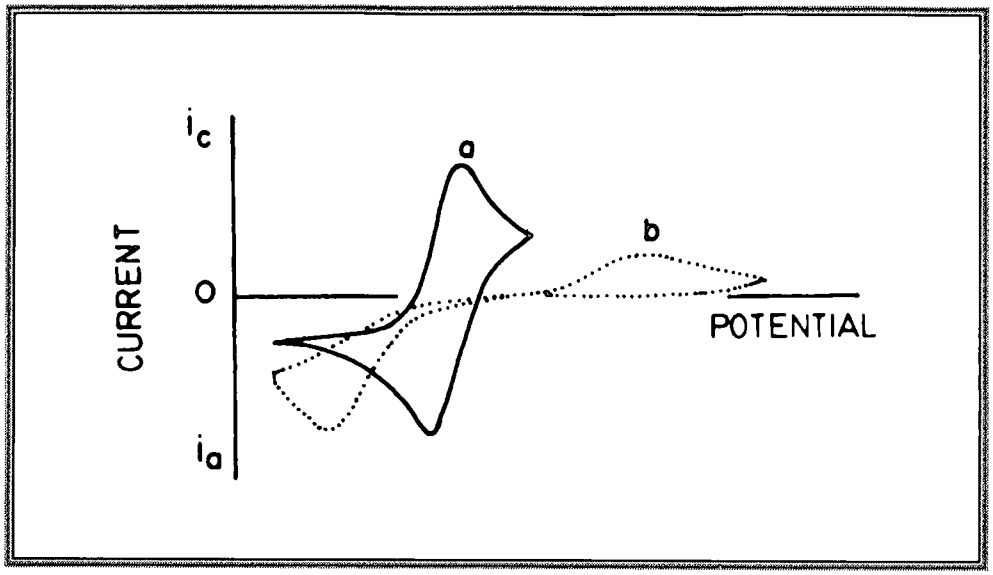

Figure 5.4: Cyclic Voltammogram exhibiting electrochemical reversibility (a) and irreversibility (b).

In the case of an irreversible system, the peak current is described by:

$I_p = (2.99 \times 10^5)n(\alpha n_a)^{1/2}AD^{1/2}C\nu^{1/2}$

α = transfer coefficient

n_a = number of electrons in the rate-determining step of the electrode process

The peak potential is no longer independent of the scan rate. In general, irreversible behavior gives voltammograms that are more spread out and flatter. It is important to recognize that electrochemical irreversibility also influences the peak current ratio. The more irreversible a couple becomes, the smaller will be the I_p on the reverse scan. This is often due to the fact that significant product has diffused away from the surface by the time the reverse E_p is reached.

The simplest case of an irreversible system is that where only oxidation or reduction is possible , for example: $O + ne^- \rightarrow R$ where R cannot be re-oxidised to O or to anything else (Figure 5.5).

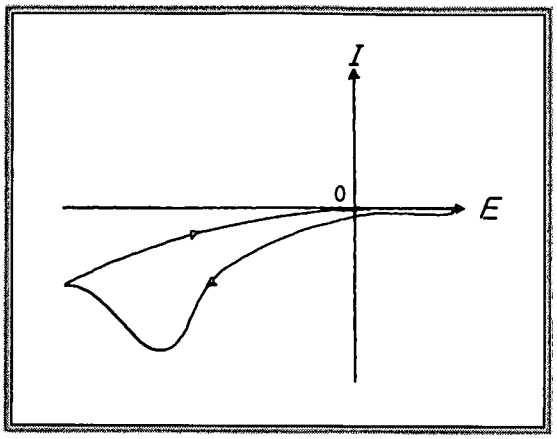

Figure 5.5: Schematic of the CV expected from an irreversible process of the form $O + ne^- \rightarrow R$.

Zone boundaries for reversible, quasi-reversible and irreversible systems were suggested by Matsuda and Ayabe[6]:

Reversible (Nernstian):	$k^\circ = 0.3\nu^{1/2}$ cm.s^{-1}
Quasi-reversible:	$k^\circ \geq 2 \times 10^{-5}\nu^{1/2}$ cm.s^{-1}
Irreversible:	$k^\circ \leq 2 \times 10^{-5}\nu^{1/2}$ cm.s^{-1}

k° = standard (intrinsic) heterogeneous rate constant

A system that appears reversible at one scan rate can "become irreversible" at faster scan rates. This illustrates the somewhat arbitrary nature of reversibility. In a reversible system, ΔE_p should be independent of the scan rate. However, due to the presence of a finite solution resistance between the reference and the working electrode, ΔE_p increases. This solution resistance couples with the cell current to produce an IR potential drop that keeps the working electrode from being at the programmed potential. Thus, if the resistance of the solution is large enough so that $I_{p,a}R$ and $I_{p,c}R$ are appreciable with respect to the accuracy of the potential measurements, then the true potential, E_{true}, of the working electrode will differ from that dictated by the potentiostat, $E_{applied}$. Instead, the potential will be greater or less than $E_{applied}$ by the IR drop. Since the peak current is proportional to $\nu^{1/2}$, this IR drop increases with scan rate and the peak potential moves apart. Scan rates faster than 100 V.s^{-1} are therefore rarely practical, because of the IR drop and charging current.

[6] Matsuda H., Ayabe Y., *Z. Electrochem.*, **59**, 494, (1955)

For any given potential, $(\delta C/\delta x)_{x=0}$ is larger for the faster scans. Consequently, the current is greater. In the faster scans less time is available for consequent depletion of the adjacent solution, resulting in steeper profiles.

5.4 Mechanisms of electrogenerated complexes

The ratio of the peak current can be significantly influenced by chemical reactions coupled to the electrode process. One of the most intriguing aspects of electrochemistry involves the homogeneous chemical reactions that often accompany heterogeneous electron transfer processes occuring at the electrode-solution interface. If one assumes that the electrochemical process involves an initial electron transfer to or from a neutral starting material, it can be anticipated that a high reactivity of the resulting charged complex to either electrophiles or nucleophiles, respectively, will occur. One of the questions to be answered for each chemical system is whether such an attack will occur at the metal or the ligand and what the consequences of each might be.

Cases where the product of the electrode reaction is lost via chemical reactions are particularly easy to identify by means of CV. The return peak will be reduced in magnitude if some chemical reaction occurs and it will be completely absent if the reaction half-life is much less than the scan duration[7].

Any step in the electrochemical mechanism must be either chemical (C) or electrochemical (E) in nature. The simplest mechanism conceivable would consist of two processes, one chemical and the other electrochemical, denoted CE or EC. An example of a CE process would be the reduction of a weak acid, such as acetic acid:

$CH_3COOH \rightleftharpoons CH_3COO^- + H^+$ C

$H^+ + e^- \rightarrow \frac{1}{2} H_2$ E

[7] Evans D.H., O'Connell K.M., Peterson R.A., Kelly M.J., *J. Chem. Ed.*, **60(4)**, 290, (1983)

An example of the EC mechanism is the oxidation of ascorbic acid[8]:

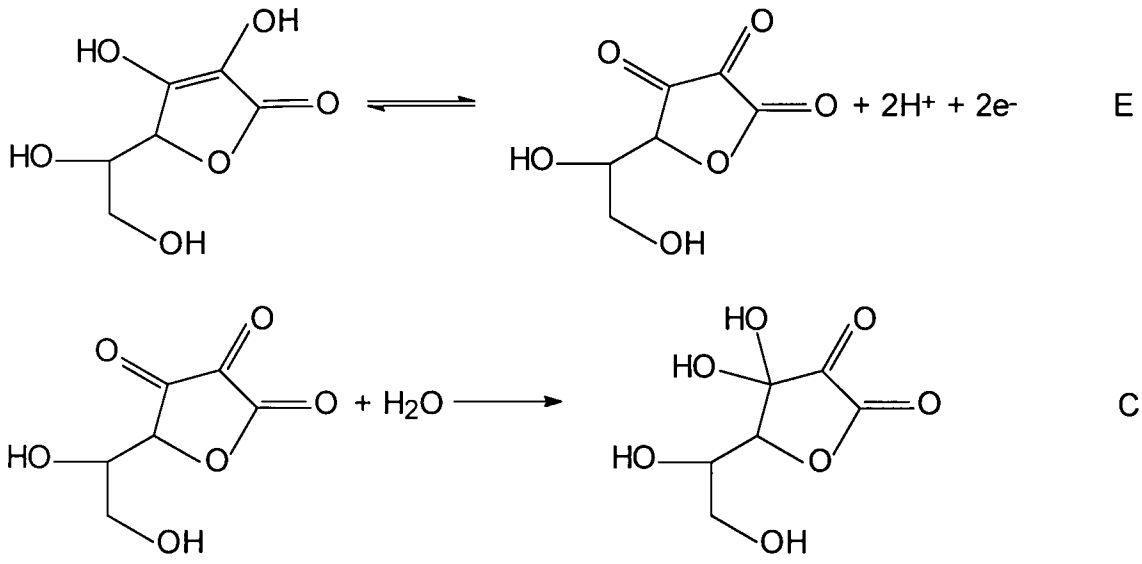

A more complicated mechanism involving regeneration of starting material is the ECC or half-regeneration mechanism:

$R \rightleftharpoons O + ne^-$ E

$O + Z \rightarrow OZ$ C

$OZ + O \rightarrow OZ^+ + R$ C

Z = some other solution component

The oxidation of 9,10-diphenylanthracene (DPA) in acetonitrile in the presence of nucleophiles such as water and pyridine (py) has been shown to follow this mechanism[9].

The ECE mechanism involves electrochemical generation of a species that then reacts with some other component in solution. The product of this reaction is more easily oxidised/reduced than the starting material and so is immediately electrolysed:

$R \rightleftharpoons O + ne^-$ E

$O + Z \rightarrow OZ$ C

$OZ \rightarrow OZ^+ + ne^-$ E

Z = some other solution component

This mechanism is encountered in the oxidation of organic compounds in the presence of a nucleophile.

---

[8] Perone S.P., Kretlow W.J., *Anal. Chem.*, **38**, 1760, (1966)
[9] Evans J.F., Blount H.N., *J. Am. Chem. Soc.*, **100**, 4191, (1978)

For the uncomplicated reduction of a metal complex, the cathodic current function ($I_{p,c}/\nu^{1/2}$) is independent of the scan rate and the ratio of $I_{p,a}/I_{p,c}$ is unity. For an EC mechanism, the current function is still practically independent of the scan rate, but $I_{p,a}/I_{p,c}$ is less than unity. For an ECE mechanism in which the second reduction occurs at a potential more positive than the first, the current function will be greater than the E or EC mechanistic case and $I_{p,a}/I_{p,c}$ will be less than unity[10].

Spectroscopic techniques (UV/Visible, IR and NMR) have been effectively coupled with electrochemistry to enable monitoring of homogeneous chemical reactions and to provide information on the identity of the species present.

5.5 Bulk Electrolysis

There are circumstances where it is desirable to alter the composition of the bulk solution appreciably by electrolysis. These include analytical measurement techniques for removal or separation of solution components and electrosynthetic methods. These bulk electrolytic methods are characterised by large *A/V* conditions and as effective mass transfer conditions as possible. Although bulk electrolytic methods are generally characterised by large currents and time scales for experiments of the order of minutes or hours, the basic principles governing electrode reactions, as decribed, still apply. Since the potential of the working electrode is the basic variable that controls the degree of completion of an electrolytic process in most cases, controlled potential techniques are usually the most desirable for bulk electrolysis.

Placement of the auxiliary electrode to provide a fairly uniform current distribution across the surface of the working electrode is usually desirable and the auxiliary electrode is usually placed in a separate compartment isolated from the working electrode.

In coulometric methods the total quantity of electricity required to carry out an exhaustive electrolysis is determined. The quantity of material or number of

[10] Kissinger P.T., Heineman W.R., *Laboratory Techniques in Electroanalytical Chemistry*, Chapter 18, BAS Press, (1984)

electrons involved in the electrode reaction can then be determined by Faraday's laws, if the reaction occurs with 100% current efficiency.

5.5.1 Coulometric Measurements

In controlled potential coulometry the total number of coulombs consumed in an electrolysis is used to determine the amount of substance electrolysed. To enable a coulometric method, the electrode reaction must satisfy the following requirements:

(i) It must be of known stoichiometry.

(ii) It must be a single reaction or at least have no side reactions of different stoichiometry.

(iii) It must occur with close to 100% current efficiency.

The current is monitored during the electrolysis, so that the background current can be determined and the completion of electrolysis observed. The shape of the I/t curve can be diagnostic of the mechanism of the electrode reaction and instrumental errors. If the final current following electrolysis is constant , but appreciably higher than the pre-electrolysis background current of the supporting electrode solution alone, a reaction of the electrolysis product may be regenerating starting material or another electroactive substance. This symptom can also indicate leakage of material from the auxiliary electrode compartment. If the current at the start of the electrolysis remains constant for some time before showing the usual exponential decay, the output current or voltage of the potentiostat is probably insufficient for the electrolysis conditions to maintain the working electrode at the potential chosen.

The total quantity of electricity Q(t) (Coulombs) consumed in the electrolysis is given by the area under the I/t curve (Figure 5.6).

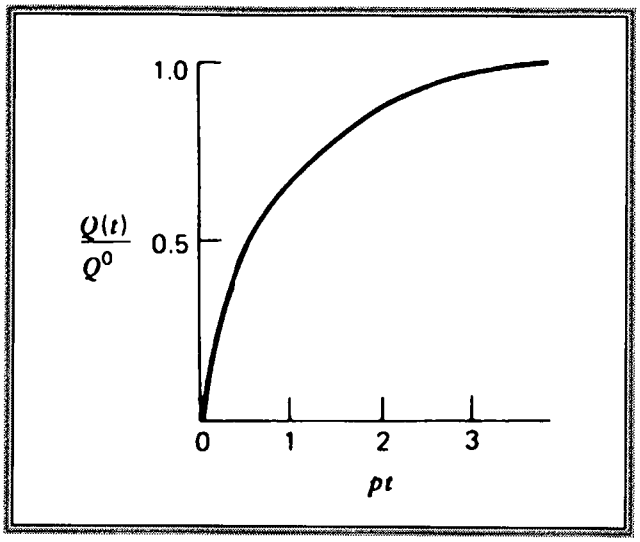

Figure 5.6: Coulombs versus time curve during controlled potential electrolysis.

$$Q(t) = \int_0^t I(t)\partial t \qquad ④$$

Q° is the value of Q at the completion of the electrolysis ($t \rightarrow \infty$) and is given as: $Q^\circ = nFN_o = nFVC_o^*$ ⑤

N_o represents the total number of moles of O initially present.

Controlled potential coulometry is also a very useful method for studying the mechanism of electrode reactions and for determining the *n* value for an electrode reaction without prior knowledge of electrode area or diffusion coefficient. (In voltammetric methods, if *n* is to be determined from the limiting current, the electrode area and diffusion coefficient must be known.) To determine *n* from potential measurements, knowledge about the reversibility of the reaction is required. However, because the time scale of coulometric measurements (~10 – 60 min) is at least one or two orders of magnitude longer than that of voltammetric methods, perturbing homogeneous chemical reactions following the electron transfer, which might not affect the voltammetric measurement, may be important. For example:

$O \rightleftharpoons R + ne^-$

$R \rightarrow A$ (slow, $t_{1/2} \sim 2 - 5$ min)

$A + ne^- \rightarrow B$ (A reduced at less negative potentials than O).

CHAPTER 6:
ELECTROCHEMICAL MECHANISTIC STUDIES

6.1 Introduction

The obvious way to study the influence of ligand sets in redox properties is by electrochemistry[1]. An increasing number of inorganic chemists have been using CV to evaluate the effect of ligands on the oxidation/reduction potentials of the central metal ion in complexes and multinuclear clusters.

When investigating a chemical system for a finite time with CV, there are several experimental considerations that need to be established. Among these are choosing the appropriate electrodes, solvent and supporting electrolyte and also determining whether O_2 and/or H_2O are interfering.

6.2 Solvents in Electrochemistry

All electrochemical phenomena occur in a medium, which generally consists of a solvent containing a supporting electrolyte. There is no universal solvent. Consideration must be given as to how the chemical and electrochemical properties of the electrode reaction in question may be affected by the solvent system.

The major requirement of the solvent is that the species under investigation must be soluble and stable in it[2]. The material under investigation must be soluble[3] to the extent of at least 1×10^{-4} mol.dm^{-3} and the concentration of the electrolyte must be at least 0.05 mol.dm^{-3}. The ideal electrochemical solvent properties are[4]:

- Electrochemical inertness
- Electrical conductivity
- Good solvent power
- Chemical inertness
- Convenient potential window

---

[1] Moock K.H., Macgregor S.A., Heath G.A., Derrick S., Boeré R.T., *J.Chem. Soc.*, **Dalton Trans.**, 2067, (1996)
[2] Van Benschoten J.J., Lewis J.Y., Heineman W.R., Roston D.A., Kissinger P.T., *J. Chem. Ed.*, **60(9)**, 772, (1983)
[3] Sawyer D.T., Roberts J.L., *Experimental Electrochemistry for Chemists*, Chapter 4, Wiley, New York, (1974)
[4] Kissinger P.T., Heineman W.R., *Laboratory Techniques in Electroanalytical Chemistry*, Chapter 13, Dekker, New York, (1984)

The solvent system should not undergo any electrochemical reaction over a range of potentials from very positive (strongly oxidising) to very negative (strongly reducing). A solution of tetrabutylammonium hexafluorophosphate, TBAHFP, in acetonitrile, CH_3CN, exhibits a very wide accessible potential range with positive and negative decomposition potentials, 3.4V and –2.9V *versus* SCE respectively[4]. The potential window is often limited[2] at the negative end by the reduction of H_2O to H_2 and also the reduction of O_2 to H_2O_2 and H_2O, and at the positive end by the oxidation of H_2O to O_2. The potential window is also influenced by the choice of working electrode, solvent and supporting electrolyte.

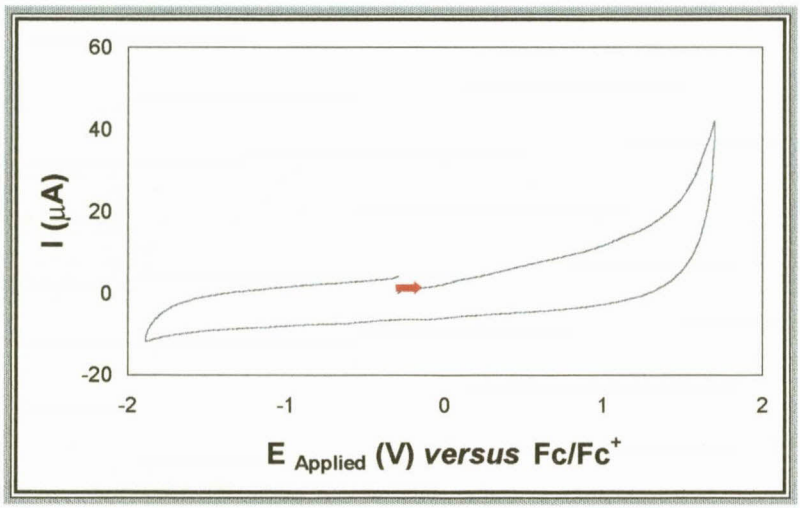

Figure 6.1: *CV of 0.1 mol.dm^{-3} TBAHFP on a Glassy Carbon working electrode in CH_3CN to define the potential window. The scan rate was equal to 0.1 V.s^{-1}.*

In order to support passage of an electrical current, the solvent system should have low electrical resistance and hence a moderately high dielectric constant ($\geq$ 10) since the prevalence of ion pairing and even multiple ionic association in less polar solvents results in low ionic mobility and conductivity in such solutions. Uncompensated IR errors can become troublesome in high resistance solvents.

The solvents most often used are the dipolar aprotic solvents. These solvents have large dielectric constants and low proton availability. CH_3CN is commonly used in anodic studies but is moderately nucleophilic. CH_3CN has a dielectric constant of 37

and is an excellent solvent for polar organic compounds and inorganic salts and is stable after purification.

6.2.1 Acetonitrile as solvent

The electrochemical studies reported here were performed with CH_3CN as solvent. CH_3CN can contain water, ammonia, methylamine, ethylamine, acetone and many more impurities. CH_3CN was therefore distilled from P_2O_5 and NaH and the resulting solvent was passed through a column of Al_2O_3, and stored under argon[5].

6.3 Supporting electrolytes in non-aqueous solvents

A supporting electrolyte is used to increase conductivity in the majority of electroanalytical or electrosynthetic experiments in non-aqueous solutions, which influences mass transfer. The provision of a conducting medium will minimise IR drop. Most of the current will be carried by ions of the supporting electrolyte. Diffusion of an electro-active species will also be affected by the viscosity of the medium and by the size of the solvating sphere.

TBAHFP, used as supporting electrolyte is readily obtained in pure form and is highly soluble in CH_3CN. The Cyclic Voltammogram of TBAHFP (Figure 6.1) shows electrochemical inertness from –1.8V to 1.8V

6.3.1 Preparation of electrode solution

The solvent-supporting electrolyte was prepared from electrochemically pure TBAHFP. TBAHFP (0.97g, 0.1 mol.dm^{-3}) was placed in a 25ml dry, argon filled volumetric flask before pure dry CH_3CN was added[5].

6.4 Electrodes for Cyclic Voltammetry

The potential of a working electrode must be measured with respect to some reference electrode whose potential is stable and reproducible. This measurement will include at least two single potentials.

---

[5] Dümmling S., Eichhorn E., Schneider S., *BAS Current Separations*, **15(2)**, 53, (1996)

The two electrode configuration is a system in which the cell current passes through both the working and the reference electrode. To avoid errors, the cell current and internal cell resistance must be kept as small as possible, and the reference electrode must be designed to have low internal resistance and a metal/solution interface of sufficient area to minimise internal polarisation.

The requirement for a counter electrode is that its interfacial potential remains constant so that any change in the cell potential produces identical changes in the working electrode's interfacial potential.

An electrode with a potential that does not vary with the current is referred to an ideal non-polarisable electrode[6] and is characterised by a vertical region on a current *versus* potential plot (Figure 6.2).

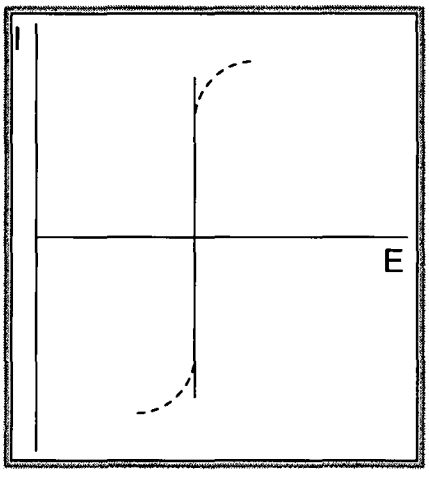

Figure 6.2: *Current/potential curves for an ideal non-polarisable electrode. Dashed lines show the behaviour of electrodes that approach the ideal.*

There is no electrode that behaves in this way, although some approach ideal non-polarisable behaviour at low currents. Consequently, the interfacial potential of the counter electrode in the two electrode configuration varies as the current is passed through the cell. This problem is overcome by using a three electrode configuration, in which the function of the counter electrode is divided between the reference and working electrodes. The cell current flows between the working electrode and the

[6] Bott A.W., *BAS Current Separations*, **14(2)**, 64, (1995)

counter or auxiliary electrode, while the potential of the working electrode is measured with respect to the reference electrode. This avoids internal polarisation of the reference electrode and compensates for the major portion of the IR drop in the cell.

Since the current that passes through the reference electrode in the three electrode configuration is many orders of magnitude lower than in the two electrode configuration, the requirements for the reference electrode are less demanding and hence smaller, more polarisable electrodes can be used.

6.5 Cell assembly

The CV experiments were performed in a three electrode cell equipped with a Glassy Carbon working electrode tip (BAS, electro-active area, A = 0.08cm^2), a Pt-wire counter electrode and an Ag/Ag^+ reference electrode (0.01mol.dm^{-3} $AgNO_3$ in CH_3CN/0.1mol.dm^{-3} TBAHFP solvent-supporting electrolyte) connected to the cell (Figure 6.3).

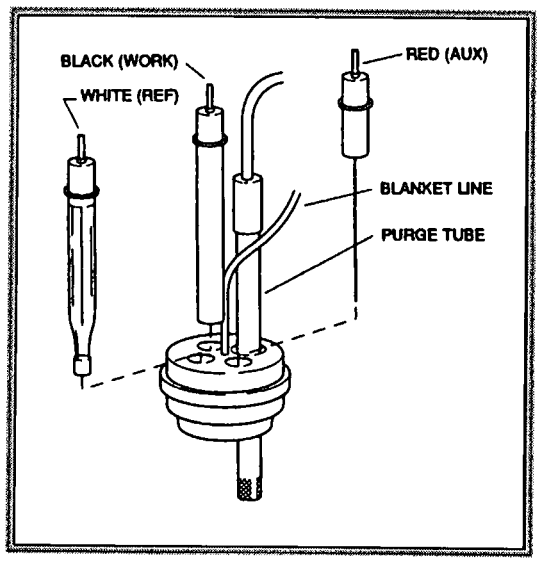

Figure 6.3: BAS electrode lead connections for a three electrode cell configuration.

The glass cell was rinsed with acetone, methanol and acetonitrile, evacuated and filled with argon. It was equipped with the Pt-wire counter electrode, which was cleaned by means of flaming to get rid of all impurities, and rinsed thereafter with acetone, methanol and acetonitrile. The Glassy Carbon working electrode was

polished on a 3-Micron Alumina sheet, cleaned in an ultrasonic bath and rinsed with acetonitrile. The Ag-wire was polished with steel wool, rinsed with acetonitrile and inserted into a $0.01mol.dm^{-3}$ $AgNO_3$, $0.1mol.dm^{-3}$ TBAHFP Ag-solvent-supporting electrolyte solution. The Ag/Ag^+ reference electrode was immerged directly, without a salt bridge, in the glass cell after the analyte solution ($2x10^{-3}$ Rh(I) complex/TBAHFP solvent-supporting electrolyte solution) was added.

The three electrode cell configuration was placed in a Faraday cage connected to a BAS CV-27 cyclic voltammograph[7], which was interfaced with an ADALAB-PC AD/DA converter, and ADALAB controlled software[8]. A locally designed software package, VOLTAMMETRY[9], was used to generate the potential sweep and to record the current signal. The software package HYPERPLOT[10] was used for the processing of all data according to the European sign convention. All the experiments reported here were studied at 25,0(2)°C.

All potentials are referred to an external Fc/Fc^+ standard (Figure 6.4) in the above mentioned solvent-supporting electrolyte[5]. The redox potential, $E°_{Fc/Fc^+}$, was determined against the Ag/Ag^+ reference electrode ($0.01mol.dm^{-3}$ $AgNO_3$ in $CH_3CN/0.1mol.dm^{-3}$ TBAHFP solvent-supporting electrolyte) on a Glassy Carbon electrode (Table 6.1). It is clear (Table 6.1) why it was decided to quote potentials *versus* Fc/Fc^+ as external standard. Although small, there is a change in oxidation and reduction potentials of Fc in the presence of the Rh(I) complexes.

	pKa	V_{ox} (V) *versus* Ag/Ag^+	V_{red} (V) *versus* Ag/Ag^+	$E°$ (V) *versus* Ag/Ag^+	ΔE_p (V) *versus* Ag/Ag^+	I_{pa}/I_{pc}
Fc (external)		0.128	0.05	0.089	0.078	1.05
Fc (internal) in Rh(dbm)(CO)(PPh_3)	9.35	0.139	0.046	0.093	0.093	
Fc (internal) in Rh(ba)(CO)(PPh_3)	8.7	0.144	0.041	0.093	0.103	
Fc (internal) in Rh(btfa)(CO)(PPh_3)	6.3	0.124	0.042	0.083	0.082	
Fc (internal) in Rh(tfaa)(CO)(PPh_3)	6.3	0.132	0.032	0.082	0.100	

Table 6.1: Oxidation and reduction potentials of Fc/Fc^+ as an internal and external standard.

[7] *BAS CV-27 Voltammograph Instruction Manual*, Bioanalytical Systems Inc., West Lafayette, Indiana, (1984)
[8] *ADALAB-PC and ADAPT Systems*, Interactive Microware Inc., State College, Pennsylvania, (1990)
[9] Erasmus J.J.C., *VOLTAMMETRY Instruction Manual*, University of the Orange Free State, (1993)
[10] *HYPERPLOT/ADALAB-PC User's Guide Version 2.0*, J.H.M. International Inc., Columbus. Ohio, (1989)

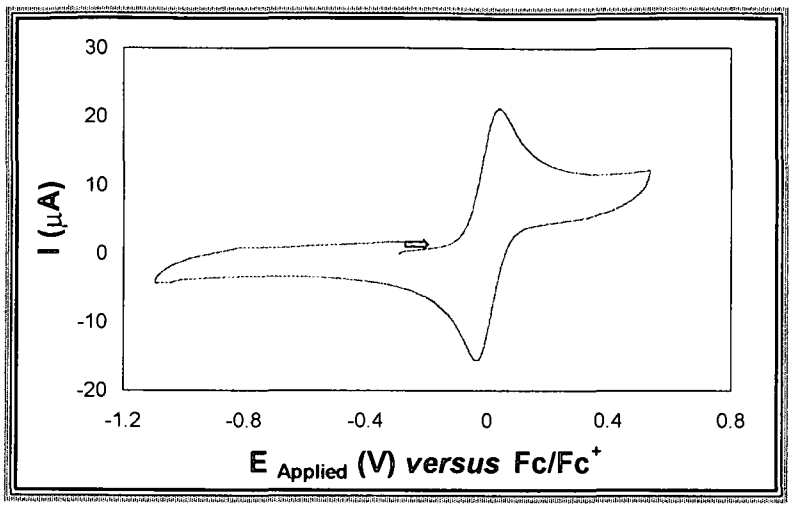

Figure 6.4: *CV of 1 x 10^{-3} mol.dm^{-3} Fc, on a Glassy Carbon working electrode in 0.1 mol.dm^{-3} TBAHFP/CH_3CN solvent-supporting electrolyte. The scan rate was equal to 0.1 V.s^{-1}.*

6.6 The dependence of the oxidation potential on the nucleophilicity of the Rhodium(I) metal centre

A CV with a large potential window was drawn to establish the oxidation and reduction potential of the analyte solution (2 x 10^{-3} Rh(I) complex/TBAHFP solvent-supporting electrolyte solution) (Figure 6.5).

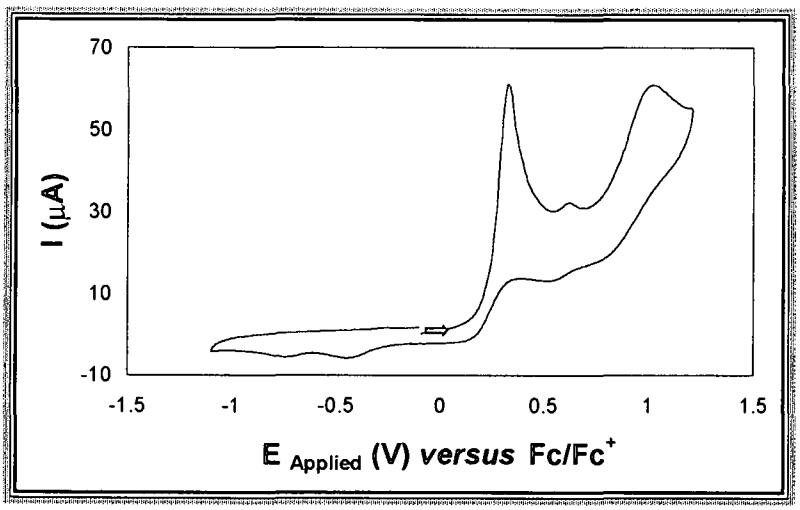

Figure 6.5: *A wide potential window CV of Rh(dbm)(CO)(PPh_3) on a Glassy Carbon working electrode in 0.1 mol.dm^{-3} TBAHFP/CH_3CN solvent-supporting electrolyte. The scan rate was equal to 0.1 V.s^{-1}.*

The oxidation peak at ~1V represents the oxidation of H_2O (Figure 6.5). The sharp oxidation potential peak between 0.3V and 0.5V obtained for the various Rh(β-diketonato)(CO)(PPh_3) complexes belong to that of the Rh(I).

Rh(I)(β-diketonato)(CO)(PPh_3) → Rh(III)(β-diketonato)(CO)(PPh_3) + $2e^-$ ①

CV's of the four Rh(β-diketonato)(CO)(PPh_3) complexes (Figure 6.6) indicated a definite relationship between the oxidation potentials of the various Rh(I) metal centres and the pKa values of the β-diketones (Table 6.2).

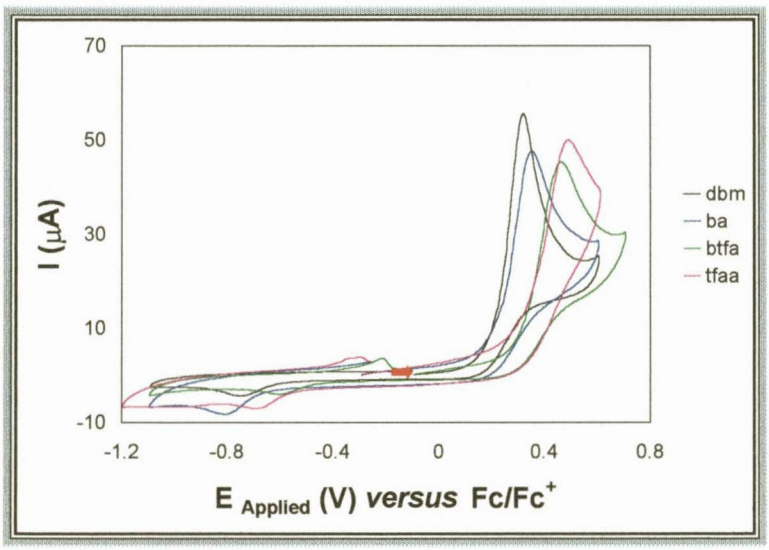

Figure 6.6: *CV's of the Rh(β-diketonato)(CO)(PPh_3) complexes on a Glassy Carbon working electrode in 0.1 mol.dm^{-3} TBAHFP/CH_3CN solvent-supporting electrolyte. The scan rate was equal to 0.1 V.s^{-1}.*

β-Diketone	pKa	V_p^{ox} (V) *versus* Fc/Fc^+	V_p^{red} (V) *versus* Fc/Fc^+
dbm	9.4	0.308	-0.76
ba	8.7	0.336	-0.80
btfa	6.3	0.448	-0.64
tfaa	6.3	0.491	-0.66

Table 6.2: *Oxidation and reduction potentials of the various Rh(β-diketonato)(CO)(PPh_3) complexes.*

The higher the pKa values of the β-diketones used and therefore the more nucleophilic the Rh(I) metal centre, the lower the oxidation potential (Figure 6.7) and

higher the reduction potential, implying that it is easier to oxidise the Rh(I) metal centre to Rh(III), but also more difficult to reduce it back. The variation of the sharp oxidation potential peak between 0.3V and 0.5V when the pKa values were varied is an indication that this peak is indeed the oxidation potential of the Rh(I) metal centre. ΔE_p (V) *versus* Fc/Fc^+ is larger than 1V, indicating a definite irreversible system. The formal redox potential could therefore not be obtained (Section 5.2.2) and hence only the half-cell potentials are given.

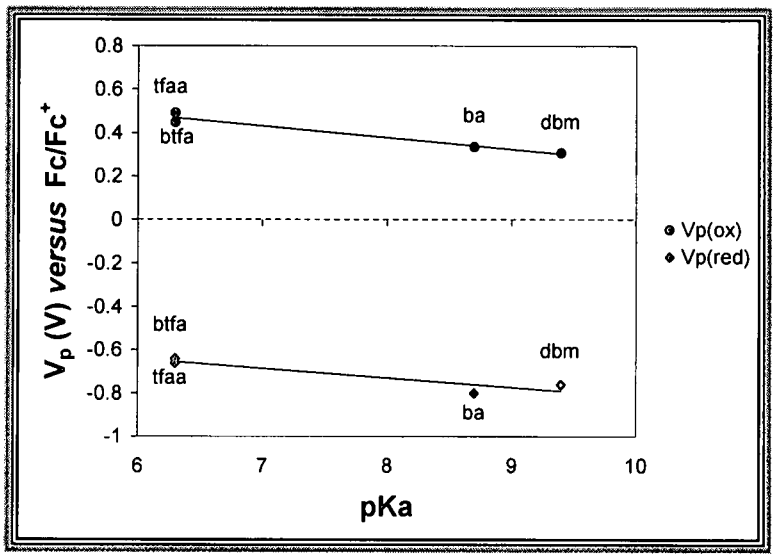

Figure 6.7: Relationship between the oxidation and reduction potentials of the various Rh(β-diketonato)(CO)(PPh_3) complexes and the pKa values of the respective β-diketones.

6.7 Effect of scan rate and scan direction

6.7.1 Cathodic scans

No reduction peak was observed during negative scans starting with the same potential ($E_{Initial}$ = -0.2V) (Figure 6.8).

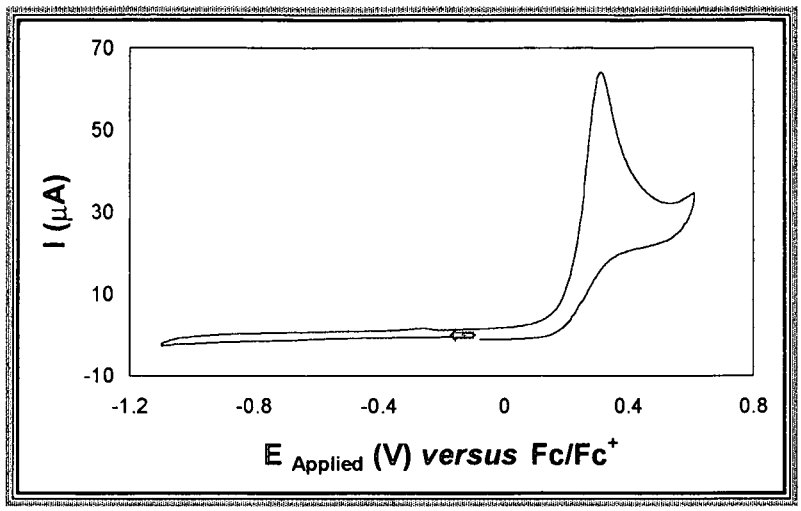

Figure 6.8: *Negative scan CV's of the Rh(dbm)(CO)(PPh_3) on a Glassy Carbon working electrode in 0.1 mol.dm^{-3} TBAHFP/CH_3CN solvent-supporting electrolyte. The scan rate was equal to 0.1 V.s^{-1}.*

There is no Rh(III) present in the analyte solution (2 x 10^{-3} Rh(I) complex/TBAHFP solvent-supporting electrolyte solution) and it can only be generated electrochemically by the oxidation of the Rh(I). During the negative scan there was no Rh(III) present in the analyte solution to be reduced back to Rh(I), but there was Rh(I) in the analyte solution to be oxidised. The small reduction peak obtained from positive scans (Figure 6.6) is therefore definitely coupled to the sharp oxidation peak between 0.3V and 0.5V.

No reduction peaks were observed with scan rates ≤ 0.05V. The reason was that chemical decomposition back to Rh(I) occurred before the Rh(III) could be electrochemically reduced back to Rh(I)

6.7.2 Successive scans

There are some systems in which a coupled chemical reaction yields electro-active by-products. In these cases multiple scans can be beneficial. Successive CV scans of the four Rh(β-diketonato)(CO)(PPh_3) complexes showed that the Glassy Carbon electrode is not poisoned by repeatedly scans and also that no by-products formed after the first CV scan (Figure 6.9).

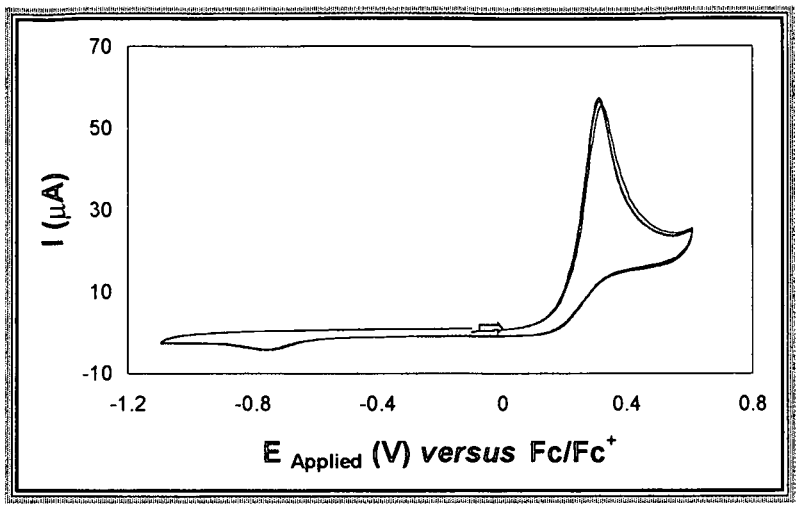

Figure 6.9: *Successive scans CV's of the Rh(dbm)(CO)(PPh_3) on a Glassy Carbon working electrode in 0.1 mol.dm^{-3} TBAHFP/CH_3CN solvent-supporting electrolyte. The scan rate was equal to 0.1 V.s^{-1}.*

6.7.3 Peak currents and Coupled Chemical reactions

The height of the current peaks can be used to determine the concentration in the bulk solution. The real forte of analysing the peak currents is the establishment of any homogeneous chemical reactions that are coupled to the electron transfer process. Diagnosis of coupled chemical reactions is often based on relative heights of the anodic and cathodic peaks.[11] The ratio of the anodic and cathodic peak currents can be used to obtain an estimate of the reaction rate, k, for the chemical step. It can be dangerous to infer quantitative information from the I_p ratio for extremely irreversible couples, because of the product diffusion away from the Glassy Carbon working electrode surface (Section 5.3).

The effect of a chemical reaction will depend on the scan rate. For example: If a very rapid chemical reaction is involved and the scan rate is slow, the CV will reflect the characteristic of the chemical step entirely. If the scan rate is rapid compared to the reaction rate, the CV will be identical to that corresponding to uncomplicated charge transfer.

[11] Mabbott G.A., *J. Chem. Ed.*, **60(9)**, 697, (1983)

An increase in the scan rates led to an increase in the cathodic peak current (Figure 6.10). By increasing the scan rate, the diffusion rate of the Rh(III) away from the working electrode surface is reached, causing more Rh(III) to be reduced back to Rh(I). Another explanation for the increase in the cathodic peak current is that the rapid scan rates forestall the decomposition of the unstable Rh(III) formed, which also causes more Rh(III) to be reduced back to Rh(I). At $0.05 V.s^{-1}$ the system behaved totally irreversibly and no reduction peak was observed.

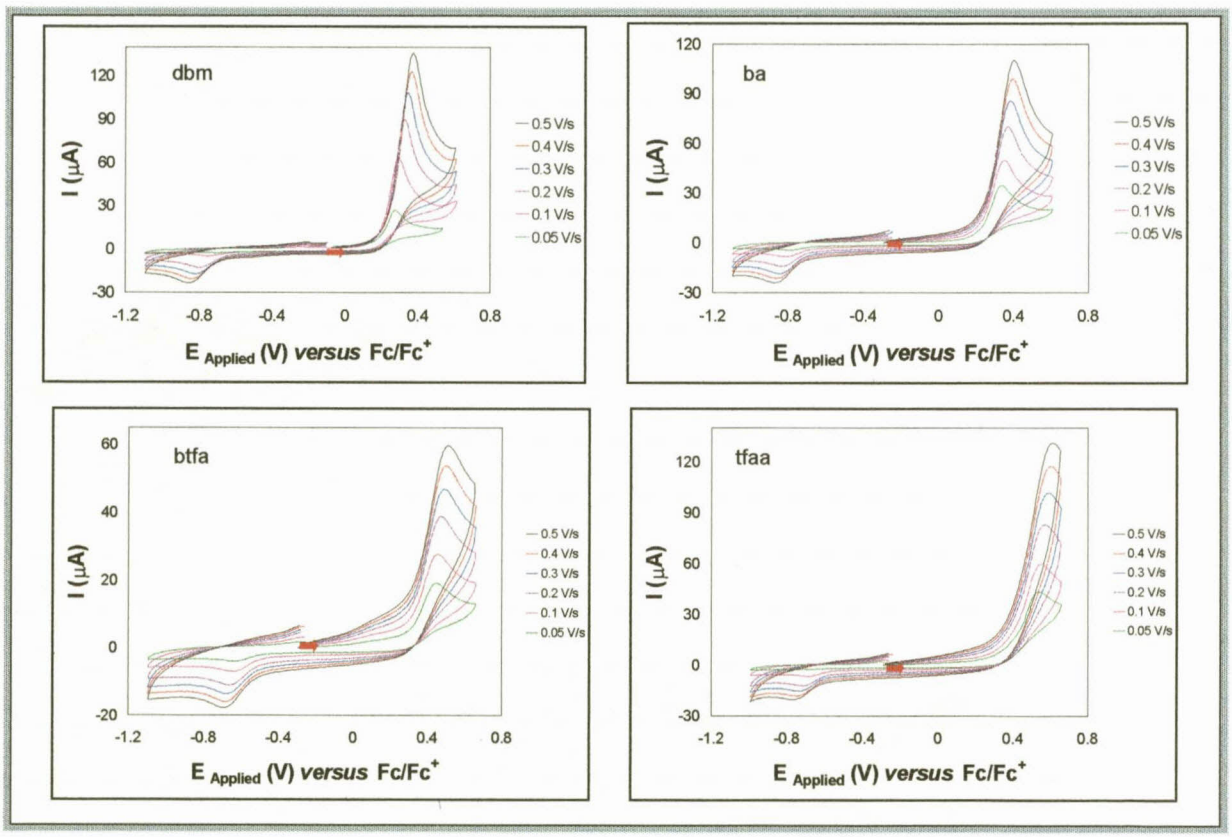

Figure 6.10: CV's of the Rh(β-diketonato)(CO)(PPh_3) complexes on a Glassy Carbon working electrode in 0.1 mol.dm^{-3} TBAHFP/CH_3CN solvent-supporting electrolyte. The scan rate was varied between 0.05 V.s^{-1} and 0.5 V.s^{-1}.

By plotting the quantity $\frac{I_p}{nFA\sqrt{Da}C_o^*}$, where $a = \frac{nF\nu}{RT}$ as a function of the voltage scan, the effect of the scan rate, ν, on the diffusion process can be separated from its effect on the kinetics[12]. For an uncomplicated charge

[12] Nicholson R.S., Shain I., *Anal. Chem.*, **36(4)**, 706, (1964)

transfer reaction, a horizontal straight line is obtained. The behaviour of any electrochemical system approaches a straight line when the rate of voltage scan is such that the chemical reaction cannot proceed significantly before the experiment is over. Experimentally, this correlation is easy to obtain (Table 6.3), since it is only necessary to plot $I_p/\nu^{1/2}$ against ν (Figure 6.11).

Scan Rate ν ($V.s^{-1}$)	V_{ox} *versus* Fc/Fc^+ (V)	I_{pa} (μA)	$I_p/\nu^{1/2}$	V_{red} *versus* Fc/Fc^+ (V)	I_{pc} (μA)
0.05	0.537	43.40	194.1	-	-
0.10	0.549	59.65	188.6	-0.68	-6.45
0.20	0.570	83.04	185.7	-0.72	-12.12
0.30	0.587	101.77	185.8	-0.74	-15.15
0.40	0.603	117.47	185.7	-0.75	-18.22
0.50	0.612	131.49	186.0	-0.77	-20.29

Table 6.3: Anodic and cathodic peak currents obtained from the CV of Rh(tfaa)(CO)(PPh_3) at various scan rates.

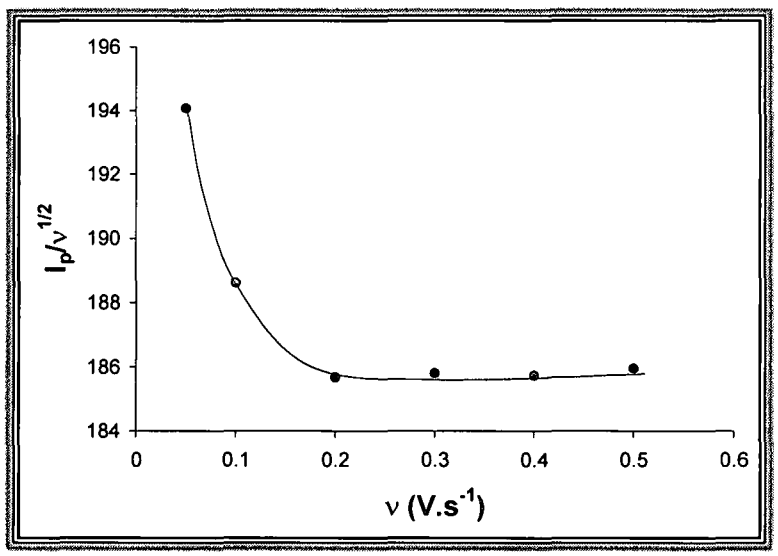

Figure 6.11: Plot of the anodic peak currents obtained during CV of Rh(tfaa)(CO)(PPh_3) against the scan rate.

The anodic peak current was directly proportional to $\nu^{1/2}$ (Section 5.3), but the cathodic peak current, although linear, was not directly proportional to $\nu^{1/2}$

(Figure 6.12). The above can only be attributed to the irreversibility of these systems and emphasises the danger of obtaining quantitative information from I_p ratios.

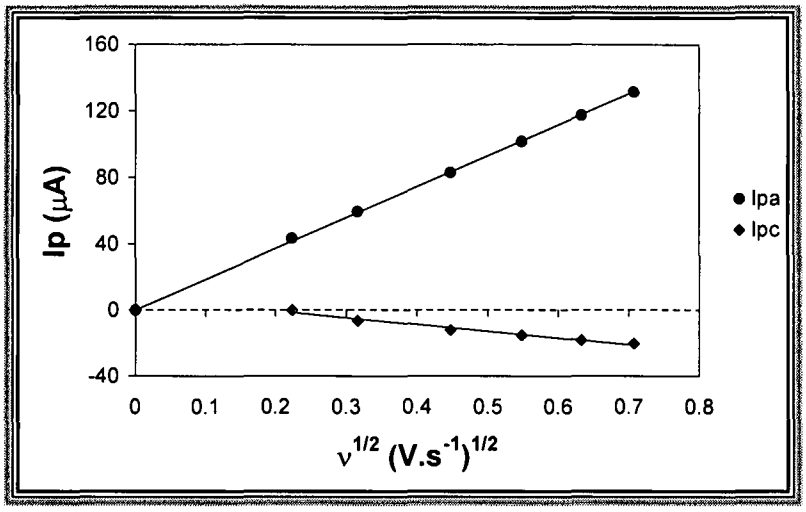

Figure 6.12: Plots of anodic and cathodic peak currents obtained from the CV of Rh(tfaa)(CO)(PPh_3) against the $\nu^{1/2}$. The Randles-Sevcik relationship for irreversible systems (Section 5.3).

6.7.4 The co-ordination of Chloride.

The effect of the co-ordination of a Cl^- ion, soluble in acetonitrile, during the electrochemical oxidation of the Rh(I)(β-diketonato)(CO)(PPh_3) complexes was investigated to prove the chemical coupling of solvents, or solvent co-ordination, during the oxidation of these Rh(I) complexes.

The Cl^- ion, Benzyltriethylammonium Chloride, $[B_ZN(Et)_3]^+Cl^-$, ($2x10^{-3}mol.dm^{-3}$) oxidises at 0.646V (Figure 6.13). The oxidation potentials of the Rh(I) complexes were between 0.3V and 0.5V (Table 6.2), preventing the Cl^- ion from being oxidised to Cl_2 before it could co-ordinate onto the Rh(I) complexes. Unfortunately the Br^- ion, tetraethylammonium bromide, oxidised at 0.311V and was therefore already oxidised to Br_2 before the Br^- ion could co-ordinate onto the Rh(I) complexes.

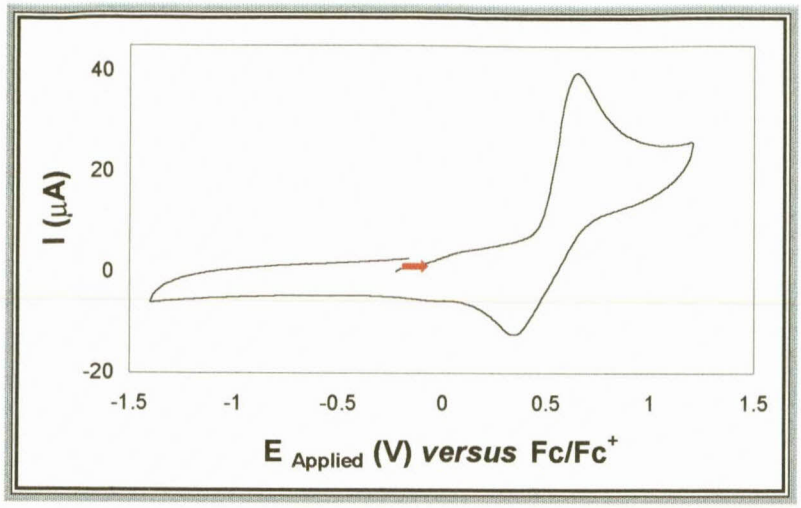

Figure 6.13: CV of $[B_ZN(Et)_3]^+Cl^-$ on a Glassy Carbon working electrode in 0.1 mol.dm^{-3} TBAHFP/CH_3CN solvent-supporting electrolyte. The scan rate was equal to 0.1 V.s^{-1}.

With the addition of $[B_ZN(Et)_3]^+Cl^-$ to the Rh(I)(β-diketonato)(CO)(PPh_3) complexes, the cathodic potential peak shifts, for example, from -0.735V to -0.947V in the case of Rh(I)(dbm)(CO)(PPh_3) (Figure 6.14). It becomes therefore more difficult to reduce the formed Rh(III) complex back to Rh(I). There is therefore a stronger co-ordination in the case of the Cl^- ion than in the case of the solvent, CH_3CN.

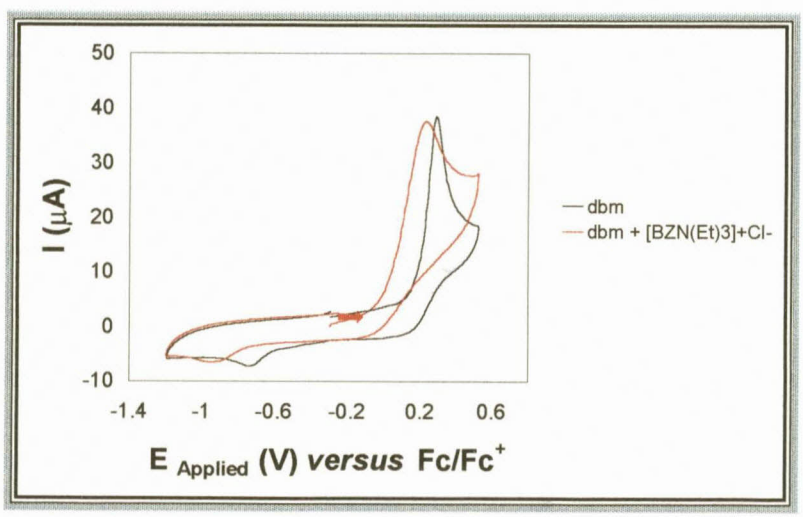

Figure 6.14: CV of Rh(dbm)(CO)(PPh_3) with the addition of $[B_ZN(Et)_3]^+Cl^-$ on a Glassy Carbon working electrode in 0.1 mol.dm^{-3} TBAHFP/CH_3CN solvent-supporting electrolyte. The scan rate was equal to 0.1 V.s^{-1}.

The oxidation potential remained constant, within the experimental error (Figure 6.14). It is therefore proved without any doubt that the sharp oxidation peaks between 0.3V and 0.5V is that of the Rh(I). These results lead to the question as to what the effect of co-ordination of different solvents with different donisity might be.

6.7.5 The effect of the solvent donisity

The effect of increasing solvent donisity on the reduction potential was studied in CH_3CN. It would have been ideal to study solvent donisity in dichloromethane due to its low donisity of 1.0, but unfortunately no reduction peak was observed in dichloromethane. Acetonitrile was therefore used as solvent to study the effect of the addition of higher donisity solvents.

Pyridine, methanol and dimethylformamide were added to the analyte solution in a mole ratio of 2:1 (5×10^{-3}) (Figure 6.15).

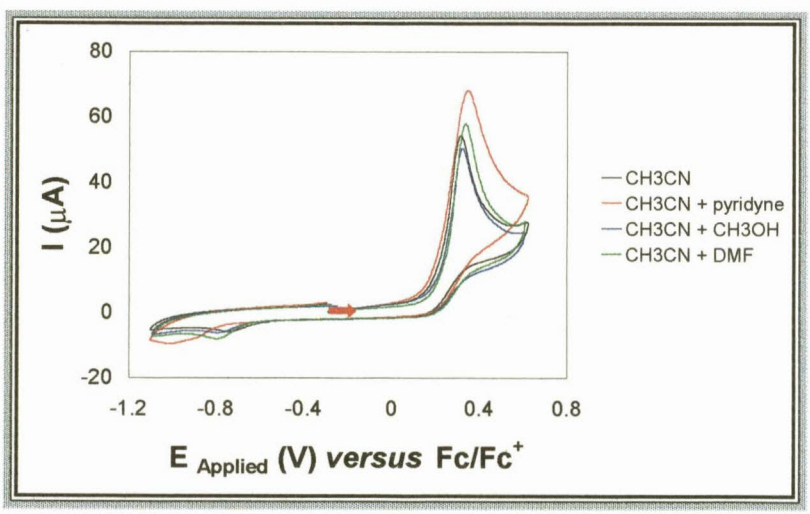

Figure 6.15: CV's of Rh(dbm)(CO)(PPh_3) with the addition of 5×10^{-3}ml pyridine, methanol and dimethylformamide in acetonitrile on a Glassy Carbon working electrode in 0.1 mol.dm^{-3} TBAHFP/CH_3CN solvent-supporting electrolyte. The scan rates were equal to 0.1 V.s^{-1}.

The larger the donisity (Table 6.4) of the added solvents, the more difficult was the reduction of the Rh(III) back to Rh(I) (Figure 6.16).

	DONISITY	V_p^{red} (V) vs, Fc/Fc^+
CH_3CN	14.1	-0.74
CH_3OH	19.0	-0.83
DMF	26.6	-0.84
PY	33.1	-1.02

Table 6.4: Reduction potentials obtained from the CV's of $Rh(dbm)(CO)(PPh_3)$ in CH_3CN with the addition of high donisity solvents.

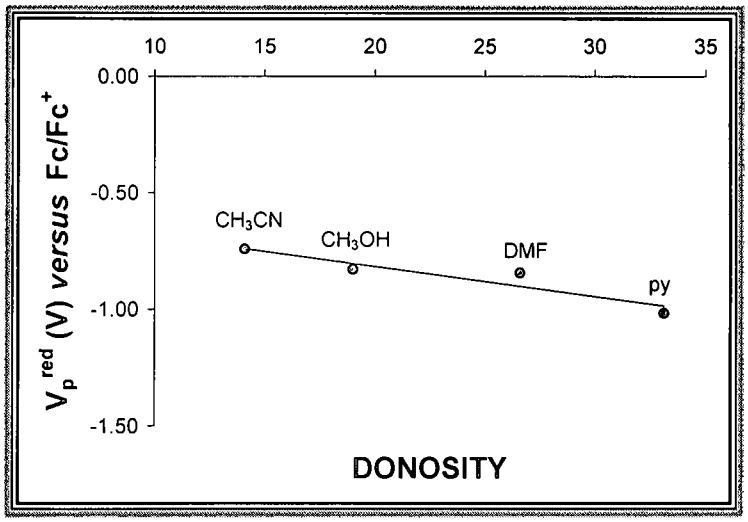

Figure 6.16: Linear relationship between the reduction potentials and solvent donisity.

6.8 Bulk Electrolysis

Peak current is proportional to the bulk concentration (Section 5.2.2). Quantitative information, although not accurate, can be gained from CV (Figure 6.17).

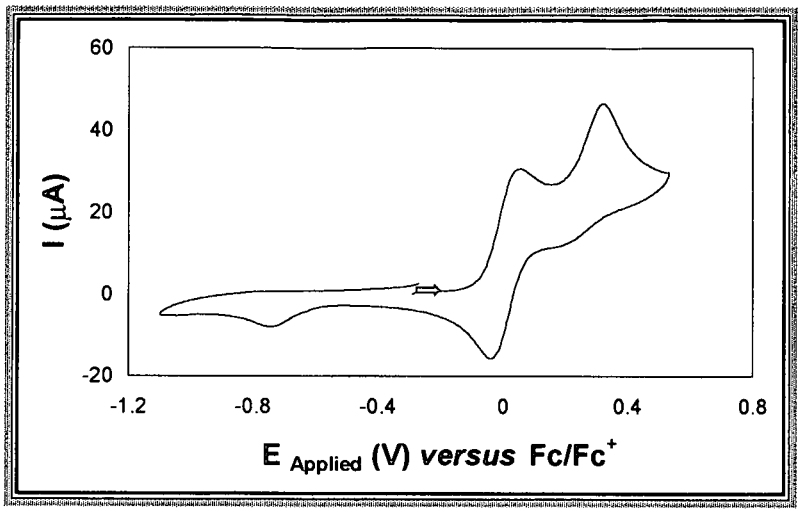

Figure 6.17: CV of 1 x 10^{-3} mol.dm^{-3} Rh(dbm)(CO)(PPh_3) together with the addition of 1x10^{-3} mol.dm^{-3} Fc in 0.1 mol.dm^{-3} TBAHFP/CH_3CN solvent-supporting electrolyte. The scan rates were equal to 0.1 V.s^{-1}.

It is known that the redox couple of Fc/Fc^+ involves $1e^-$ (Table 6.1) and if the oxidation peak current of Rh(I) to Rh(III) is twice as large as that of the Fc/Fc^+ couple, then it is certain that the sharp oxidation peak at ~0.3V is that of the Rh(I) to Rh(III).

Bulk electrolysis was carried out on a BAS CV-27 voltammograph[7]. The cell design for bulk electrolysis was the same as for the CV experiments. The only exception was the use of a much larger Glassy Carbon electrode (electro-active area, A = 3cm^2) and the use of a salt bridge (0.1mol.dm^{-3} TBAHFP solvent-supporting electrolyte in CH_3CN) for the Pt-wire counter electrode and Ag/Ag^+ reference electrode (0.01mol.dm^{-3} $AgNO_3$ in CH_3CN/0.1mol.dm^{-3} TBAHFP solvent-supporting electrolyte).

The oxidation peak current of the Rh(I) to Rh(III) reached a minimum at 0.62V (Figure 6.6) and the applied potential was therefore set at 0.62V. Considering the time factor and also the output gain (ampere *versus* volts) values of the apparatus, it was decided upon a total count of 0.9 coulombs to determine the amount of electron flow. 4.66 x 10^{-6} mole (0.0029g) Rh(dbm)(CO)(PPh_3) was added quantitatively into the cell before the cell design was completed. For the oxidation of 0.0029g Rh(I) to Rh(III), a two electron process, 0.9 coulombs should therefore be accounted for (Figure 6.18).

The total amount of $2e^-$ could not be reached during the bulk electrolysis. The only explanation for the failure of the experiment was the instability of the formed Rh(III) and it was therefore decided to stabilise the formation of the Rh(III) by means of the addition of $[BzN(Et)_3]^+Cl^-$ in a 1:2 mole ratio $Rh(dbm)(CO)(PPh_3)$:$[BzN(Et)_3]^+Cl^-$. The experiment was repeated and a total flow of 2 e^-'s was accounted for when the background current (Section 5.5.1) of 29μA was reached (Table 6.5 and Figure 6.18).

t (min)	Q (C)	I (μA)
1	0.027	370
2	0.048	346
5	0.116	347
10	0.222	325
15	0.32	317
20	0.408	288
25	0.483	252
30	0.555	233
35	0.618	201
40	0.673	165
45	0.721	147
50	0.763	129
55	0.799	111
60	0.829	90
65	0.854	78
70	0.875	62
75	0.89	47
80	0.907	42
85	0.919	39
90	0.931	35
95	0.942	31
100	0.952	31
105	0.962	29
120	0.989	30

Table 6.5: The total amount of coulombs calculated during bulk electrolysis of $Rh(dbm)(CO)(PPh_3)$ with the addition of $[BzN(Et)_3]^+Cl^-$.

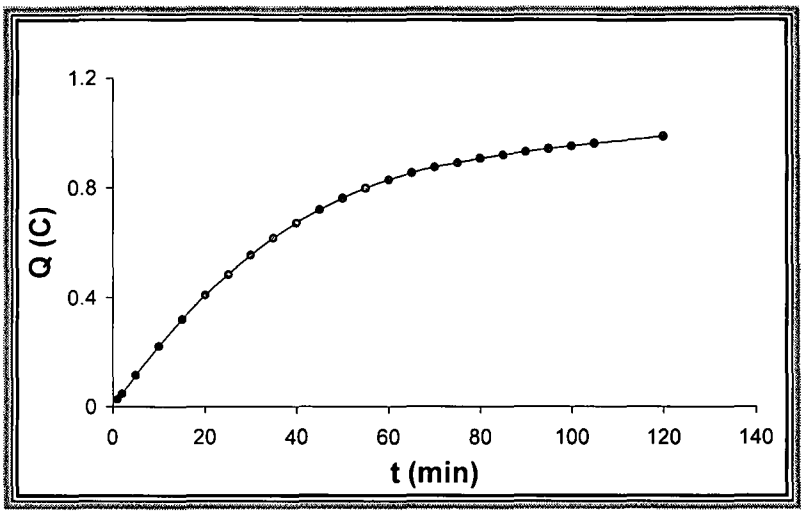

Figure 6.18: Plot of total amounts of coulomb (Q) against time.

6.9 The electrochemical oxidation in perspective

6.9.1 Electronic and steric effects

The effect of the different substituents on the β-diketone showed that the chemical oxidation rate increases with an increase of the pKa-values of the free β-diketones (Section 4.5.5 and Figure 4.7 and 4.8). The same effect was observed in the electrochemical oxidation (Figure 6.7) where it was proved once again that when electron density is removed from the Rh(I) centre, it becomes more difficult to oxidise Rh(I) to Rh(III). There is, however, a significant difference between the two relations, pKa *versus* second order constant (Figure 4.7 and 4.8) and pKa *versus* electrochemical oxidation potential (Figure 6.7). In spite of possessing the same pKa-values, the chemical oxidation of the more bulky Rh(btfa)(CO)(PPh_3) was slower than that of Rh(tfaa)(CO)(PPh_3) (Figure 4.7 and 4.8). It was expected that steric parameters would not have an influence during electrochemical oxidation. This was indeed proved to be true since the oxidation potentials of Rh(btfa)(CO)(PPh_3) and Rh(tfaa)(CO)(PPh_3) are the same, within experimental error (Figure 6.7). The technique of electrochemical oxidation can therefore be used to quantify steric effects during chemical oxidation. This observation is of special importance since steric effects play an important role in the industrial application of oxidative addition reactions.

6.9.2 Solvent co-ordination

During the electrochemical oxidation of square planar Rh(I) to the octahedral Rh(III) (Section 6.6) the only possible co-ordination ligand is the solvent, CH_3CN. The results of the different solvent donisities (Section 6.7.5) prove the postulation of solvent co-ordination. The addition of solvents with higher donosities and therefore better co-ordinating properties makes it more difficult to reduce the Rh(III) species formed, back to Rh(I) (Table 6.4 and Figure 6.16). A further proof of solvent co-ordination is that during negative scans (Figure 6.8) no reduction peaks were observed. Positive scans with slow scan rates ($\nu \leq 0.05V.s^{-1}$) also showed no reduction peaks, indicating the weak co-ordination of the solvents (Figure 6.10).

6.9.3 Electrochemical oxidation mechanism

Based upon the CV results (Figure 6.8 and 6.10) as well as the discussion above (Section 6.9.2), an EC mechanism (Figure 6.19, Step ① and ②) is suggested in the case of slow scan rates during the electrochemical oxidation of Rh(I) to Rh(III).

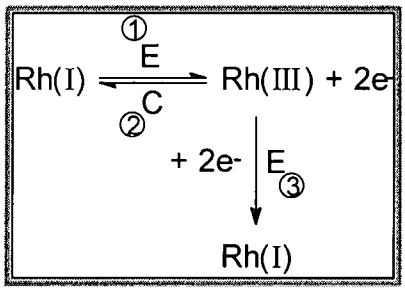

Figure 6.19: An EC, ECE and EE mechanism for the electrochemical oxidation of Rh(I) to Rh(III).

Successive CV scans (Section 6.7.2) showed that no by-products formed after the first CV scans (Figure 6.9). Other than the chemical regeneration of Rh(III) back to Rh(I), no other chemical path was observed. The chemical regeneration was also observed during bulk electrolysis (Section 6.8), where a total amount of $2e^-$ could not be accounted for before the addition of $[B_ZN(Et)_3]^+Cl^-$, due to the instability of the Rh(III) formed.

An increase in the scan rates ($\nu \geq 0.1V.s^{-1}$) leads to an increase in the reducibility of the Rh(III) back to Rh(I) (Section 6.7.3). An ECE mechanism in the case of fast scan rates was therefore suggested (Figure 6.19, Step ①, ② and ③). The diffusion rate of the Rh(III) away from the working electrode, as well as decomposition of the formed Rh(III), is forestalled, causing more Rh(III) to be reduced back to Rh(I) (Figure 6.19, Step ③).

In the presence of a stronger co-ordination ligand, $[B_ZN(Et)_3]^+Cl^-$, it became more difficult to reduce Rh(III) back to Rh(I) (Figure 6.14). The electrochemically generated Rh(III) in the presence of Cl^- is therefore much more stable than in the case of solvent co-ordination. The stability of the electrochemically formed Rh(III) was also observed during bulk electrolysis (Section 6.8) where a total amount of $2e^-$ could be accounted for in the presence of $[B_ZN(Et)_3]^+Cl^-$. An EE mechanism (Figure 6.19, Step ① and ③) is therefore suggested during the electrochemical oxidation of Rh(I) to Rh(III) in the presence of $[B_ZN(Et)_3]^+Cl^-$ where no chemical regeneration of Rh(I) was observed.

PART 3
MOLECULAR MECHANICS

THE DEVELOPMENT AND APPLICATIONS OF A RHODIUM(I) CARBONYL PHOSPHINE FORCE FIELD

CHAPTER 7:

EXTENSION OF MOLECULAR MECHANICS FOR THE MODELLING OF CO-ORDINATION COMPOUNDS

7.1 Introduction

Computational chemistry, a multidisciplinary science that transcends the traditional barriers separating biology, chemistry, mathematics and physics, is becoming a mature field of chemistry influencing science and technology in both the academic field and in industry[1]. The challenges for computational chemistry are to characterise and predict the structure and stability of chemical systems and to estimate energy differences between states as well as to explain reaction pathways and mechanisms at atomic level. Meeting these challenges could eliminate time consuming experiments.

A variety of computational techniques, ranging from ab initio to semi-empirical to completely empirical techniques, can be employed in the estimation of molecular structure and energetics[2].

---

[1] Lipkowitz K.B., Boyd D.B., *Reviews in Computational Chemistry, Chapter 10*, Boyd D.B., **Vol. 1**, VCH, New York, (1990)
[2] Fruhbeis H., Klein R., Wallmeier H., *Angew. Chem., Int. Ed. Engl.*, **26**, 403, (1987)

7.1.1 Molecular mechanics *versus* quantum mechanics

Molecular mechanics does not consider the electrons in the molecule explicitly, but rather treats the atoms and their associated electrons as units interconnected by a potential function. Quantum mechanics is more concerned with the three-dimensional distribution of electrons around the nuclei and freeze the position of the nuclei (Born-Oppenheimer approximation) for each structure of which the electronic wavelength is described[3].

Molecular mechanics is a quick calculation due to the fact that the potential energy of the molecule is obtained as a simple sum of terms for each set of atomic co-ordinates. Quantum mechanics is very accurate but requires a great deal of computer time. Molecular mechanics is conceptually easier to understand than quantum mechanics. Since molecular mechanics is an interpolation of experimental data, the predicted geometry of a molecule is often very near what would be obtained experimentally.

There are some pitfalls regarding molecular mechanics. Molecular mechanics requires as input some initial atomic co-ordinates for each atom in the molecule. If related molecules have been studied by means of X-ray crystallography, their unit cell co-ordinates may be used. If the starting geometry of the molecule is near some potential well on the potential energy surface, there is no way that an even lower potential well will be recognised during the minimisation process and they can cause some trouble. Molecular mechanics is not appropriate for studying properties where electronic effects like orbital interactions, bond breaking and bond formation predominate[3]. A quantum mechanical approach is better in these cases.

[3] Boyd D.B., Lipkowitz K.B., *J. Chem. Ed.*, **59(4)**, 269, (1982)

Factors limiting the application of empirical force fields methods to the study of transition metal complexes can be divided into[4]:

(i) Limitations inherent in the generalised valence force fields.

(ii) Difficulties in parameterisation of the force field.

7.2 Basic principles of molecular mechanics

Molecular mechanics is an empirical method requiring less computer time than ab initio or semi-empirical approaches[5]. Molecular mechanics interpolates the structure of an unknown complex on the basis of a set of parameters that were derived from fitting a number of crystal structures[6].

Consider a molecule as a collection of atoms held together by elastic forces (Figure 7.1). These forces can be described by potential energy functions of structural features like bond lengths, bond angles, rotation angles, non-bonding interactions, etc. The combination of these potential energy functions is called the force field. The energy, E, of the molecule in the force field arises from the deviations from the "ideal" structural features and can be approximated by the sum of all energy contributions[3,7]:

$$E = E_{\text{stretching}} + E_{\text{bending}} + E_{\text{rotating}} + E_{\text{non-bonding}} + \ldots \qquad ①$$

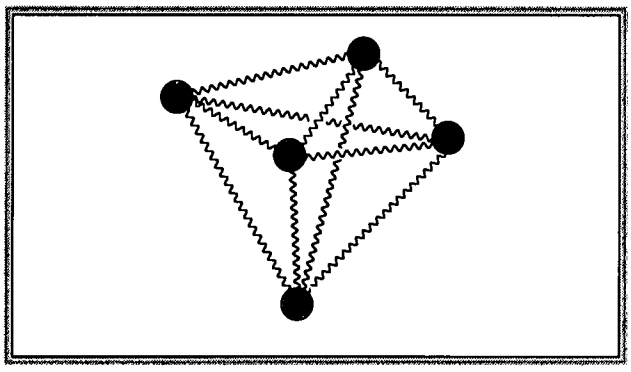

Figure 7.1: Schematic representation of the molecular mechanics model.

[4] Allured V.S., Kelly C.M., Landis C.R., *J. Chem. Soc.*, **113 (1)**, 1, (1991)
[5] Canales C., Egan L., Zimmer M., *J. Chem. Ed.*, **69 (1)**, 21, (1992)
[6] Comba P., Zimmer M., *J. Chem. Ed.*, **73 (2)**, 108, (1996)
[7] Cox P.J., *J. Chem. Ed.*, **59 (4)**, 275, (1982)

Molecular mechanics is an attempt to formulate as reliable a recipe as possible for reproducing the potential energy surface for the movement of atoms within a molecule. A potential energy surface is simply a specification of the classical potential energy as a function of molecular structure. Minima on the potential surface correspond to stable conformations of the molecule. Molecular mechanics is able to locate these minima and therefore identify stable conformations.

Molecular mechanics calculations lead to relatively precise quantitative information on intramolecular steric effects. The other two types of data resulting these calculations are structural (optimised geometries) and thermodynamic (minimised strain energies).

One major problem with molecular mechanics is that the species calculated usually does not include any environment. However, it is also not fully consistent with the model to call them "gas phase molecules" since most of the force field parameters have been fitted to solid state or solution properties.

A promising extension in the area of applications of molecular mechanics is the calculation of the structures of short-lived intermediates[8]. The problem here is that the calculated structures cannot be compared with experimental data and therefore rather large uncertainties have to be contended with.

7.2.1 Constructing a force field

Force fields are developed to treat classes of compounds that are composed of the same atom types. Molecular mechanics force fields use the equation of classical mechanics to describe the potential energy surface and physical properties of molecules.

By applying Hooke's law[3,6,7,9,10] it is possible to calculate how much energy is involved in stretching or bending bonds from their "ideal" values (Equation ②).

[8] Comba P., *Co-ord. Chem. Rev.*, **123**, 1, (1993)
[9] Hopfinger A.J., Pearlstein R.A., *J. Comp. Chem.*, **5 (5)**, 486, (1984)
[10] *HyperChem™, Computational Chemistry, Molecular Visualization and Simulation*, Hypercube, Inc.,(1994)

$$E_r = \sum \frac{1}{2} k_r (r - r^\circ)^2 \text{ and } E_\theta = \sum \frac{1}{2} k_\theta (\theta - \theta^\circ)^2 \qquad ②$$

k_r and k_θ are the stretching and bending force constants

r and θ are the actual bond lengths and bond angles (Figure 7.2)

r° and θ° are the "ideal" bond lengths and bond angles

Standard values of r° and θ° can be selected from X-ray data or from compiled structure lists. The larger the force constants, k_r or k_θ, the greater the tendency for the bond or angle to remain at their equilibrium distance or angle. It takes more energy to stretch a bond than to bend it; therefore, the values of k_θ are more or less a tenth the magnitude of k_r. If a molecule is distorted, it is therefore expected that most of the distortion will be found in the bond angles rather than in the bond lengths.

Harmonic potentials are only good approximations for small deformations in bond lengths and bond angles[11].

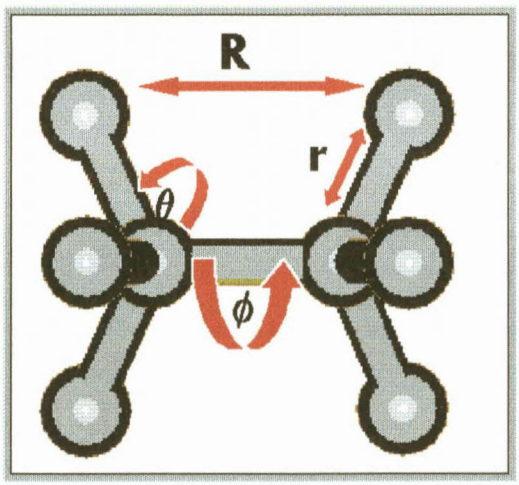

Figure 7.2: Schematic representation of a force field.

Rotation about bonds changes the molecular energy. Rotation around a double bond involves bond breaking and is therefore a very high-energy process. Internal free rotation about single bonds is expressed in terms of torsion angles. The barriers of free rotation must therefore also be built into

[11] Hay B.P., *Co-ord. Chem. Rev.*, **126**, 177, (1993)

the force fields. The dihedral potential function is implemented as a Fourier series[10]:

$$E\phi = \sum\left[\frac{1}{2}V_1(1+\cos\phi)+\frac{1}{2}V_2(1-\cos 2\phi)+\frac{1}{2}V_3(1+\cos 3\phi)\right] \qquad ③$$

V is the dihedral force constant

ϕ is the dihedral angle (Figure 7.2)

It takes less energy to distort a dihedral angle from its preferred value than it does to bend an angle from its "ideal" values. The precision of these fits regarding individual torsional minima is partially sacrificed for the overall fit. Rotation around a metal-ligand axis does not seem to be measurably restricted and the corresponding potential is therefore generally omitted[12].

As two atoms approach one another, there is an attraction due to London dispersion forces and a van der Waals repulsion as the atoms get too close. A Lennard-Jones function simulates the above[6]:

$$E_{nb} = \sum\left(\frac{A}{R_{ij}^{12}}-\frac{B}{R_{ij}^{6}}\right) \qquad ④$$

A and B are van der Waals parameters

R_{ij} is the non-bonding distance between atom i and j (Figure 7.2)

R^{-6} describes the attracting London dispersion interaction and R^{-12} describes the repulsing interaction caused by Pauli exclusion. These non-bonded potential functions describe the two atoms as the same regardless of what other atoms are in the vicinity of the two.

In-plane and out-of-plane bending force constants are important at sp^2-hybridised atoms. A simple potential function is used to describe the energy contribution arising from the out-of-plane deformation:

[12] Kim P.H., *J. Phys. Soc. Jpn.*, **15**, 445, (1960)

$$E_{\delta} = \sum \frac{1}{2} k_{\delta} \delta^2 \qquad ⑤$$

k_δ is the out-of-plane force constant

δ is the distance of the sp^2-atom from the plane defined by the three attached atoms.

The electrostatic potential is determined by:

$$E_{elec} = \sum \left(\frac{q_i q_j}{\varepsilon R_{ij}} \right) \qquad ⑥$$

q_i and q_j are point charges of atom i and j

ε is the dielectric constant

R_{ij} is the non-bonding distance between atom i and j (Figure 7.2)

Experimental force constants for any specific bond are clearly dependent on the environment and so are molecule specific. In molecular mechanics, however, generally applicable and therefore molecule independent force constants are needed. Force constants used in molecular mechanics are therefore not related to experimental observations, but are usually the result of extensive fittings.

Force fields are usually developed for specific types of molecules and their use in other situations will either fail or give poor results. Once the appropriate force field has been established, it is used in the minimisation of the strain energy of the complex.

7.2.2 Force field parameters

In order to use these equations (Equation ②-⑥) to calculate the total strain in the molecule, the following parameters must be known[6]:

- The force constant for all the bonds and angles.
- The "ideal" bond lengths, r°, and bond angles, θ°.
- The periodicity of the dihedral angle.
- The barriers of free rotation, V.
- The van der Waals parameters, A_{ij} and B_{ij}, between atom i and j.

Force field parameters can be derived from experimental data, most notably from X-ray crystallographic data. Force field parameters have also been estimated from quantum mechanics. To insure that the optimised structure retains bond lengths and bond angles close to the "ideal" bond lengths, r°, and bond angles, θ°, unknown force constants should each be set equal to relatively high values. The pitfall of this approach is the unrealistic distortion of other bond lengths and bond angles that are correctly parameterised. The initial values of the parameters obtained are only rough estimates and can therefore be adjusted by a trail-and-error[13] method or by least square calculations[14]. The quality of the force field derived is then judged by its ability to reproduce data with an accuracy rivalling that achieved by experimental methods.

7.2.3 Geometry optimisation and energy minimisation

Once the force field has been constructed and suitable parameters have been chosen, trail geometry is specified in terms of atomic co-ordinates in the input data and the initial steric energy is calculated by means of single point calculations. The geometry is then optimised, meaning that the energy is minimised. Molecular mechanics involves the refinement of a structure by modification of the initial trail co-ordinates in order to minimise the strain energy. Minimisation may be achieved by a number of different algorithms such as steepest descent, Newton-Raphson, simplex and others.

A single point calculation determines molecular properties such as energies of a defined molecular structure for stationary points on the potential energy surface.

Geometry optimisation finds the co-ordinates of a molecular structure that represent a potential energy minimum. For potential energy, V, and Cartesian co-ordinates, r_i, the optimised co-ordinates satisfy the equation: $\frac{\partial(V)}{\partial(r_i)} = 0$

[13] Allinger N.L., *Adv. Phys. Org. Chem.*, **13**, 1, (1976)
[14] Lifson S., Warshel A., *J. Chem. Phys.*, **49**, 5116, (1968)

The goal of performing a geometry optimisation calculation is to characterise a potential energy minimum. A geometry optimisation procedure results in the formation of a new structure with minimum steric energy.

It is very important to find the global minimum of a complex and not a local minimum during geometry optimisation.

7.3 Force fields for co-ordination compounds

One of the most prominent and fascinating features of transition metal complexes is their large variability in molecular geometry which can be attributed to the electronic structures of the metal ions possessing partially filled d- and f-orbitals. The ligand sphere and the co-ordination geometry obviously have a large influence on the kinetic, thermodynamic and electronic properties of the transition metal. Ligand exchange reactivities, isomer stabilities and selectivities, together with spectroscopic properties, are related to structural parameters, but what determines the co-ordination geometry of a transition metal complex? Each structure is a compromise between the demands of the metal ion (mainly electronic effects) and that of the ligand (primarily steric effects). The metal ion demands are rather weak[8] and the limitations of the co-ordinated ligand are only given by chemical instability. Therefore, models have been proposed which interpret and predict structures of transition metal complexes while completely ignoring electronic effects.

Molecular mechanics force fields that have been developed for co-ordination compounds are very limited in the type of ligands and metal ions that can be treated. Those who conduct molecular mechanics on co-ordination compounds have had to and will continue to have to build the force fields needed. Since the bulk of the structure in many co-ordination compounds is composed of organic constituents, the natural tendency has been to adapt existing organic force fields to allow the addition of a metal ion. In this way it is not necessary to develop an entire new force field, but only the portion of the force field that is needed to treat the new interactions incurred by the presence of the metal ion[11].

Only a few methods have evolved to extend an organic force field to treat metal complexes. These methods differ in the type of terms that are added to the potential energy equations to describe the interactions that involve the metal ion

7.3.1 Valence force field method

The valence force field method is the most commonly used. It is based upon the logical extension of an organic valence force field; i.e. the metal ion is treated like any other atom in an organic molecule. In theory, this means that terms are added to the potential energy equation for each M—L bond, M—L—X angle, L—M—L angle, M—L—X—X torsion angle, L—M—L—X torsion angle and each M•••X non-bonding interaction (M = metal ion, L = ligand donor atom, X = any other atom type).

The L—M—L—X torsion terms are omitted because the rotation barriers about M—L bonds are, in general, very low[15]. This can be done by setting the barriers of free rotation to zero.

The first modification of an organic force field is to allow for an increased number of attachments per atom because organic force fields are limited to four attachments per atom. In addition, it is necessary to make some provision for the fact there are two types of L—M—L angles in the complex[4], *cis* and *trans*. This provision is necessary because organic force fields assign parameters to potential functions based on the atom types that are involved. The above is called the *unique labelling problem.*

Due to the difficulties associated with the assignment of preferred angles at the metal centre, the valence force field method is best suited for geometries with two or less L—M—L angle types, i.e. complexes with co-ordination number of ≤ 6. One solution to the angle assignment problem is to define each ligand donor atom as a different atom type and to assign the appropriate ideal value to each of the individual angles.

[15] Buckingham D.A., Sargeson A.M., *Top. Stereochem.*, **6**, 219, (1971)

7.3.2 Points-on-a-sphere method

The points-on-a-sphere method states that the donor atoms attached to the metal ion tend to distribute themselves in such a way as to minimise donor atom - donor atom repulsion. Most co-ordination geometries can be explained by merely considering the distribution of points on the surface of a sphere with an appropriate repulsing force between them[16]. The points-on-a-sphere method treats the inner co-ordination sphere of the metal in a similar fashion. All L—M—L terms are replaced by L•••L van der Waals terms. The points-on-a-sphere method allows therefore the L—M—L angles to be dictated by van der Waals interactions between the ligand donor atoms. All other metal dependent interactions are treated exactly as in the valence force field approach. An exception for the use of the points-on-a-sphere method arises with four co-ordinate metal complexes, where L•••L repulsing forces alone always favour a tetrahedral arrangement.

7.3.3 Ionic method

The ionic method, also known as the pair potential method, is quite different from the preceding two methods. In the ionic method, the interactions of the metal ion with the ligands are modelled entirely by M•••L non-bonded terms. All M•••L and M•••X van der Waals interactions and electrostatic interactions are included in the potential energy equations and all M—L, M—L—X, L—M—L and M—L—X—X terms are omitted from the potential energy equation.

The simplicity of the ionic method can be a disadvantage, because it is not clear whether this method provides an adequate potential energy surface for the accurate modelling of structures in metal complexes and whether it will yield transferable force fields.

[16] Kepert D.L., *Prog. Inorg. Chem.*, **23**, 1, (1977)

7.3.4 Parameterisation of co-ordinated compounds

Most molecular mechanics force fields already contain parameters for common organic functional groups. When modelling co-ordination compounds, it is generally assumed that the complexation of the ligand to a metal ion does not significantly alter the nature of the interactions within the ligand. The parameters used for modelling the ligand structure within a metal complex are therefore assumed to be transferable from organic force fields. The metal dependent parameters are obtained by the same techniques, such as experimental data, that are used for the development of organic parameter sets. The performance of the initial set of parameters is tested by comparing calculated and experimental structures, together with their respective energies. If necessary, the initial parameters are then modified to minimise the errors in the calculated output.

Bond stretching and angle bending parameters:

The valence force field method uses parameters for M—L stretches, M—L—X bends and L—M—L bends. The parameters needed for M—L bond stretching deformations are the strain-free bond lengths, $r°$, and the force constant, k_r. The parameters needed for M—L—X and L—M—L bending deformation are the strain-free bond angle, $\theta°$, and the force constant, k_θ. Values for $r°$ and $\theta°$ are assigned by comparison with experimental bond lengths and bond angles in complexes that are deemed to be relatively unstrained, or by the use of ideal geometries, i.e. $\theta° = 90°$ for a *cis* L—M—L angle in an octahedral geometry. The force constants, k_r and k_θ, are derived from vibration data or by means of quantum mechanics. It is also possible to estimate initial values for k_r and k_θ by comparison with values that have been used in organic force fields. Some groups have assumed that the M—L—X bending interaction has the same k_θ value as the analogous $C(sp^3)$—L—X[11].

Torsion angle parameters:

The valence force field method requires the definition of parameters for M—L—X—X torsional interaction. The parameters needed for the torsional

interaction are the effective barriers of free rotation, V. These parameters are usually obtained by a trial-and-error fitting process in organic force fields. Much less information is available for rotational barriers in metal complexes and one approach has also been to assume that the M—L—X—X torsional interaction will contribute the same amount to a rotational barrier as the corresponding $C(sp^3)$—L—X—X interaction.

Non-bonding parameters:

For transition metals, van der Waals parameters have been roughly estimated by comparison with values that are used for the elements found in organic force fields. The valence force field method does not require the addition of non-bonded interactions with the metal ion and it remains to be shown that the addition of metal ion non-bonded terms actually improves the performance of the force field.

It is important that the force field is reasonably balanced, i.e. no one component is so unrealistic that the other components must compensate for it in order to yield the net result in agreement with experimental data.

The popularity of molecular mechanics is based on the simplicity of the model, which sometimes might be misleading, in the sense that the high degree of parameterisation still allows a number of effects not explicitly treated by the model to be accounted for.

CHAPTER 8:

THE COMPUTATION OF THE STRUCTURE OF $Rh(dbm)(CO)(PPh_3)$ AND THE OXIDATIVE ADDITION TRANSITION STATE

8.1 Introduction

Molecular mechanics involves three important concepts:

- Functional forms
- Atom types
- Parameter sets

To run a molecular mechanics calculation, a force field must be chosen. HyperChem(TM)[1] is a modelling and simulation programme of which input is straightforward and computation of the molecular mechanics structures is based on MM^+, AMBER, BIO^+ and OPLS methods (Figure 8.1). The functional form, force field, describes the analytical form of each of the terms on the potential energy surface. AMBER, BIO^+ and OPLS methods are primarily designed to explore macromolecules.

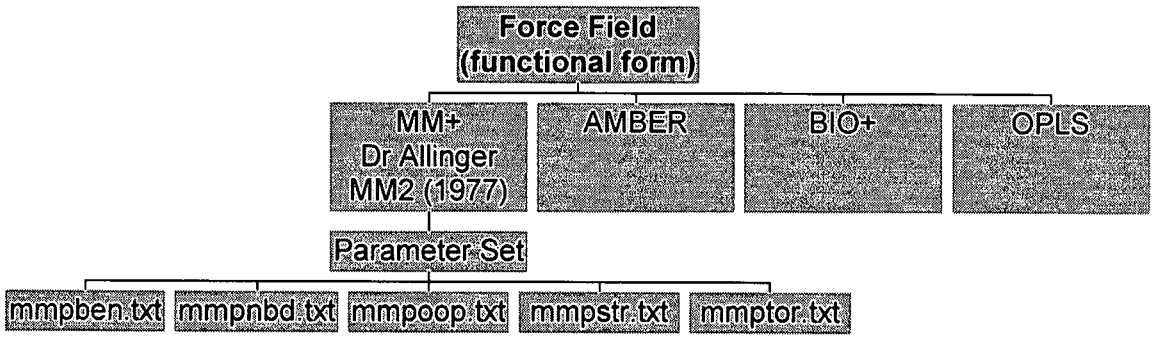

Figure 8.1: Functional forms of HyperChem(TM) and MM^+ parameter sets

[1] *HyperChem(TM), Getting Started, Molecular Visualization and Simulation*, Hypercube, Inc.,(1994)

8.2: The MM$^+$ force field

MM$^+$ is derived from Dr Allinger's MM2 force field[2], which was developed in 1977. The MM2 force field will fail in many situations where no parameters exist, but the MM$^+$ force field will perform a calculation with the existing parameters and will therefore use default values when parameters do not exist. MM$^+$ force field parameters are given in ASCII text file formats, which are easily available for modification and additions. A disadvantage of parameter sets in ASCII text form is that it makes comparison between parameter sets difficult.

8.2.1 The Rhodium(I) Carbonyl Phosphine force field

The Rh(I) Carbonyl Phosphine force field was developed by the fitting of fifteen known, square planar Rh(I) Carbonyl Phosphine structures[3]. The X-ray crystallographic input data, of which the Rh(acac)(CO)(PPh_3) data is given as an example, (Table 8.1) was read into PCMODEL[4] and converted to a Z-matrix mopac file, which was then imported in HyperChem(TM) (Figure 8.2).

a(Å)	*b(Å)*	*c(Å)*	*α(°)*	*β(°)*	*γ(°)*
Acac.xra					
13.200	10.450	8.900	97.050	110.850	103.150
	0.2392	-0.00467	0.06724	RH	
	0.3421	0.1945	0.2433	P	
	-0.0286	0.1157	-0.2812	C	
	0.4204	-0.1173	0.2486	O	
	X	*Y*	*Z*		

Table 8.1: The triclinic $P\bar{1}$ space group and selected fractional atomic co-ordinates of Rh(acac)(CO)(PPh_3).

---

[2] Allinger N.L., *J. Am. Chem. Soc.*, **99**, 8127, (1977)

[3] (i) Rh(acac)(CO)(PPh_3): Leipoldt J.G., Basson S.S., Bok L.D.C., Gerber T.I.A., *Inorg. Chim. Acta*, **26**, L35, (1978)
[3] (ii) Rh(bpha)(CO)(PPh_3): Leipoldt J.G., Grobler E.C., *Inorg. Chim. Acta*, **60**, 141, (1982)
[3] (iii) Rh(bzaa)(CO)(PPh_3): Roodt A., Leipoldt J.G., Swarts J.C., Steyn G.J.J., *Acta Cryst.* , **C48**, 547, (1992)
[3] (iv) Rh(cupf)(CO)(PPh_3): Basson S.S., Leipoldt J.G., Roodt A., Venter J.A., *Inorg. Chim. Acta*, **118**, L45, (1986)
[3] (v) Rh(cacsm)(CO)(PPh_3): Steyn G.J.J., Roodt A. *to be published*
[3] (vi) Rh(hacsm)(CO)(PPh_3): Steyn G.J.J., Roodt A., Poletaeva I., Varshavsky Y.S., *J., Organomet. Chem.*, **536**, 197, (1997)
[3] (vii) Rh(macsm)(CO)(PPh_3): Steyn G.J.J., Roodt A., Leipoldt J.G., *Inorg. Chem.*, **31**, 3477, (1992)
[3] (viii) Rh(ox)(CO)(PPh_3): Leipoldt J.G., Basson S.S., Dennis C.R., *Inorg. Chim. Acta*, **50**, 121, (1981)
[3] (ix) Rh(pic)(CO)(PPh_3): Leipoldt J.G., Lamprecht G.J., Graham D.E., *Inorg. Chim. Acta*, **101**, 123, (1985)
[3] (x) Rh(sacac)(CO)(PPh_3): Botha L.J., Basson S.S., Leipoldt J.G., *Inorg. Chim. Acta*, **126**, 25, (1987)
[3] (xi) Rh(salNR)(CO)(PPh_3): Leipoldt J.G., Basson S.S., Grobler E.C., Roodt A., *Inorg. Chim. Acta*, **99**, 13, (1985)
[3] (xii) Rh(tfdmaa)(CO)(PPh_3): Leipoldt J.G., Basson S.S., Nel J.T., *Inorg. Chim. Acta*, **74**, 85, (1983)
[3] (xiii) Rh(tfhd)(CO)(PPh_3): Steynberg E.C., Lamprecht G.J., Leipoldt J.G., *Inorg. Chim. Acta*, **133**, 33, (1987)
[3] (xiv) Rh(tftmaa)(CO)(PPh_3): Leipoldt J.G., Basson S.S., *Inorg. Chim. Acta*, **117**, L3, (1986)
[3] (xv) Rh(trop)(CO)(PPh_3): Leipoldt J.G., Bok L.D.C., Basson S.S., Meyer H., *Inorg. Chim. Acta*, **42**, 105, (1980)

[4] *PCMODEL, Molecular modelling software*, **IBM RS/6000**, Serena Software, Bloomington, (1990)

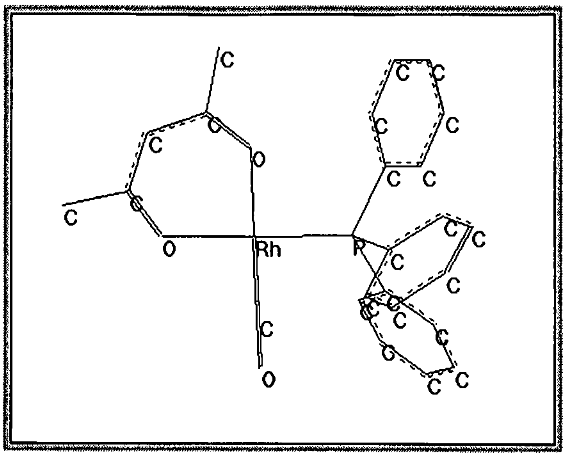

Figure 8.2: Rh(acac)(CO)(PPh$_3$) structure imported from PCMODEL.

A force field contains atom types and parameters that must be assigned to the molecule before a molecular mechanics calculation is performed. The atom types represent sets of atoms of the same element and define the classical environment of an atom together with its stereochemical properties. It is possible to distinguish between atoms by means of hybridisation, formal charge on the atoms and immediate bonded neighbours. A sp-hybridised carbon, C2, can therefore be distinguished from a sp^2-hybridised carbon, C3, and a sp^3-hybridised carbon, C4, by the fact that these carbons are different types. Molecular mechanics calculations treat all atoms of the same type in similar ways. Force fields require atom types to assign calculation parameters.

Atom types

Atom types are defined in a Rule file. Atom typing rules can be added and modified in the Rule file. For each atom in a molecular structure, HyperChem(TM) scans the Rule file and makes the following decisions:

- What is the force field?
- What is the element?
- For this element, does the atom satisfy the test in the first clause (Appendix 5)?
- When the atom satisfies the test in a clause, HyperChem(TM) assigns the atom type.

The MM$^+$ force field has a default set of atom types together with their parameter sets which was used for the organic constituents in the structures

(Section 7.3). New atom types were added to the existing MM^+ force field and compiled to treat the new interactions incurred by the presence of the Rh(I) metal ion (Appendix 5).

The new atom types defined in the Rule file (Appendix 5) must also be added in a Type Parameter file (Table 8.2). Atom types in the Type Parameter file are used to calculate strain energies during molecular mechanics and are also used for the assignment of parameters in the various parameters sets, whereas the Rule file is used for the prediction of similar Rh(I) Carbonyl Phosphine structures.

```
TYPE  MASS  REMARK
c2    12.000      4.  C CSP ALKYNE, C=C=O"
c3    12.000      2.  C CSP2 ALKENE
c4    12.000      1.  C CSP3
c5    12.000      68. C sp3 CARBON bonded to Fluoride
c6    12.000      74. C CARBONYL TO RHODIUM
c7    12.000      44. C sp3 CARBON bonded to Sulphur
ca    12.000      50. C BENZENE
cx    12.000      76. C AROMATIC CARBON in bidentate ligands (6-ring)
cy    12.000      77. C AROMATIC CARBON in bidentate ligands (5-ring)
h       1.0079    5.  H EXCEPT ON N/O
hn      1.008     23. H NH AMINE
n4    14.0067     82. N Co-ordinated NITROGEN; bonded to C; (6-ring)
n4tp  14.0067     87. N n4 trans to P
n4tc  14.0067     88. N n4 trans to CO
n5    14.0067     83. N Co-ordinated NITROGEN; bonded to C; (5-ring)
n5tp  14.0067     89. N n5 trans to P
n6    14.0067     80. N in bidentate ligand; bonded to O; (5-ring)
o+    15.9994     75. O MONO POSITIVE OXYGEN; bonded to c6 (carbonyl)
o1    15.9994     7.  O =O CARBONYL
o2    15.9994     6.  O C-O-H, C-O-C"
o3    15.9994     78. O Co-ordinated OXYGEN; bonded to C; (6-ring)
o3tp  15.9994     90. O o3 trans to P
o3tc  15.9994     91. O o3 trans to CO
o5    15.9994     85. O Co-ordinated OXYGEN; bonded to C; (5-ring)
o5tp  15.9994     92. O o5 trans to P
o5tc  15.9994     93. O o5 trans to CO
o7    15.9994     86. O Co-ordinated OXYGEN; bonded to N; (5-ring)
o7tp  15.9994     94. O o7 trans to P
o7tc  15.9994     95. O o7 trans to CO
p1    30.994      84. P >P- PHOSPHINE bonded to Rh
rh1   102.91      73. Rh RHODIUM (I)
s2    31.972      15. S -S- SULPHIDE
s5    31.972      81. S Co ordinated SULPHUR; bonded to C; (5-ring)
s7    31.972      79. S Co-ordinated SULPHUR; bonded to C; (6-ring)
s7tp  31.972      96. S s7 trans to P
s7tc  31.972      97. S s7 trans to CO
```

Table 8.2: Selected atom types from the mmptyp.txt Type Parameter file.

It was necessary to make some provision for the fact there are two types of L—M—L angles in the complex, namely *cis* and *trans* (Section 7.3.1). A solution to the angle assignment problem was to make use of the valence force field method to define each ligand donor atom as a different atom type and to assign the appropriate ideal values to each of the individual angles. Unfortunately, there is no clause available in the Rule file of HyperChem(TM) to distinguish between the above. Subdividing the atom types of the ligand donor atoms in the Type Parameter file into two, those *trans* to the carbonyl group and those *trans* to the phosphine group, solved the problem (Figure 8.3). For example: The atom type, o3, is an oxygen ligand donor atom in a six membered chelate ring, which is subdivided into o3tp and o3tc (Figure 8.3). The atom types o3tp and o3tc refer to an o3 atom type *trans* to the phosphine group and *trans* to the carbonyl group respectively.

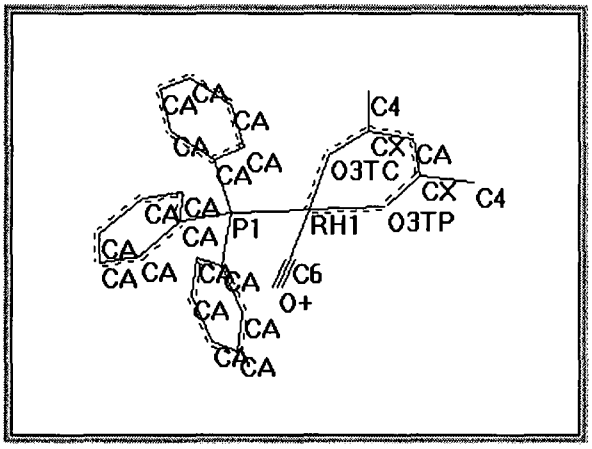

Figure 8.3: Atom type selection of Rh(acac)(CO)(PPh_3)

Parameter sets

There is a strong case for keeping parameterisation as simple as possible[5]. The parameter sets contain ASCII text files that define the interactions between atoms and include information about bond lengths and bond angles, torsion angles and electrostatic interactions (Figure 8.1), as well as the force constants for these interactions. New parameters can be added or existing parameters can be modified in these text files before they are compiled.

[5] Bernhardt P.V. Comba P., *Inorg. Chem.*, **31**, 2638, (1992)

Atom types are used to introduce specific chemical environments, but require knowledge of force constants specific to that chemical environment. HyperChem(TM) includes a default system so that when MM^+ fails to find a force constant, it will substitute a default value[6]. A wild card approach is followed. For example: The parameters for a torsion angle X—A—B—Y can be found in the mmptor.txt file (Figure 8.1). If the parameters for above torsion angle are not found, an automatic search for parameters of a torsion angle **—A—B—** will be followed. If no parameters can be found, the torsion angle **—**—**—** will be used as a default where ** refers to any atom type. The status line of HyperChem(TM) will notify if a default value is used. The default force constant value for single bonds is 700 $kcal.mol^{-1}.Å^{-1}$, for a double bond force constant 1400 $kcal.mol^{-1}.Å^{-1}$ and for a triple bond force constant 2100 $kcal.mol^{-1}.Å^{-1}$.

"Ideal" bond lengths and "ideal" bond angles in the Rh(I) Carbonyl Phosphine force field were calculated by averaging the bond lengths and bond angles of the fifteen mentioned X-ray structural data for a specific atom type. The barriers of free rotation of the MM^+ force field were copied to torsion angles in the Rh(I) Carbonyl Phosphine force field with the same valence geometry. The torsion terms around the Rh(I) metal centre were omitted because the rotation barriers about Rh—L bonds are, in general, very low[7]. This was done by setting the barriers of free rotation to zero[8].

The problem of force constants was also solved by copying force constants with similar chemical environments in the MM^+ force field to the Rh(I) Carbonyl Phosphine force field where applicable. Force constants for the Rh—L bonds, Rh—L—X angles, L—Rh—L angles, Rh—L—X—X torsion angles and each Rh∘∘∘X non-bonding interaction (M = metal ion, L = ligand donor atom, X = any other atom type) which did not appear in the MM^+ force field, were obtained by substituting the Rh(I) metal ion with a sp^3-hybridised carbon after which the routine of copying was continued (Appendix 6). The Rh(I)

---

[6] *HyperChem(TM), Computational Chemistry, Molecular Visualization and Simulation*, Hypercube, Inc.,(1994)
[7] Buckingham D.A., Sargeson A.M., *Top. Stereochem.*, **6**, 219, (1971)
[8] Boeyens J.C.A., Cotton F.A., Han S., *J. Inorg. Chem.*, **24**, 1750, (1985)

Carbonyl Phosphine force field was therefore only an extension of the MM^+ force field where the parameter sets (Figure 8.1) contained all the bonding parameters of a purely organic force field together with parameters of a Rh(I) transition metal complex force field (Appendix 6).

8.2.2 Energy minimisation and geometry optimisation of the structures in the Rhodium(I) Carbonyl Phosphine force field

The goal of performing a geometry optimisation calculation is to characterise the potential energy minimum of an unknown Rh(I) structure, which is similar to that of the Rh(I) Carbonyl Phosphine structures. Before the Rh(I) Carbonyl Phosphine force field can be used to predict similar Rh(I) structures, the credibility of the parameters used in constructing it must be tested.

Geometry optimisation was done on the series of fifteen Rh(I) Carbonyl Phosphine structures by using a Newton-Raphson minimisation procedure coded by Boyd[9].

A single point calculation (Section 7.2.3) was done on both the minimised structures and the experimental structures to determine the total energy of their respective stationary molecular conformation. The structural properties of the minimised system were then compared with those of the X-ray crystallographic input data (Figure 8.4) by means of a Turbo Pascal programme. All strain energy minimised structures reproduced the observed X-ray structures to a tolerance of 0.02Å in the Rh—L bonds lengths and 3° in the Rh—L—X and L—Rh—L bond angles[5]. The Rh(I) bond length and bond angle parameters outside the above criteria are listed below (Table 8.3).

[9] Boyd R.H., *J. Chem. Phys.*, **49**, 2574, (1968)

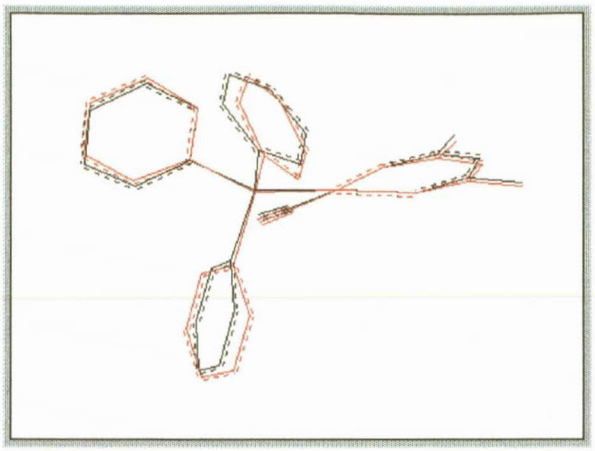

Figure 8.4: *An overlay view of the minimised structure*  *and the experimental X-ray determined structure*  .

	X-ray parameters	Computed parameters	Difference	
c:\mm8b\com02\acach.com				
RH(2) - P1(6)	2.2372	2.2678	-0.030600	**
c:\mm8b\com02\bphah.com				
RH(2) - P1(18)	2.2328	2.2670	-0.034200	**
O7(3)-RH(2)-P1(18)	94.310	97.564	-3.254000	**
RH(2)-P1(18)-CA(20)	117.317	114.107	3.210000	**
c:\mm8b\com02\bzaah.com				
O3(1) - RH(2)	2.0476	2.0724	-0.024800	**
RH(2) - P1(14)	2.2420	2.2667	-0.024700	**
c:\mm8b\com02\cacsmh.com				
RH(2) - C6(12)	1.8294	1.7925	0.036900	**
RH(2)-P1(11)-CA(13)	117.288	114.228	3.060000	**
RH(2)-C6(12)-O+(41)	171.503	176.181	-4.678000	**
c:\mm8b\com02\cupfh.com				
RH(2) - P1(6)	2.2314	2.2667	-0.035300	**
RH(2)-P1(6)-CA(11)	117.454	113.994	3.460000	**
c:\mm8b\com02\hacsmh.com				
RH(2) - C6(12)	1.8227	1.7976	0.025100	**

```
=============================================================
c:\mm8b\com02\macsmh.com
=============================================================
N4(  1) - RH(  2)     2.0877    2.1150   -0.027300          **
RH(  2) - C6( 10)     1.8365    1.7924    0.044100          **
=============================================================
c:\mm8b\com02\oxh.com
=============================================================
N5(  1) - RH(  2)     2.0981    2.1311   -0.033000          **
O5(  3)-RH(  2)-P1( 10)  91.312   95.789   -4.477000        **
=============================================================
c:\mm8b\com02\pich.com
=============================================================
RH(  2) - O5(  3)     2.0666    2.0414    0.025200          **
RH(  2)-P1( 10)-CA( 14) 121.164  116.612    4.552000        **
=============================================================
c:\mm8b\com02\sacach.com
=============================================================
RH(  2) - O3(  3)     2.0145    2.0350   -0.020500          **
RH(  2) - P1(  6)     2.2961    2.2664    0.029700          **
RH(  2)-C6(  7)-O+( 29) 180.000  175.358    4.642000        **
=============================================================
c:\mm8b\com02\salnrh.com
=============================================================
=============================================================
c:\mm8b\com02\tfdmaah.com
=============================================================
RH(  2) - O3(  3)     2.0588    2.0370    0.021800          **
=============================================================
c:\mm8b\com02\tfhdh.com
=============================================================
=============================================================
c:\mm8b\com02\tftmaah.com
=============================================================
RH(  2) - O3(  3)     2.0624    2.0346    0.027800          **
RH(  2) - P1(  9)     2.2366    2.2666   -0.030000          **
RH(  2) - C6( 10)     1.7646    1.7931   -0.028500          **
=============================================================
c:\mm8b\com02\troph.com
=============================================================
RH(  2) - P1( 11)     2.2328    2.2679   -0.035100          **
```

Table 8.3: *Rh(I) bond length and bond angle parameters outside the given tolerance criteria set for reproducibility of the minimised structures.*

*** = bond lengths greater than 0.02Å and bond angles greater than 3°.*

8.3 The prediction of the molecular structure of Rh(dbm)(CO)(PPh_3)

The credibility of the parameters used in constructing the Rh(I) Carbonyl Phosphine force field was further tested by the prediction of the molecular structure of Rh(dbm)(CO)(PPh_3) (Figure 8.5), a Rh(I) structure of which the X-ray crystallographic data is now known (Section 3.4.3) but were not added to the force field during its construction.

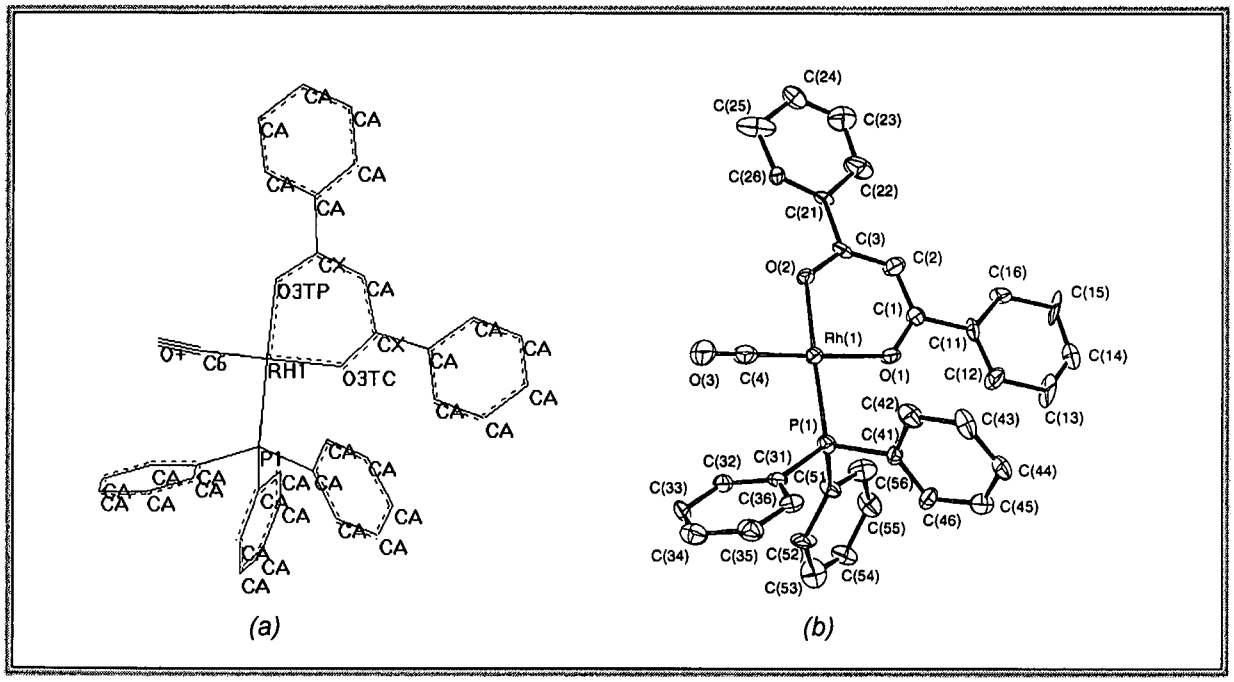

Figure 8.5: The structure of Rh(dbm)(CO)(PPh_3) predicted by the Rh(I) Carbonyl Phosphine force field, (a), versus the X-ray determined structure, (b).

The minimised Rh(dbm)(CO)(PPh_3) structure (Figure 8.5 (a)) reproduced the X-ray determined Rh(dbm)(CO)(PPh_3)[10] structure (Figure 8.5 (b)) also to a tolerance of 0.02Å in the Rh—L bonds lengths and 3° in the Rh—L—X and L—Rh—L bond angles (Table 8.4).

[10] Lamprecht Delanie, Lamprecht G.J., Botha J.M., Umakoshi K., Sasaki Y, *Acta Cryst.* **C53**, 1403, (1997)

Predicted structure of $Rh(dbm)(CO)(PPh_3)$		X-ray determined structure of $Rh(dbm)(CO)(PPh_3)$	
Rh1—P1	2.268 Å	Rh1—P1	2.237 Å
Rh1—O3TC	2.032 Å	Rh1—O1	2.038 Å
Rh1—O3TP	2.071 Å	Rh1—O2	2.081 Å
Rh1—C6	1.793 Å	Rh1—C4	1.812 Å
P1—Rh1—O3TC	92.4°	P1—Rh1—O1	87.7°
P1—Rh1—O3TP	176.0°	P1—Rh1—O2	175.2°
P1—Rh1—C6	89.4°	P1—Rh1—C4	91.1°
O3TC—Rh1—O3TP	87.1°	O1—Rh1—O2	88.5°
O3TC—Rh1—C6	176.5°	O1—Rh1—C4	175.3°
O3TP—Rh1—C6	90.8°	O2—Rh1—C4	92.9°
Rh1—P1—CA	114.0°	Rh1—P1—C31	119.8°
Rh1—P1—CA	115.5°	Rh1—P1—C51	113.4°
Rh1—P1—CA	111.9°	Rh1—P1—C51	110.7°
Rh1—O3TC—CX	131.3°	Rh1—O1—C1	127.5°
Rh1—O3TP—CX	129.3°	Rh1—O2—C3	125.1°
Rh1—C6—O+	176.7°	Rh1—C4—O3	177.4°

Table 8.4: Comparative bond lengths and bond angles of the predicted and X-ray determined structures of $Rh(dbm)(CO)(PPh_3)$.

8.4 The computation of a transition state during the oxidative addition of CH_3I to Rh(I) Carbonyl Phosphine complexes

The ligand "surface" in the space-filling mechanical models is representative of the points in space at which a repulsing interaction with other non-bonded atoms becomes important[11]. The cone angle is a rough measure of the extent of this repulsing surface from the vantage point of a metal centre. The cone angle, the most widely accepted approach assessing ligand steric effects, is that suggested by Tolman (Section 2.2). A limitation of Tolman's approach is that it is difficult to decide on an appropriate cone angle for complex ligands, in which the van der Waals "surface" is highly irregular.

In molecular mechanics, steric effects are exerted through the van der Waals interactions between all atoms separated by at least two other atoms in the connectivity diagram for the molecule[12].

An effective computational measure of ligand steric requirements must take into account that steric forces are short range and repulsing[13]. Secondly, it must permit

[11] Caffery M.L., Brown T.L., *Inorg. Chem.*, **30**, 3907, (1991)
[12] Brown T.L., *Inorg. Chem.*, **31**, 1286, (1992)
[13] Lee K.J., Brown T.L., *Inorg. Chem.*, **31**, 289, (1992)

evaluation of the steric effect of each ligand in an appropriate conformation; that is, one that is more or less typical of a ligand bound to a metal centre. Given the predominantly non-bonded repulsing nature of the steric term, the focus should be, not on the van der Waals interaction between ligand and metal, but only on the repulsing part of that interaction, for the lowest energy structure for the complex.

The steric parameter should be a measure of the steric effect exerted by the ligand in its reactions with a metal centre or that exerted when the ligand is bound to a metal undergoing a reaction. Individual ligands exert different effective steric demands from one reaction to the next, as a result of the steric and electronic characteristics of the transition state.

Based on the kinetic studies (Chapter 4), the proposed mechanism of the oxidative addition of CH_3I to Rh(I) Carbonyl Phosphine complexes is a nucleophilic attack by the Rhodium atom on the Carbon atom of the methyl iodide where a linear polar transition state (Figure 4. 21(a)) is formed which leads to *trans* addition. The possibility of a three-centred polar transition state (Figure 4.22), which normally leads to *cis* addition, cannot be ruled out[14]. The question as to whether the transition state is linear or three-centred was answered by the computation of the steric energy when CH_3I approaches the Rh(I) metal centre.

The optimised structure file of CH_3I was merged into the optimised $Rh(dbm)(CO)(PPh_3)$ structure file. The co-ordinates of the Rh(I) metal atom were translated to the origin (0 0 0). The x and y co-ordinates of CH_3I remained constant at their respective origin positions after translating whereas the z co-ordinates was varied from 0.5 Å to 5 Å. After each variation of the z co-ordinates of the Carbon atom in CH_3I, the CH_3I molecule was optimised relative to the stationary $Rh(dbm)(CO)(PPh_3)$ molecule. A single point calculation was then performed on the entire system[15] to determine the steric energy in $kcal.mol^{-1}$ (Figure 8.7).

The force field predicted only three approaches of the CH_3I to the Rh(I) metal centre, two of which would lead to a concerted three-centred mechanism and one of which would lead to a S_N2 mechanism (Figure 8.6).

---

[14] van Zyl G.J., Lamprecht G.J., Leipoldt J.G., Swaddle T.W., *Inorg. Chim. Acta*, **143**, 223, (1988)
[15] *HyperChem(TM), Reference, Molecular Visualization and Simulation*, Hypercube, Inc.,(1994)

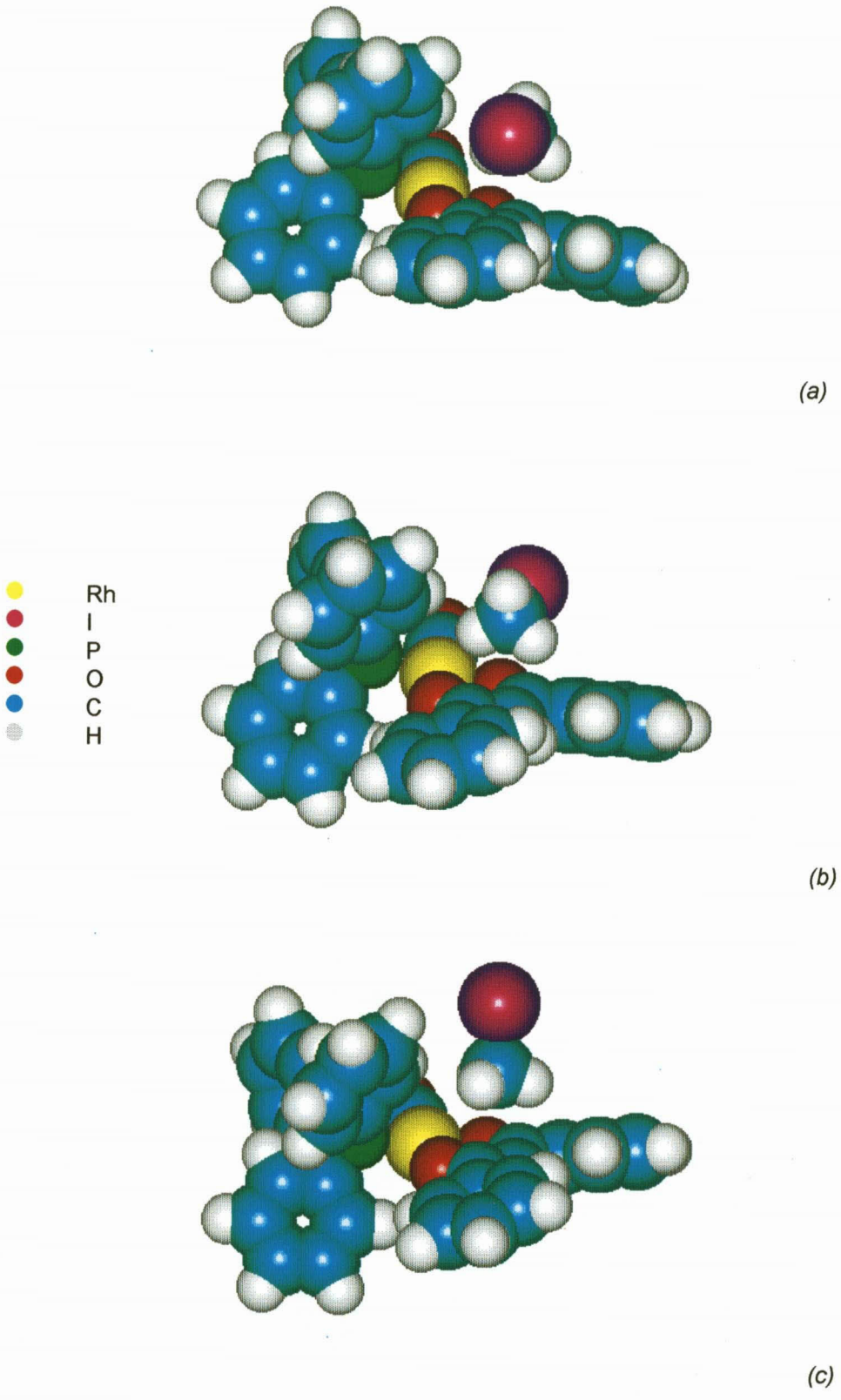

Figure 8.6: *The three CH_3I approaches calculated by the force field.*
(a) and (b) approaches a concerted three-centred mechanism
(c) approaches a linear S_N2 mechanism

The S_N2 approach was more stable, with lower steric energy values, than the concerted three-centred approach (Figure 8.7) and was independent of the initial z co-ordinate translation of the carbon atom in CH_3I.

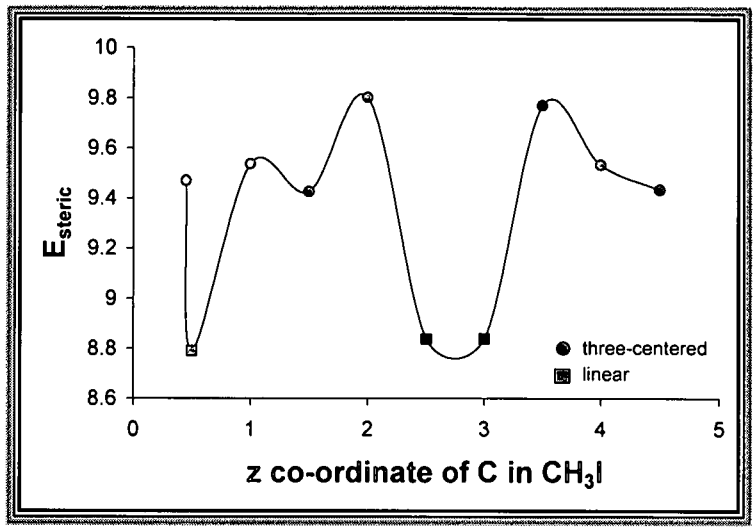

Figure 8.7: *Plot of the steric energy obtained during optimisation of CH_3I approaching $Rh(dbm)(CO)(PPh_3)$ versus the initial z co-ordinate of the Carbon atom in CH_3I.*

8.5 The molecular mechanics in perspective

The main purpose of the development of a Rh(I) Carbonyl Phosphine force field was to predict the molecular structure of Rh(I) complexes as well as to compute possible intermediates or transition states during the oxidative addition of CH_3I to these complexes.

8.5.1 The prediction of $Rh(dbm)(CO)(PPh_3)$

The excellent agreement between the observed and computed structures suggests that the set of parameters chosen for molecular mechanics calculation was appropriate (Figure 8.4).

Comparing the predicted square planar $Rh(dbm)(CO)(PPh_3)$ structure with the X-ray crystallographic structure (Figure 8.5 and Table 8.4) also suggests that the parameters chosen for constructing the force field were appropriate. The most conspicuous deviation in the bond length and bond angle criteria of

0.02Å and 3° was the Rh1—P1 bond length. Considering X-ray crystallographic data of Rh(I) Carbonyl Phosphine complexes, the estimated standard deviation of a Rh—P bond is very small (0.001 Å) relative to the estimated standard deviations of the other bond lengths and can therefore explain the relatively large deviation in the computed and X-ray determined Rh—P bond lengths.

8.5.2 The prediction of S_N2 mechanism

The computation of the transition state during the oxidative addition of CH_3I to $Rh(dbm)(CO)(PPh_3)$ suggests a concerted three-centred transition state (Figure 8.6 (a) and (b)) and a linear transition state (Figure 8.6 (c)).

The steric energy calculated for the above was lower for the linear transition state than for the concerted three-centred transition state. Oxidative addition of CH_3I to the Rh(I) Carbonyl Phosphine complexes will therefore rather occur via a S_N2 mechanics than a concerted three-centred mechanism. These results were also observed during ab initio calculations[16].

The second reaction path during oxidative addition of CH_3I to Rh(I) carbonyl Phosphine complexes is an isomerisation step (Figure 4.21). A linear transition state will lead to *trans* addition (Section 2.2.1) of CH_3I and isomerisation will therefore form a *cis* Rh(III) Carbonyl Phosphine isomer as final product (Section 4.5.4).

The *cis* final isomer was only proved by means of X-ray determined structures of similar Rh(I) Carbonyl Phosphine complexes[17,18]. Unfortunately only a few Rh(III) Carbonyl Phosphine structures have been isolated to date and it was therefore not possible to develop an accurate Rh(III) Carbonyl Phosphine force field which could have been used to predict the most stable final isomer (*trans* Rh(III) Carbonyl Phosphine or *cis* Rh(III) Carbonyl Phosphine) formed during oxidative addition of CH_3I to Rh(I) Carbonyl Phosphine complexes.

---

[16] Griffin T.R., Cook D.B., Haynes A., Pearson J.M., Monti D., Morris G.E., *J. Am. Chem. Soc.*, **118**, 3029, (1996)
[17] Basson S.S., Leipoldt J.G., Roodt A., Venter J.A., *Inorg. Chim. Acta*, **128**, 31, (1987)
[18] Conradie J., Lamprecht G.J., Swarts J.C., *to be published*

APPENDIX 1:
ABBREVIATIONS

$\Delta\overline{V}^{\circ *}$	Molar volume of activation
$\Delta G^{\circ *}$	Standard free energy of activation
$\Delta H^{\circ *}$	Standard enthalpy of activation
$\Delta S^{\circ *}$	Standard entropy of activation
Å	Angstrom
CV	Cyclic Voltammetry
Fc	Ferrocene
K*	Equilibrium constant of the activation state
k_1	First order rate constant
k_2	Second order rate constant
Ka	Acid dissociation constant
k_{obs}	Observed rate constant
L	Ligand
M	Metal
Ph	Phenyl
py	Pyridine
SCE	Standard Calomel Electrode

APPENDIX 2:
REAGENTS

Rhodium(III)chloride Trihydrate: $(RhCl_3.3H_2O)$
Merck for synthesis
38 % Rhodium
$M_r = 263.31\ g.mol^{-1}$

N N'-Dimethylformamide (DMF): $((CH_3)_2N(CO)H)$
Merck
99.5 %
b.p. = 153 °C (760 mmHg)

1,3-Diphenyl-1,3-propanedione (Dibenzoylmethane) (dbm): $C_{15}H_{12}O_2$
Merck for synthesis
$M_r = 224.26\ g.mol^{-1}$

1-Phenyl-1,3-propanedione (Benzoylacetone) (ba): $C_{10}H_{10}O_2$
Merck for synthesis
$M_r = 162.19\ g.mol^{-1}$

1-Phenyl-4,4,4-trifluoro-1,3-butanedione (Benzoyltrifluoroacetone) (btfa): $C_{10}H_7O_2F_3$
Merck for synthesis
$M_r = 216.16\ g.mol^{-1}$

1,1,1-Triflouro-2,4-pentanedione (Triflouroacethylacetone) (tfaa): $C_5H_5O_2F_3$
Merck for synthesis
$M_r = 154.09\ g.mol^{-1}$

Triphenylphosphine (PPh_3): $(C_6H_5)_3P$
Merck for synthesis
$M_r = 262.26\ g.mol^{-1}$

Methyl Iodide: CH_3I
Merck for synthesis
Stabilised in Silver
$M_r = 141.94\ g.mol^{-1}$

Tetrabutylammonium hexafluorophosphate (TBAHFP): $C_{16}H_{36}F_6NP$
Fluka
$M_r = 387{,}43\ g.mol^{-1}$

Silver nitrate: $AgNO_3$
BDH Chemicals
$M_r = 169{,}87\ g.mol^{-1}$

Benzyltriethylammonium chloride $[B_ZN(Et)_3]^+Cl^-$:	$C_6H_5CH_2N(C_2H_5)_3Cl$
	Aldrich
	M_r = 227.78 g.mol^{-1}
Tetraethylammonium bromide:	$C_8H_{20}BrN$
	Fluka
	M_r = 210.16 g.mol^{-1}

APPENDIX 3:

THE BEER - LAMBERT LAW

The reduction of intensity, δI, that occurs when light passes through a layer of thickness, $\delta \ell$, containing an absorbing species, C, at a molar concentration, [C], is proportional to the thickness of the layer, the concentration of the absorbing species and the intensity of the light.

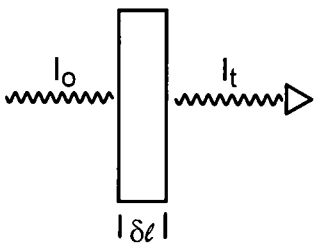

$$\frac{-\partial I_t}{\partial \ell} \propto IC = \varepsilon IC$$

$$\ln\left(\frac{I_t}{I_\circ}\right) = -\varepsilon C \ell$$

$$\log\left(\frac{I_t}{I_\circ}\right) = -\frac{\varepsilon}{2.303} C\ell \text{ or } = -\varepsilon' C\ell$$

but $\frac{I_t}{I_\circ} = T$ and $A = -\log T$

therefor $A = \varepsilon' C\ell$

ε = molar absorption coeficient (extinction coeficient)

T = transmission

A = absorption

APPENDIX 4:

THE EYRING RELATIONSHIP

Consider the following chemical equation:

$$A + B \overset{K^*}{\rightleftharpoons} (A,B)^* \xrightarrow{k_2} AB$$

The reaction rate is given by $-\frac{\partial[(A,B)^*]}{\partial t} = \nu[(A,B)^*]$.

The transition state or activated complex, $[(A,B)^*]$, is regarded as a normal molecule in every respect except that one of its vibrations is equivalent to a translational degree of freedom along the reaction co-ordinate which leads to the formation of products. It this degree of freedom is treated as a classical vibration, its frequency ν, at temperature T, is given by:

$\nu = \frac{k_B T}{h}$ k_B = Boltzman constant and h = Planck constant

Therefore:

$$-\frac{\partial[(A,B)^*]}{\partial t} = \frac{k_B T}{h}[(A,B)^*], \text{but} -\frac{\partial[(A,B)^*]}{\partial t} = k_2[A][B] \text{because} -\frac{\partial[(A,B)^*]}{\partial t} = \frac{\partial[(A,B)^*]}{\partial t}$$

$$\therefore k_2[A][B] = \frac{k_B T}{h}[(A,B)^*]$$

$$k_B = \frac{R}{N}$$

$$k_2[A][B] = \frac{RT}{Nh}[(A,B)^*]$$

$$k_2 = \frac{RT}{Nh} \cdot \frac{[(A,B)^*]}{[A][B]}$$

$$\therefore k_2 = \frac{RT}{Nh} \cdot K^*$$

R = gas constant and N = Avogradro's constant

Like any other equilibrium constant, K* is related to the free energy of formation $\Delta G^{\circ *}$ of the activated complex by the thermodynamic expression: $\Delta G^{\circ *} = -RT\ln K^{*}$

$$K^{*} = e^{-\frac{\Delta G^{\circ *}}{RT}}$$

$$\therefore k_2 = \frac{RT}{Nh} e^{-\frac{\Delta G^{\circ *}}{RT}}$$

Since $\Delta G^{\circ *}$ is related to the heat of activation, $\Delta H^{\circ *}$, and the entropy of activation, $\Delta S^{\circ *}$, by the thermodynamic relationship of $\Delta G^{\circ *} = \Delta H^{\circ *} - T\Delta S^{\circ *}$,

$$k_2 = \frac{RT}{Nh} e^{\frac{\Delta S^{\circ *}}{R}} \cdot e^{-\frac{\Delta H^{\circ *}}{RT}}$$

APPENDIX 5:

NEW ATOM TYPES ENTRIES IN THE *CHEM.RUL* FILE

```
; Type rules for the MM+ force field
;
forcefield(mm+)

Rh:
;Rhodium
        =RH1.    ; numerical type 73    (ADDED 6/2/95)

C:
; Carbon

; carbon in a metal carbonyl    (ADDED,16/6/98)
      is it sp?
      connected to (#O)?
      =C6.  ; numerical type 74

; aromatic carbons in bidentate ligand (6-ring) (ADDED,16/6/98)
      in 6 ring?
      connected to (~*)(~*)?
      =CX.  ; numerical type 76

; aromatic carbons in bidentate ligand (5-ring) (ADDED,16/6/98)
      in 5 ring?
      connected to (~*)(~*)?
      =CY.  ; numerical type 77

; alkane carbons (ADDED,16/6/98)
      is it sp3?
      connected to (-X)?
      =C5.  ; numerical type 68

      connected to (-S)?
      =C7.  ; numerical type 44

      connected to (-*)?
      =C4.  ; numerical type 1

N:
; Nitrogen

; sp2 nitrogen in bidentate ligand (6-ring) (ADDED,17/6/98)
      is it sp2?
      in 5 ring?
      connected to (~O)?
      =N6.  ; numerical type 80

      is it sp2?
      in 5 ring?
      connected to (~C)?
      =N5.  ; numerical type 83

      is it sp2?
      in 6 ring?
      connected to (~C)?
```

```
      =N4.   ; numerical type 82

O:
; Oxygen

; metallic carbonyl oxygen  (ADDED 6/2/95)
      connected to #C?
      =O+.   ;numerical type 75

; aromatic oxygen in bidentate ligand (5-ring) (ADDED 17/6/98)
      is it sp2?
      in 5 ring?
      connected to (C)?
      =O5.   ; numerical type 85

; aromatic oxygen in bidentate ligand (5-ring) (ADDED 17/6/98)
      is it sp2?
      in 5 ring?
      connected to (N)?
      =O7.   ; numerical type 86

; aromatic oxygen in bidentate ligand (6-ring) (ADDED 17/6/98)
      is it sp2?
      in 6 ring?
      connected to (C)?
      =O3.   ; numerical type 78

P:
; Phosphorus

; phosphine
      connected to (-C)(-C)(-C)?
      =P1.   ; numerical type 84

S:
; Sulphur

; aromatic sulfide in bidentate ligand (5-ring) (ADDED 18/6/98)
      in 5 ring?
      connected to (C)?
      =S5. ; numerical type 81

; aromatic sulfide in bidentate ligand (6-ring) (ADDED 18/6/98)
      in 6 ring?
      connected to (C)?
      =S7. ; numerical type 79
```

APPENDIX 6:

PARAMETER SETS OF THE RH(I) CARBONYL PHOSPHINE FORCE FIELD

Bond Length Parameter file (mmpstr.txt)

T1	T2	KS	L0	L1	DIPOLE	REMARK
c4	c4	4.400	1.520	0.000	0.000	"average"
c4	h	4.600	1.027	0.000	0.000	"average"
c3	h	4.600	0.930	0.000	0.000	"average"
o2	ho	4.600	0.820	0.000	-1.115	"average"
ca	ca	8.065	1.394	0.000	0.000	"average"
c3	ca	9.600	1.492	0.000	0.000	"average"
ca	h	4.600	1.051	0.000	0.000	"average"
ca	o2	6.000	1.354	0.000	0.001	"average"
o3tp	rh1	5.360	2.075	0.000	0.440	"Lamprecht, c4-o2, MM2"
o3tp	cx	6.000	1.272	0.000	0.001	"Lamprecht, ca-o2, MM2"
rh1	o3tc	5.360	2.037	0.000	0.440	"Lamprecht, c4-o2, MM2"
rh1	p1	2.910	2.256	0.000	0.830	"Lamprecht, c4-p, MM2"
rh1	c6	4.400	1.800	0.000	0.300	"Lamprecht, c4-co, MM2"
o3tc	cx	6.000	1.278	0.000	0.001	"Lamprecht, ca-o2, MM2"
cx	ca	8.065	1.417	0.000	0.000	"Lamprecht, ca-ca, MM2"
cx	c4	4.400	1.525	0.000	0.300	"Lamprecht, c4-ca, MM2"
p1	ca	2.910	1.827	0.000	1.040	"Lamprecht, ca-p, c3->ca"
c6	o+	10.80	1.168	0.000	2.600	"Lamprecht, co-o1, MM2"
o5tp	rh1	5.360	2.085	0.000	0.440	"Lamprecht, c4-o2, MM2"
o5tp	cy	6.000	1.301	0.000	0.001	"Lamprecht, ca-o2, MM2"
rh1	o7tc	5.360	2.035	0.000	0.440	"Lamprecht, c4-o2, MM2"
o7tc	n6	10.000	1.349	0.000	0.000	"Lamprecht, o2-n2, MM2"
n6	cy	10.000	1.311	0.000	1.300	"Lamprecht, ca-n2, c3->ca"
n6	ca	10.000	1.443	0.000	1.300	"Lamprecht, ca-n2, c3->ca"
cy	ca	8.065	1.480	0.000	0.000	"Lamprecht, ca-ca, MM2"
n4tp	rh1	3.520	2.102	0.000	1.470	"Lamprecht, c4-n2, MM2"
n4tp	cx	10.00	1.304	0.000	1.300	"Lamprecht, ca-n2, c3->ca"
n4tp	c4	3.520	1.491	0.000	1.470	"Lamprecht, c4-n2, MM2"
rh1	s7tc	3.213	2.295	0.000	1.200	"Lamprecht, c4-s2, MM2"
s7tc	cx	6.471	1.712	0.000	1.925	"Lamprecht, ca-sa, c3->ca"
cx	s2	6.471	1.770	0.000	1.925	"Lamprecht, ca-sa, c3->ca"
s2	c7	3.213	1.774	0.000	1.200	"Lamprecht, c4-s2, MM2"
c7	h	4.600	1.080	0.000	0.000	"Lamprecht, c4-h, MM2"
o7tp	rh1	5.360	2.064	0.000	0.440	"Lamprecht, c4-o2, MM2"
o7tp	n6	10.000	1.300	0.000	0.000	"Lamprecht, o2-n2, MM2"
n6	n6	10.720	1.277	0.000	0.000	"Lamprecht, na-na, MM2"
s7tp	rh1	3.213	2.297	0.000	1.200	"Lamprecht, c4-s2, MM2"
s7tp	cx	6.471	1.710	0.000	1.925	"Lamprecht, ca-sa, c3->ca"
rh1	n4tc	3.520	2.019	0.000	1.470	"Lamprecht, c4-n2, MM2"
n4tc	cx	10.00	1.299	0.000	1.300	"Lamprecht, ca-n2, c3->ca"
n4tc	hn	5.900	0.762	0.000	-1.310	"Lamprecht, n2-hv, MM2"
n5tp	rh1	3.520	2.095	0.000	1.470	"Lamprecht, c4-n2, MM2"
n5tp	ca	10.00	1.362	0.000	1.300	"Lamprecht, ca-n2, c3->ca"
n5tp	cx	10.00	1.362	0.000	1.300	"Lamprecht, ca-n2, c3->ca"
rh1	o5tc	5.360	2.047	0.000	0.440	"Lamprecht, c4-o2, MM2"
o5tc	ca	6.000	1.328	0.000	0.001	"Lamprecht, ca-o2, MM2"
cx	h	4.600	1.080	0.000	0.000	"Lamprecht, ca-h, MM2"
o5tc	co	5.050	1.219	0.000	-0.200	"Lamprecht, co-o2, MM2"
n4tp	ca	10.00	1.473	0.000	1.300	"Lamprecht, ca-n2, c3->ca"
o3tc	ca	6.000	1.296	0.000	0.001	"Lamprecht, ca-o2, MM2"

```
cx      c5      4.400    1.518    0.000   0.300    "Lamprecht, c4-ca, MM2"
c5      f       5.100    1.312    0.000   1.820    "Lamprecht, c4-f, MM2"
o5tc    cy      6.000    1.300    0.000   0.001    "Lamprecht, ca-o2, MM2"
cy      cy      8.065    1.461    0.000   0.000    "Lamprecht, ca-ca, MM2"
cy      c3      9.600    1.404    0.000   0.000    "Lamprecht, c3-ca, c3->ca"
```

Bond Angle Parameter file (mmpben.txt)

```
T1      T2      T3      KS       TYPE1    TYPE2    TYPE3    REMARK
c4      c4      c4      0.450    111.0    109.5    109.5    "average"
c4      c4      h       0.360    109.0    109.4    110.0    "average"
h       c4      h       0.320    108.9    109.0    109.5    "average"
hn      n3      hn      0.500    120.0    0.0      0.0      "average"
h       ca      ca      0.360    120.9    120.5    0.0      "average"
ca      ca      ca      0.430    120.0    0.0      0.0      "average"
c3      ca      ca      0.430    121.3    0.0      0.0      "average"
ca      c3      h       0.360    112.4    120.5    0.0      "average"
ca      ca      o2      0.700    120.3    0.0      0.0      "average"
rh1     o3tp    cx      0.770    125.7    0.0      0.0      "Lamprecht, c4-c2-ca, c3->ca"
o3tp    rh1     o3tc    0.460    87.6     97.0     102.2    "Lamprecht, o2-c4-o2, MM2"
o3tp    rh1     p1      0.480    176.8    0.0      0.0      "Lamprecht, c4-c4-p, MM2"
o3tp    rh1     c6      0.700    92.0     0.0      0.0      "Lamprecht, co-c4-o2, MM2"
o3tc    rh1     p1      0.480    90.6     0.0      0.0      "Lamprecht, c4-c4-p, MM2"
o3tc    rh1     c6      0.700    177.1    0.0      0.0      "Lamprecht, co-c4-o2, MM2"
p1      rh1     c6      0.480    88.8     0.0      0.0      "Lamprecht, c4-c4-p, MM2"
rh1     o3tc    cx      0.770    129.8    0.0      0.0      "Lamprecht, c4-o2-ca, c3->ca"
o3tc    cx      ca      0.700    127.7    0.0      0.0      "Lamprecht, ca-ca-o2, c3->ca"
o3tc    cx      c4      0.500    116.2    0.0      0.0      "Lamprecht, c4-ca-o2, c3->ca"
ca      cx      c4      0.550    115.1    122.0    120.0    "Lamprecht, c4-ca-ca, MM2"
o3tp    cx      ca      0.700    130.1    0.0      0.0      "Lamprecht, ca-ca-o2, c3->ca"
o3tp    cx      c4      0.500    113.5    0.0      0.0      "Lamprecht, c4-ca-o2, c3->ca"
rh1     p1      ca      0.480    114.6    0.0      0.0      "Lamprecht, c4-p-ca, c3->ca"
ca      p1      ca      0.480    103.9    0.0      0.0      "Lamprecht, ca-p-ca, c3->ca"
rh1     c6      o+      0.460    176.8    0.0      0.0      "Lamprecht, ca-p-ca, MM2"
p1      ca      ca      0.380    120.0    0.0      0.0      "Lamprecht, ca-ca-p, c3->ca"
cx      ca      cx      0.430    123.1    0.0      0.0      "Lamprecht, ca-ca-ca, c3->ca"
cx      ca      h       0.360    119.8    120.5    0.0      "Lamprecht, h-ca-ca, c3->ca"
cx      c4      h       0.360    109.7    109.4    110.0    "Lamprecht, h-c4-ca, MM2"
rh1     o5tp    cy      0.770    113.5    0.0      0.0      "Lamprecht, c4-o2-ca, c3->ca"
o5tp    rh1     o7tc    0.460    78.4     97.0     102.2    "Lamprecht, o2-c4-o2, MM2"
o5tp    rh1     p1      0.480    173.4    0.0      0.0      "Lamprecht, c4-c4-p, MM2"
o5tp    rh1     c6      0.700    98.0     0.0      0.0      "Lamprecht, co-c4-o2, MM2"
o7tc    rh1     p1      0.480    95.6     0.0      0.0      "Lamprecht, c4-c4-p, MM2"
o7tc    rh1     c6      0.700    174.7    0.0      0.0      "Lamprecht, co-c4-o2, MM2"
rh1     o7tc    n6      0.770    111.1    0.0      0.0      "Lamprecht, c4-o2-ca, c3->ca"
o7tc    n6      cy      0.700    119.1    0.0      0.0      "Lamprecht, ca-ca-o2, c3->ca"
o7tc    n6      ca      0.700    115.6    0.0      0.0      "Lamprecht, ca-ca-o2, c3->ca"
cy      n6      ca      0.400    127.1    0.0      0.0      "Lamprecht, ca-n2-ca, c3->ca"
o5tp    cy      n6      0.700    119.0    0.0      0.0      "Lamprecht, ca-ca-o2, c3->ca"
o5tp    cy      ca      0.700    117.7    0.0      0.0      "Lamprecht, ca-ca-o2, c3->ca"
n6      cy      ca      0.500    123.4    0.0      0.0      "Lamprecht, ca-ca-n2, c3->ca"
cy      ca      ca      0.430    119.5    0.0      0.0      "Lamprecht, ca-ca-ca, MM2"
n6      ca      ca      0.500    118.4    0.0      0.0      "Lamprecht, ca-ca-n2, c3->ca"
cx      ca      c4      0.550    116.7    122.0    120.0    "Lamprecht, c4-ca-ca, MM2"
rh1     n4tp    cx      0.630    126.8    0.0      0.0      "Lamprecht, c4-n2-ca, c3->ca"
rh1     n4tp    c4      0.760    117.2    0.0      0.0      "Lamprecht, c4-n2-c4, MM2"
cx      n4tp    c4      0.630    114.8    0.0      0.0      "Lamprecht, c4-n2-ca, c3->ca"
n4tp    rh1     s7tc    0.580    93.7     108.0    114.8    "Lamprecht, n2-c4-s2, MM2"
n4tp    rh1     p1      0.480    177.3    0.0      0.0      "Lamprecht, c4-c4-p, MM2"
n4tp    rh1     c6      0.820    95.3     111.1    109.8    "Lamprecht, co-c4-n2, MM2"
s7tc    rh1     p1      0.480    86.6     0.0      0.0      "Lamprecht, c4-c4-p, MM2"
s7tc    rh1     c6      0.420    169.4    0.0      0.0      "Lamprecht, co-c4-s2, MM2"
rh1     s7tc    cx      0.680    111.6    0.0      0.0      "Lamprecht, ca-sa-ca, c3->ca"
s7tc    cx      s2      0.420    116.6    0.0      0.0      "Lamprecht, s2-c4-s2, MM2"
s7tc    cx      ca      0.380    128.2    0.0      0.0      "Lamprecht, ca-ca-sa, c3->ca"
s2      cx      ca      0.380    114.8    0.0      0.0      "Lamprecht, ca-ca-sa, c3->ca"
cx      s2      c7      0.720    105.8    0.0      0.0      "Lamprecht, c4-s2-c4, MM2"
```

n4tp	cx	ca	0.500	128.6	0.0	0.0	"Lamprecht, ca-ca-n2, c3->ca"
n4tp	cx	c4	0.550	123.1	122.0	120.0	"Lamprecht, c4-ca-ca, MM2"
cx	c4	c4	0.450	108.2	109.5	109.5	"Lamprecht, c4-c4-ca, MM2"
n4tp	c4	c4	0.500	112.7	110.8	109.3	"Lamprecht, c4-c4-n2, MM2"
n4tp	c4	h	0.420	108.6	0.0	0.0	"Lamprecht, h-c4-n2, MM2"
s2	c7	h	0.360	109.4	112.0	109.3	"Lamprecht, h-c4-s2, MM2"
h	c7	h	0.320	109.5	109.0	109.5	"Lamprecht, h-c4-h, MM2"
rh1	o7tp	n6	0.770	115.4	0.0	0.0	"Lamprecht, c4-o2-ca, c3->ca"
o7tp	rh1	o7tc	0.460	76.6	97.0	102.2	"Lamprecht, o2-c4-o2, MM2"
o7tp	rh1	p1	0.480	172.6	0.0	0.0	"Lamprecht, c4-c4-p, MM2"
o7tp	rh1	c6	0.700	98.1	0.0	0.0	"Lamprecht, co-c4-o2, MM2"
o7tc	n6	n6	0.400	123.5	0.0	0.0	"Lamprecht, ca-na-na, c3->ca"
n6	n6	ca	0.400	119.0	0.0	0.0	"Lamprecht, ca-na-na, c3->ca"
o7tp	n6	n6	0.400	113.6	0.0	0.0	"Lamprecht, ca-na-na, c3->ca"
rh1	s7tp	cx	0.680	111.2	0.0	0.0	"Lamprecht, ca-sa-ca, c3->ca"
s7tp	rh1	n4tc	0.580	91.3	108.0	114.8	"Lamprecht, n2-c4-s2, MM2"
s7tp	rh1	p1	0.480	177.9	0.0	0.0	"Lamprecht, c4-c4-p, MM2"
s7tp	rh1	c6	0.420	88.9	0.0	0.0	"Lamprecht, co-c4-s2, MM2"
n4tc	rh1	p1	0.480	90.9	0.0	0.0	"Lamprecht, c4-c4-p, MM2"
n4tc	rh1	c6	0.820	177.2	111.1	109.8	"Lamprecht, co-c4-n2, MM2"
rh1	n4tc	cx	0.630	133.8	0.0	0.0	"Lamprecht, c4-n2-ca, c3->ca"
rh1	n4tc	hn	0.440	120.3	0.0	0.0	"Lamprecht, c4-n2-hv, MM2"
cx	n4tc	hn	0.500	105.9	0.0	0.0	"Lamprecht, ca-n2-hv, c3->ca"
n4tc	cx	ca	0.500	127.8	0.0	0.0	"Lamprecht, ca-ca-n2, c3->ca"
n4tc	cx	c4	0.550	122.1	122.0	120.0	"Lamprecht, c4-ca-ca, MM2"
s7tp	cx	ca	0.380	128.4	0.0	0.0	"Lamprecht, ca-ca-sa, c3->ca"
s7tp	cx	s2	0.420	118.1	0.0	0.0	"Lamprecht, s2-c4-s2, MM2"
rh1	n5tp	ca	0.630	112.3	0.0	0.0	"Lamprecht, c4-n2-ca, c3->ca"
rh1	n5tp	cx	0.630	127.1	0.0	0.0	"Lamprecht, c4-n2-ca, c3->ca"
ca	n5tp	cx	0.400	120.6	0.0	0.0	"Lamprecht, ca-n2-ca, c3->ca"
n5tp	rh1	o5tc	0.700	79.5	0.0	0.0	"Lamprecht, ca-c4-o2, c3->ca"
n5tp	rh1	p1	0.480	170.1	0.0	0.0	"Lamprecht, c4-c4-p, MM2"
n5tp	rh1	c6	0.820	96.6	111.1	109.8	"Lamprecht, co-c4-n2, MM2"
o5tc	rh1	p1	0.480	93.0	0.0	0.0	"Lamprecht, c4-c4-p, MM2"
o5tc	rh1	c6	0.700	175.1	0.0	0.0	"Lamprecht, co-c4-o2, MM2"
rh1	o5tc	ca	0.770	144.4	0.0	0.0	"Lamprecht, c4-o2-ca, c3->ca"
o5tc	ca	ca	0.700	120.4	0.0	0.0	"Lamprecht, ca-ca-o2, c3->ca"
n5tp	ca	ca	0.500	120.7	0.0	0.0	"Lamprecht, ca-ca-n2, c3->ca"
n5tp	cx	ca	0.500	119.3	0.0	0.0	"Lamprecht, ca-ca-n2, c3->ca"
n5tp	cx	h	0.300	120.3	0.0	0.0	"Lamprecht, h-ca-n2, c3->ca"
ca	cx	h	0.360	118.9	120.5	0.0	"Lamprecht, h-ca-ca, MM2"
ca	ca	cx	0.430	120.1	0.0	0.0	"Lamprecht, ca-ca-ca, MM2"
rh1	o5tc	co	0.600	116.6	0.0	0.0	"Lamprecht, c4-o2-co, MM2"
o5tc	co	ca	0.700	115.7	0.0	0.0	"Lamprecht, ca-co-o2, c3->ca"
o5tc	co	o1	0.800	125.4	0.0	0.0	"Lamprecht, o2-co-o1, MM2"
n5tp	ca	co	0.600	115.1	117.6	0.0	"Lamprecht, ca-ca-co, c3->ca"
s7tp	rh1	o3tc	0.700	91.9	0.0	0.0	"Lamprecht, ca-c4-o2, c3->ca"
s7tp	cx	c4	0.550	112.1	122.0	120.0	"Lamprecht, c4-ca-ca, MM2"
rh1	n4tp	ca	0.630	121.7	0.0	0.0	"Lamprecht, c4-n2-ca, c3->ca"
cx	n4tp	ca	0.400	113.9	0.0	0.0	"Lamprecht, ca-n2-ca, c3->ca"
n4tp	rh1	o3tc	0.700	88.7	0.0	0.0	"Lamprecht, ca-c4-o2, c3->ca"
rh1	o3tc	ca	0.770	129.3	0.0	0.0	"Lamprecht, c4-o2-ca, c3->ca"
o3tc	ca	ca	0.700	120.5	0.0	0.0	"Lamprecht, ca-ca-o2, c3->ca"
n4tp	cx	h	0.300	116.2	0.0	0.0	"Lamprecht, h-ca-n2, c3->ca"
n4tp	ca	ca	0.500	116.8	0.0	0.0	"Lamprecht, ca-ca-n2, c3->ca"
o3tp	cx	c5	0.500	111.8	0.0	0.0	"Lamprecht, c4-ca-o2, c3->ca"
c5	cx	ca	0.550	115.9	122.0	120.0	"Lamprecht, c4-ca-ca, MM2"
cx	c5	f	0.650	113.3	0.0	0.0	"Lamprecht, ca-c4-f, c3->ca"
f	c5	f	1.070	105.2	0.0	0.0	"Lamprecht, f-c4-f, MM2"
o5tp	rh1	o5tc	0.460	77.8	97.0	102.2	"Lamprecht, o2-c4-o2, MM2"
rh1	o5tc	cy	0.770	116.1	0.0	0.0	"Lamprecht, c4-o2-ca, c3->ca"
o5tc	cy	cy	0.700	115.9	0.0	0.0	"Lamprecht, ca-ca-o2, c3->ca"
o5tc	cy	c3	0.700	118.1	0.0	0.0	"Lamprecht, c3-ca-o2, c3->ca"
cy	cy	c3	0.430	126.8	0.0	0.0	"Lamprecht, c3-ca-ca, c3->ca"
o5tp	cy	cy	0.700	115.2	0.0	0.0	"Lamprecht, ca-ca-o2, c3->ca
o5tp	cy	c3	0.700	117.3	0.0	0.0	"Lamprecht, c3-ca-o2, c3->ca
cy	c3	c3	0.430	128.3	0.0	0.0	"Lamprecht, c3-c3-ca, c3->ca"
cy	c3	h	0.360	115.9	120.5	0.0	"Lamprecht, ca-c3-h, c3->ca"

Torsion Parameter file (mmptor.txt)

T1	T2	T3	T4	V1	V2	V3	REMARK
c4	c4	c4	c4	0.20	0.27	0.09	"Allinger, MM2 (1991)"
c4	c4	c4	h	0.00	0.00	0.27	"Allinger, MM2 (1991)"
h	c4	c4	h	0.00	0.00	0.24	"Allinger, MM2 (1991)"
c4	c4	c4	ca	0.17	0.27	0.09	"Allinger, MM2 (1991)"
h	c4	c4	ca	0.00	0.00	0.50	"Allinger, MM2 (1991)"
c4	c4	ca	ca	-0.44	0.24	0.06	"Allinger, MM2 (1991)"
c4	ca	ca	c4	-0.10	9.00	0.00	"Allinger, MM2 (1991)"
c4	ca	ca	h	0.00	9.00	0.00	"Allinger, MM2 (1991)"
h	c4	ca	ca	0.00	0.00	-0.24	"Allinger, MM2 (1991)"
h	ca	ca	h	0.00	15.00	0.00	"theoretical"
c4	ca	ca	ca	-0.27	9.00	0.00	"Allinger, MM2 (1991)"
ca	c4	ca	ca	0.10	0.00	0.50	"Allinger, MM2 (1991)"
h	ca	ca	ca	0.00	5.41	-1.06	"Allinger, MM2 (1991)"
ca	ca	ca	ca	-0.93	4.80	0.00	"theoretical"
o3tp	rh1	o3tc	cx	0.00	0.00	0.00	"Lamprecht"
o3tp	rh1	p1	ca	0.00	0.00	0.00	"Lamprecht"
o3tp	rh1	c6	o+	0.00	0.00	0.00	"Lamprecht"
o3tp	cx	ca	cx	0.00	16.25	0.00	"Lamprecht, ca-ca-ca-o2, c3->ca"
o3tp	cx	ca	h	0.00	16.25	0.00	"Lamprecht, h-ca-ca-o2, c3->ca"
o3tp	cx	c4	h	0.00	0.00	0.54	"Lamprecht, h-c4-ca-o2, c3->ca"
rh1	o3tp	cx	ca	3.53	2.30	-3.53	"Lamprecht, ca-ca-o2-c4, c3->ca"
rh1	o3tp	cx	c4	2.30	4.00	0.00	"Lamprecht, c4-ca-o2-c4, c3->ca"
rh1	o3tc	cx	ca	3.53	2.30	-3.53	"Lamprecht, ca-ca-o2-c4, c3->ca"
rh1	o3tc	cx	c4	2.30	4.00	0.00	"Lamprecht, c4-ca-o2-c4, c3->ca"
rh1	p1	ca	ca	0.00	0.00	0.40	"Lamprecht, ca-ca-p-c4, c3->ca"
o3tc	rh1	p1	ca	0.00	0.00	0.00	"Lamprecht"
o3tc	rh1	o3tp	cx	0.00	0.00	0.00	"Lamprecht"
o3tc	rh1	c6	o+	0.00	0.00	0.00	"Lamprecht"
o3tc	cx	ca	cx	0.00	16.25	0.00	"Lamprecht, ca-ca-ca-o2, c3->ca"
o3tc	cx	ca	h	0.00	16.25	0.00	"Lamprecht, h-ca-ca-o2, c3->ca"
o3tc	cx	c4	h	0.00	0.00	0.54	"Lamprecht, h-c4-ca-o2, c3->ca"
cx	o3tc	rh1	p1	0.00	0.00	0.00	"Lamprecht"
cx	o3tp	rh1	p1	0.00	0.00	0.00	"Lamprecht"
cx	o3tc	rh1	c6	0.00	0.00	0.00	"Lamprecht"
cx	ca	cx	c4	-0.27	9.00	0.00	"Lamprecht, c4-ca-ca-ca, MM2"
cx	o3tp	rh1	c6	0.00	0.00	0.00	"Lamprecht"
p1	rh1	c6	o+	0.00	0.00	0.00	"Lamprecht"
p1	ca	ca	ca	0.00	16.25	0.00	"Lamprecht, ca-ca-ca-p, c3->ca"
p1	ca	ca	h	0.00	16.25	0.00	"Lamprecht, h-ca-ca-p, c3->ca"
c6	rh1	p1	ca	0.00	0.00	0.00	"Lamprecht"
ca	p1	ca	ca	0.00	0.00	0.33	"Lamprecht, ca-ca-p-ca, c3->ca"
ca	cx	c4	h	0.00	0.00	-0.24	"Lamprecht, h-c4-ca-ca, MM2"
c4	cx	ca	h	0.00	9.00	0.00	"Lamprecht, c4-ca-ca-h, MM2"
o5tp	rh1	o7tc	n6	0.00	0.00	0.00	"Lamprecht"
o5tp	rh1	p1	ca	0.00	0.00	0.00	"Lamprecht"
o5tp	rh1	c6	o+	0.00	0.00	0.00	"Lamprecht"
o5tp	cy	n6	o7tc	-2.00	16.25	0.00	"Lamprecht, o2-ca-ca-o2, c3->ca"
o5tp	cy	n6	ca	0.00	16.25	0.00	"Lamprecht, ca-ca-ca-o2, c3->ca"
o5tp	cy	ca	ca	0.00	16.25	0.00	"Lamprecht, ca-ca-ca-o2, c3->ca"
rh1	o5tp	cy	n6	3.53	2.30	-3.53	"Lamprecht, ca-ca-o2-c4, c3->ca"
rh1	o5tp	cy	ca	3.53	2.30	-3.53	"Lamprecht, ca-ca-o2-c4, c3->ca"
rh1	o7tc	n6	cy	3.53	2.30	-3.53	"Lamprecht, ca-ca-o2-c4, c3->ca"
rh1	o7tc	n6	ca	3.53	2.30	-3.53	"Lamprecht, ca-ca-o2-c4, c3->ca"
o7tc	rh1	o5tp	cy	0.00	0.00	0.00	"Lamprecht"
o7tc	rh1	p1	ca	0.00	0.00	0.00	"Lamprecht"
o7tc	rh1	c6	o+	0.00	0.00	0.00	"Lamprecht"
o7tc	n6	cy	ca	0.00	16.25	0.00	"Lamprecht, ca-ca-ca-o2, c3->ca"
o7tc	n6	ca	ca	0.00	16.25	0.00	"Lamprecht, ca-ca-ca-o2, c3->ca"
n6	o7tc	rh1	p1	0.00	0.00	0.00	"Lamprecht"
n6	o7tc	rh1	c6	0.00	0.00	0.00	"Lamprecht"
n6	cy	ca	ca	0.00	15.00	0.00	"Lamprecht, ca-ca-ca-n2, c3->ca"
n6	ca	ca	ca	0.00	15.00	0.00	"Lamprecht, ca-ca-ca-n2, c3->ca"
n6	ca	ca	h	0.00	15.00	0.00	"Lamprecht, h-ca-ca-n2, c3->ca"

```
cy    o5tp  rh1   p1    0.00    0.00    0.00    "Lamprecht"
cy    o5tp  rh1   c6    0.00    0.00    0.00    "Lamprecht"
cy    n6    ca    ca    0.00    0.00    1.49    "Lamprecht, ca-ca-n2-ca, c3->ca"
cy    ca    ca    ca    -0.93   4.80    0.00    "Lamprecht, ca-ca-ca-ca, theory"
cy    ca    ca    h     0.00    5.41    -1.06   "Lamprecht, h-ca-ca-ca, MM2"
ca    cy    n6    ca    0.00    0.00    1.49    "Lamprecht, ca-ca-n2-ca, c3->ca"
o3tp  cx    ca    c4    -1.20   16.25   0.00    "Lamprecht, c4-ca-ca-o2, c3->ca"
o3tc  cx    ca    c4    -1.20   16.25   0.00    "Lamprecht, c4-ca-ca-o2, c3->ca"
cx    ca    c4    ca    0.10    0.00    0.50    "Lamprecht, ca-c4-ca-ca, MM2"
cx    ca    c4    h     0.00    0.00    -0.24   "Lamprecht, h-c4-ca-ca, MM2"
c4    ca    cx    c4    -0.10   9.00    0.00    "Lamprecht, c4-ca-ca-c4, MM2"
n4tp  rh1   s7tc  cx    0.00    0.00    0.00    "Lamprecht"
n4tp  rh1   p1    ca    0.00    0.00    0.00    "Lamprecht"
n4tp  rh1   c6    o+    0.00    0.00    0.00    "Lamprecht"
n4tp  cx    ca    cx    0.00    15.00   0.00    "Lamprecht, ca-ca-ca-n2, c3->ca"
n4tp  cx    ca    c4    -0.27   9.00    0.00    "Lamprecht, c4-ca-ca-ca, MM2"
n4tp  cx    c4    c4    -0.44   0.24    0.06    "Lamprecht, c4-c4-ca-ca, MM2"
n4tp  cx    c4    h     0.00    0.00    -0.24   "Lamprecht, h-c4-ca-ca, MM2"
n4tp  c4    c4    c4    0.00    0.00    0.40    "Lamprecht, c4-c4-c4-n2, MM2"
n4tp  c4    c4    h     0.00    0.00    0.40    "Lamprecht, h-c4-c4-n2, MM2"
rh1   n4tp  cx    ca    0.00    0.50    0.00    "Lamprecht, ca-ca-n2-c4, c3->ca"
rh1   n4tp  cx    c4    -0.10   9.00    0.00    "Lamprecht, c4-ca-ca-c4, MM2"
rh1   n4tp  c4    c4    0.00    0.00    0.91    "Lamprecht, c4-c4-n2-c4, MM2"
rh1   n4tp  c4    h     0.00    0.00    -0.20   "Lamprecht, h-c4-n2-c4, MM2"
rh1   s7tc  cx    s2    0.00    15.00   2.60    "Lamprecht, ca-ca-ca-sa, c3->ca"
rh1   s7tc  cx    ca    0.00    1.70    0.40    "Lamprecht, ca-ca-sa-ca, c3->ca"
s7tc  rh1   n4tp  cx    0.00    0.00    0.00    "Lamprecht"
s7tc  rh1   n4tp  c4    0.00    0.00    0.00    "Lamprecht"
s7tc  rh1   p1    ca    0.00    0.00    0.00    "Lamprecht"
s7tc  rh1   c6    o+    0.00    0.00    0.00    "Lamprecht"
s7tc  cx    s2    c7    0.00    1.70    0.40    "Lamprecht, ca-ca-sa-ca, c3->ca"
s7tc  cx    ca    cx    0.00    15.00   2.60    "Lamprecht, ca-ca-ca-sa, c3->ca"
s7tc  cx    ca    c4    0.00    15.00   2.60    "Lamprecht, ca-ca-ca-sa, c3->ca"
cx    s7tc  rh1   p1    0.00    0.00    0.00    "Lamprecht"
cx    s7tc  rh1   c6    0.00    0.00    0.00    "Lamprecht"
cx    s2    c7    h     0.00    1.70    0.00    "Lamprecht, h-ca-sa-ca, c3->ca"
cx    ca    c4    c4    -0.44   0.24    0.06    "Lamprecht, c4-c4-ca-ca, MM2"
s2    cx    ca    cx    0.00    15.00   2.60    "Lamprecht, ca-ca-ca-sa, c3->ca"
s2    cx    ca    c4    0.00    15.00   2.60    "Lamprecht, ca-ca-ca-sa, c3->ca"
ca    cx    s2    c7    0.00    1.70    0.40    "Lamprecht, ca-ca-sa-ca, c3->ca"
ca    cx    n4tp  c4    0.00    0.50    0.00    "Lamprecht, ca-ca-n2-c4, c3->ca"
ca    cx    c4    c4    -0.44   0.24    0.06    "Lamprecht, c4-c4-ca-ca, MM2"
cx    n4tp  rh1   p1    0.00    0.00    0.00    "Lamprecht"
cx    n4tp  rh1   c6    0.00    0.00    0.00    "Lamprecht"
cx    n4tp  c4    c4    0.00    0.00    0.00    "Lamprecht, c4-c4-n2-ca, c3->ca"
cx    n4tp  c4    h     0.00    0.00    0.00    "Lamprecht, c4-c4-n2-ca, c3->ca"
cx    c4    c4    c4    0.17    0.27    0.09    "Lamprecht, c4-c4-c4-ca, MM2"
cx    c4    c4    h     0.00    0.00    0.50    "Lamprecht, h-c4-c4-ca, MM2"
c4    cx    n4tp  c4    -0.10   9.00    0.00    "Lamprecht, c4-ca-ca-c4, MM2"
p1    rh1   n4tp  c4    0.00    0.00    0.00    "Lamprecht"
c6    rh1   n4tp  c4    0.00    0.00    0.00    "Lamprecht"
o7tp  rh1   o7tc  n6    0.00    0.00    0.00    "Lamprecht"
o7tp  rh1   p1    ca    0.00    0.00    0.00    "Lamprecht"
o7tp  rh1   c6    o+    0.00    0.00    0.00    "Lamprecht"
o7tp  n6    n6    o7tc  0.00    10.00   0.00    "Lamprecht, ca-na-na-ca, c3->ca"
o7tp  n6    n6    ca    0.00    10.00   0.00    "Lamprecht, ca-na-na-ca, c3->ca"
rh1   o7tp  n6    n6    0.00    10.00   0.00    "Lamprecht, ca-ca-na-na, c3->ca"
rh1   o7tc  n6    n6    0.00    10.00   0.00    "Lamprecht, ca-ca-na-na, c3->ca"
o7tc  rh1   o7tp  n6    0.00    0.00    0.00    "Lamprecht"
n6    o7tp  rh1   p1    0.00    0.00    0.00    "Lamprecht"
n6    o7tp  rh1   c6    0.00    0.00    0.00    "Lamprecht"
n6    n6    ca    ca    0.00    10.00   0.00    "Lamprecht, ca-ca-na-na, c3->ca"
s7tp  rh1   n4tc  cx    0.00    0.00    0.00    "Lamprecht"
s7tp  rh1   n4tc  hn    0.00    0.00    0.00    "Lamprecht"
s7tp  rh1   p1    ca    0.00    0.00    0.00    "Lamprecht"
s7tp  rh1   c6    o+    0.00    0.00    0.00    "Lamprecht"
s7tp  cx    ca    cx    0.00    15.00   2.60    "Lamprecht, ca-ca-ca-sa, c3->ca"
s7tp  cx    ca    c4    0.00    15.00   2.60    "Lamprecht, ca-ca-ca-sa, c3->ca"
```

s7tp	cx	s2	c7	0.00	1.70	0.40	"Lamprecht, ca-ca-sa-ca, c3->ca"
rh1	s7tp	cx	ca	0.00	1.70	0.40	"Lamprecht, ca-ca-sa-ca, c3->ca"
rh1	n4tc	cx	c4	-0.10	9.00	0.00	"Lamprecht, c4-ca-ca-c4, MM2"
n4tc	rh1	s7tp	cx	0.00	0.00	0.00	"Lamprecht"
n4tc	rh1	p1	ca	0.00	0.00	0.00	"Lamprecht"
n4tc	rh1	c6	o+	0.00	0.00	0.00	"Lamprecht"
n4tc	cx	ca	cx	0.00	15.00	0.00	"Lamprecht, ca-ca-ca-n2, c3->ca"
n4tc	cx	ca	c4	-0.27	9.00	0.00	"Lamprecht, c4-ca-ca-ca, MM2"
n4tc	cx	c4	c4	-0.44	0.24	0.06	"Lamprecht, c4-c4-ca-ca, MM2"
n4tc	cx	c4	h	0.00	0.00	-0.24	"Lamprecht, h-c4-ca-ca, MM2"
cx	n4tc	rh1	p1	0.00	0.00	0.00	"Lamprecht"
cx	n4tc	rh1	c6	0.00	0.00	0.00	"Lamprecht"
ca	cx	n4tc	hn	1.85	7.20	0.00	"Lamprecht, ca-ca-n2-hv, c3->ca"
c4	cx	n4tc	hn	1.85	7.20	0.00	"Lamprecht, ca-ca-n2-hv, c3->ca"
cx	s7tp	rh1	p1	0.00	0.00	0.00	"Lamprecht"
cx	s7tp	rh1	c6	0.00	0.00	0.00	"Lamprecht"
p1	rh1	n4tc	hn	0.00	0.00	0.00	"Lamprecht"
c6	rh1	n4tc	hn	0.00	0.00	0.00	"Lamprecht"
rh1	s7tp	cx	s2	0.00	15.00	2.60	"Lamprecht, ca-ca-ca-sa, c3->ca"
rh1	n4tc	cx	ca	0.00	0.50	0.00	"Lamprecht, ca-ca-n2-c4, c3->ca"
n5tp	rh1	o5tc	ca	0.00	0.00	0.00	"Lamprecht"
n5tp	rh1	p1	ca	0.00	0.00	0.00	"Lamprecht"
n5tp	rh1	c6	o+	0.00	0.00	0.00	"Lamprecht"
n5tp	ca	ca	o5tc	0.00	16.25	0.00	"Lamprecht, ca-ca-ca-o2, c3->ca"
n5tp	ca	ca	ca	0.00	15.00	0.00	"Lamprecht, ca-ca-ca-n2, c3->ca"
n5tp	cx	ca	ca	0.00	15.00	0.00	"Lamprecht, ca-ca-ca-n2, c3->ca"
n5tp	cx	ca	h	0.00	15.00	0.00	"Lamprecht, h-ca-ca-n2, c3->ca"
rh1	n5tp	ca	ca	0.00	0.50	0.00	"Lamprecht, ca-ca-n2-c4, c3->ca"
rh1	n5tp	cx	ca	0.00	0.50	0.00	"Lamprecht, ca-ca-n2-c4, c3->ca"
rh1	n5tp	cx	h	0.00	0.50	0.00	"Lamprecht, ca-ca-n2-c4, c3->ca"
rh1	o5tc	ca	ca	3.53	2.30	-3.53	"Lamprecht, ca-ca-o2-c4, c3->ca"
o5tc	rh1	n5tp	ca	0.00	0.00	0.00	"Lamprecht"
o5tc	rh1	n5tp	cx	0.00	0.00	0.00	"Lamprecht"
o5tc	rh1	p1	ca	0.00	0.00	0.00	"Lamprecht"
o5tc	rh1	c6	o+	0.00	0.00	0.00	"Lamprecht"
o5tc	ca	ca	ca	0.00	16.25	0.00	"Lamprecht, ca-ca-ca-o2, c3->ca"
o5tc	ca	ca	h	0.00	16.25	0.00	"Lamprecht, h-ca-ca-o2, c3->ca"
ca	o5tc	rh1	p1	0.00	0.00	0.00	"Lamprecht"
ca	o5tc	rh1	c6	0.00	0.00	0.00	"Lamprecht"
ca	ca	n5tp	cx	0.00	0.00	1.49	"Lamprecht, ca-ca-n2-ca, c3->ca"
ca	n5tp	rh1	p1	0.00	0.00	0.00	"Lamprecht"
ca	n5tp	rh1	c6	0.00	0.00	0.00	"Lamprecht"
ca	n5tp	cx	ca	0.00	0.00	1.49	"Lamprecht, ca-ca-n2-ca, c3->ca"
ca	n5tp	cx	h	0.00	0.00	1.49	"Lamprecht, ca-ca-n2-ca, c3->ca"
ca	ca	n5tp	cx	0.00	0.00	1.49	"Lamprecht, ca-ca-n2-ca, c3->ca"
ca	ca	ca	cx	-0.93	4.80	0.00	"Lamprecht, ca-ca-ca-ca, theory"
ca	ca	cx	h	0.00	5.41	-1.06	"Lamprecht, h-ca-ca-ca, MM2"
p1	rh1	n5tp	cx	0.00	0.00	0.00	"Lamprecht"
c6	rh1	n5tp	cx	0.00	0.00	0.00	"Lamprecht"
cx	ca	ca	h	0.00	5.41	-1.06	"Lamprecht, h-ca-ca-ca, MM2"
h	cx	ca	h	0.00	15.00	0.00	"Lamprecht, h-ca-ca-h, theory"
n5tp	rh1	o5tc	co	0.00	0.00	0.00	"Lamprecht"
n5tp	ca	co	o5tc	0.00	16.25	0.00	"Lamprecht, ca-ca-co-o2, c3->ca"
n5tp	ca	co	o1	1.53	6.50	0.83	"Lamprecht, ca-ca-co-o1, c3->ca"
n5tp	ca	ca	h	0.00	15.00	0.00	"Lamprecht, h-ca-ca-n2, c3->ca"
rh1	n5tp	ca	co	0.00	15.00	0.00	"Lamprecht, c4-ca-ca-co, c3->ca"
rh1	o5tc	co	ca	0.00	11.10	0.00	"Lamprecht, c4-ca-co-ca, c3->ca"
rh1	o5tc	co	o1	2.75	15.00	0.00	"Lamprecht, c4-ca-co-o1, c3->ca"
o5tc	co	ca	ca	0.00	16.25	0.00	"Lamprecht, ca-ca-co-o2, c3->ca"
co	o5tc	rh1	p1	0.00	0.00	0.00	"Lamprecht"
co	o5tc	rh1	c6	0.00	0.00	0.00	"Lamprecht"
co	ca	n5tp	cx	0.00	15.00	0.00	"Lamprecht, ca-ca-ca-co, c3->ca"
s7tp	rh1	o3tc	cx	0.00	0.00	0.00	"Lamprecht"
s7tp	cx	ca	h	0.00	15.00	0.00	"Lamprecht, h-ca-ca-sa, c3->ca"
s7tp	cx	c4	h	0.00	15.00	0.00	"Lamprecht, h-ca-ca-sa, c3->ca"
rh1	s7tp	cx	c4	-0.10	9.00	0.00	"Lamprecht, c4-ca-ca-c4, MM2"
o3tc	rh1	s7tp	cx	0.00	0.00	0.00	"Lamprecht"
n4tp	rh1	o3tc	ca	0.00	0.00	0.00	"Lamprecht"

```
n4tp  cx    ca    ca    0.00    15.00   0.00    "Lamprecht, ca-ca-ca-n2, c3->ca"
n4tp  ca    ca    ca    0.00    15.00   0.00    "Lamprecht, ca-ca-ca-n2, c3->ca"
n4tp  ca    ca    h     0.00    15.00   0.00    "Lamprecht, h-ca-ca-n2, c3->ca"
n4tp  ca    ca    c4    0.00    15.00   0.00    "Lamprecht, ca-ca-ca-n2, c3->ca"
rh1   n4tp  cx    h     0.00    9.00    0.00    "Lamprecht, c4-ca-ca-h, MM2"
rh1   n4tp  ca    ca    0.00    0.50    0.00    "Lamprecht, ca-ca-n2-c4, c3->ca"
rh1   o3tc  ca    ca    3.53    2.30    -3.53   "Lamprecht, ca-ca-o2-c4, c3->ca"
o3tc  rh1   n4tp  cx    0.00    0.00    0.00    "Lamprecht"
o3tc  rh1   n4tp  ca    0.00    0.00    0.00    "Lamprecht"
o3tc  ca    ca    ca    0.00    16.25   0.00    "Lamprecht, ca-ca-ca-o2, c3->ca"
o3tc  ca    ca    h     0.00    16.25   0.00    "Lamprecht, h-ca-ca-o2, c3->ca"
o3tc  ca    ca    cx    0.00    16.25   0.00    "Lamprecht, ca-ca-ca-o2, c3->ca"
ca    o3tc  rh1   c6    0.00    0.00    0.00    "Lamprecht"
ca    o3tc  rh1   p1    0.00    0.00    0.00    "Lamprecht"
ca    cx    n4tp  ca    0.00    0.00    1.49    "Lamprecht, ca-ca-n2-ca, c3->ca"
cx    n4tp  ca    ca    0.00    0.00    1.49    "Lamprecht, ca-ca-n2-ca, c3->ca"
ca    n4tp  rh1   c6    0.00    0.00    0.00    "Lamprecht"
ca    n4tp  rh1   p1    0.00    0.00    0.00    "Lamprecht"
ca    n4tp  cx    h     0.00    5.41    -1.06   "Lamprecht, h-ca-ca-ca, MM2"
o3tp  cx    c5    f     1.24    1.45    -1.24   "Lamprecht, f-c4-ca-ca, c3->ca"
rh1   o3tp  cx    c5    2.30    4.00    0.00    "Lamprecht, c4-ca-o2-c4, c3->ca"
o3tc  cx    c4    c4    0.00    0.00    0.00    "Lamprecht, c4-c4-ca-o2, c3->ca"
cx    ca    cx    c5    -0.27   9.00    0.00    "Lamprecht, c4-ca-ca-ca, MM2"
c5    cx    ca    h     0.00    9.00    0.00    "Lamprecht, c4-ca-ca-h, MM2"
ca    cx    c5    f     1.24    1.45    -1.24   "Lamprecht, f-c4-ca-ca, c3->ca"
o5tp  rh1   o5tc  cy    0.00    0.00    0.00    "Lamprecht"
o5tp  cy    cy    o5tc  -2.00   16.25   0.00    "Lamprecht, o2-ca-ca-o2, c3->ca"
o5tp  cy    cy    c3    0.00    16.25   0.00    "Lamprecht, c3-ca-ca-o2, c3->ca"
o5tp  cy    c3    c3    0.00    16.25   0.00    "Lamprecht, c3-c3-ca-o2, c3->ca"
o5tp  cy    c3    h     0.00    16.25   0.00    "Lamprecht, h-c3-ca-o2, c3->ca"
rh1   o5tp  cy    cy    3.53    2.30    -3.53   "Lamprecht, ca-ca-o2-c4, c3->ca"
rh1   o5tp  cy    c3    3.53    2.30    -3.53   "Lamprecht, c3-ca-o2-c4, c3->ca"
rh1   o5tc  cy    cy    3.53    2.30    -3.53   "Lamprecht, ca-ca-o2-c4, c3->ca"
rh1   o5tc  cy    c3    3.53    2.30    -3.53   "Lamprecht, c3-ca-o2-c4, c3->ca"
o5tc  rh1   o5tp  cy    0.00    0.00    0.00    "Lamprecht"
o5tc  cy    cy    c3    0.00    16.25   0.00    "Lamprecht, c3-ca-ca-o2, c3->ca"
o5tc  cy    c3    c3    0.00    16.25   0.00    "Lamprecht, c3-c3-ca-o2, c3->ca"
o5tc  cy    c3    h     0.00    16.25   0.00    "Lamprecht, h-c3-ca-o2, c3->ca"
cy    o5tc  rh1   p1    0.00    0.00    0.00    "Lamprecht"
cy    o5tc  rh1   c6    0.00    0.00    0.00    "Lamprecht"
cy    cy    c3    c3    -0.93   8.00    0.00    "Lamprecht, c3-c3-ca-ca, c3->ca"
cy    cy    c3    h     0.00    9.00    -1.06   "Lamprecht, h-c3-ca-ca, c3->ca"
cy    c3    c3    c3    -0.93   8.00    0.00    "Lamprecht, c3-c3-c3-ca, c3->ca"
cy    c3    c3    h     0.00    9.00    -1.06   "Lamprecht, h-c3-c3-ca, c3->ca"
c3    cy    cy    c3    -0.93   8.00    0.00    "Lamprecht, c3-ca-ca-c3, c3->ca"
```

Out-of-plane Bending Parameter file (mmpoop.txt)

```
C     A     COPB    REMARK
ca    c4    0.050   "Allinger, MM2 (1991)"
ca    h     0.050   "Allinger, MM2 (1991)"
ca    ca    0.050   "Allinger, MM2 (1991)"
ca    p1    0.500   "Lamprecht, (ca p), c3->ca"
ca    cx    0.050   "Lamprecht, (ca ca), MM2"
ca    cy    0.050   "Lamprecht, (ca ca), MM2"
ca    n6    0.050   "Lamprecht, (ca n2), c3->ca"
ca    o5tc  0.050   "Lamprecht, (ca o2), c3->ca"
ca    n5tp  0.050   "Lamprecht, (ca n2), c3->ca"
co    o5tc  0.800   "Lamprecht, (co o2), MM2"
ca    o3tc  0.050   "Lamprecht, (ca o2), c3->ca"
ca    n4tp  0.050   "Lamprecht, (ca n2), c3->ca"
c3    cy    0.050   "Lamprecht, (c3 ca), c3->ca"
```

Non-Bonded Parameter file (mmpnbd.txt)

TYPE	RSTAR	EPS	REMARKS
c4	1.9000	0.0440	"Allinger, MM2 (1991)"
h	1.5000	0.0470	"Allinger, MM2 (1991)"
ca	1.9400	0.0440	"Allinger, MM2 (1991)"
o3tp	1.7400	0.0500	"Lamprecht, o2, MM2"
rh1	1.9000	0.0440	"Lamprecht, c4, MM2"
o3tc	1.7400	0.0500	"Lamprecht, o2, MM2"
cx	1.9400	0.0440	"Lamprecht, ca, MM2"
p1	2.1800	0.1680	"Lamprecht, p, MM2"
c6	1.9400	0.0440	"Lamprecht, co, MM2"
o+	1.7400	0.0660	"Lamprecht, o1, MM2"
o5tp	1.7400	0.0500	"Lamprecht, o2, MM2"
o7tc	1.7400	0.0500	"Lamprecht, o2, MM2"
n6	1.8200	0.0550	"Lamprecht, n2, MM2"
cy	1.9400	0.0440	"Lamprecht, ca, MM2"
n4tp	1.8200	0.0550	"Lamprecht, n2, MM2"
s7tc	2.1100	0.2020	"Lamprecht, s2, MM2"
c7	1.9000	0.0440	"Lamprecht, c4, MM2"
o7tp	1.7400	0.0500	"Lamprecht, o2, MM2"
s7tp	2.1100	0.2020	"Lamprecht, s2, MM2"
n4tc	1.8200	0.0550	"Lamprecht, n2, MM2"
n5tp	1.8200	0.0550	"Lamprecht, n2, MM2"
o5tc	1.7400	0.0500	"Lamprecht, o2, MM2"
c5	1.9000	0.0440	"Lamprecht, c4, MM2"

SUMMARY

Four Rh(I)(β-diketonato)(CO)(PPh_3) complexes, in which the β-diketone has different electronegativities and steric hindrances, were successfully synthesised and characterised by means of Infrared and NMR spectroscopy.

The crystal structure of (1,3-Diphenyl-1,3-propanedionato-κO, κO) Triphenyl Phosphine Rhodium(I) showed that the asymmetric unit consists of two crystallographically independent molecules. The molecules form a close centrosymmetric pair, but not a crystallographic inversion centre. The partial overlapping of the chelate ring of the one molecule with the phenyl ring of the other molecule can be attributed to π-π interactions between atoms of the two molecules.

The oxidative addition kinetics of CH_3I to Rh(I)(β-diketonato)(CO)(PPh_3) complexes was studied in the Visible, Infrared and NMR regions.

The proposed oxidative addition mechanism of CH_3I to Rh(I)(β-diketonato)(CO)(PPh_3) complexes is a nucleophilic attack by the Rhodium atom on the Carbon atom of the methyl iodide, where a linear or a three-centred polar transition state is formed which leads to *trans* and *cis* addition respectively. The main purpose of the development of a Rh(I) Carbonyl Phosphine force field was not only to predict the molecular structure of Rh(I) complexes, but also to compute a possible transition states during the oxidative addition of CH_3I to Rh(I)(β-diketonato)(CO)(PPh_3) complexes. Steric energy calculations indicated that the oxidative addition of CH_3I to the Rh(I) Carbonyl Phosphine complexes would rather occur via a S_N2 mechanism than a concerted three-centred mechanism.

The negative entropy of activation and the negative experimental volume of activation obtained during oxidative addition of CH_3I to Rh(I)(β-diketonato)(CO)(PPh_3) complexes pointed towards an associative mechanism.

An increase in solvent polarity leads to an increase in the second order rate constant. These results are indicative of a mechanism where a polar transition state is formed.

During the electrochemical oxidation of Rh(I)(β-diketonato)(CO)(PPh_3) the only possible co-ordination ligand was the solvent, CH_3CN. The addition of solvents with different donosities revealed the co-ordination of the solvents during electrochemical oxidation. The addition of solvents with higher donosities and therefore better co-ordinating properties made it more difficult to reduce the Rh(III) species formed, back to Rh(I).

The two electron irreversible electrochemical oxidation of Rh(I) to Rh(III) was confirmed during bulk electrolysis and Cyclic Voltammetric studies, where the addition of $[B_ZN(Et)_3]^+Cl^-$ to the solution stabilised the formation of Rh(III).

The electronic effect of the substituents on the β-diketones showed that the reaction rate increases with the increase of the pKa-values of the free β-diketones. The effect of more electronegative substituents on the reactivity of the Rh(I) centre is explained by the fact that electron density is removed from the Rhodium metal, making the complex a stronger Lewis acid and less reactive towards oxidative addition.

Steric effects were also perceptible in the present study where the β-diketones, btfa and tfaa, had the same pKa-values. The reaction rate of the bulkier btfa was slower than that of tfaa.

Electrochemical oxidation justified the electronic effect, with the exception that steric parameters had no effect during electrochemical oxidation. The oxidation potentials of Rh(btfa)(CO)(PPh_3) and Rh(tfaa)(CO)(PPh_3), which have the same pKa-values, are the same, within experimental error. The technique of electrochemical oxidation can therefore be used to quantify steric effects during chemical oxidation.

The final isomer formed during oxidative addition of CH_3I to Rh(I)(β-diketonato)(CO)(PPh_3) complexes depends on the nature and nucleophilicity of the ligands. A linear transition state leads to *trans* addition of CH_3I, and isomerisation forms a *cis* Rh(III) Carbonyl Phosphine isomer in the case of Rh(dbm)(CO)(PPh_3) and Rh(ba)(CO)(PPh_3) as final product. From IR spectroscopy it is clear that the final oxidative addition product of Rh(btfa)(CO)(PPh_3) and Rh(tfaa)(CO)(PPh_3) is the Rh(III) acyl complex.

OPSOMMING

Vier Rh(I)(β-diketoon)(CO)(PPh_3) komplekse, waar die β-diketone verskillende elektroniese en steriese parameters besit, is suksesvol berei en met behulp van Infrarooi en KMR spektrofotometrie gekarakteriseer.

Die kristalstruktuurstudie van (1,3-Difeniel-1,3-propaandionato-κO, κO) trifenielfosfienrodium(I) toon aan dat die asimetriese eenheidsel uit twee onafhanklike molekule bestaan. Die oorvleueling van die chelaatring van die een molekuul met die fenielring van die ander molekuul kan toegeskryf word aan π-π interaksies tussen die atome van die twee molekule.

Oksidatiewe addisie kinetika van CH_3I aan Rh(I)(β-diketoon)(CO)(PPh_3) komplekse is in die Sigbare, Infrarooi en KMR gebied bestudeer en word voorgestel deur ´n nukleofiele aanval van die Rodiumatoom op die Koolstofatoom van CH_3I. ´n Liniêre oorgandstoestand of ´n drie-senter oorgangstoestand word voorgestel. Die liniêre oorgangstoestand lei tot *trans*-addisie van CH_3I en die drie-senter oorgangstoestand lei tot *cis*-addisie van CH_3I.

Molekulêre meganika is gebriuk om ´n Rh(I)-karbonielfosfien kragveld te ontwerp waarmee nuwe Rh(I)-karbonielfosfien strukture voorspel kan word, asook om die oorgangstoestand tydens oksidatiewe addisie te bereken. Die berekening van die steriese energië van beide die liniêre oorgangstoestand en drie-senter oorgangstoestand het aangetoon dat die liniêre oorgangstoestand meer stabiel is en dat oksidatiewe addisie van CH_3I dus eerder via ´n S_N2-meganisme sal plaasvind.

Negatiewe aktiveringsentropie en aktiveringsvolume waardes wat verkry is tydens oksidatiewe addisie van CH_3I aan Rh(I)(β-diketoon)(CO)(PPh_3) komplekse dui op ´n assosiatiewe meganisme.

´n Verhoging in die polariteit van die oplosmiddels tydens oksidatiewe addisie het gelei tot ´n verhoging in die reaksietempo, wat dui op ´n polêre oorgangstoestand.

Slegs die oplosmiddel, CH_3CN, is beskikbaar om te koördineer tydens die elektrochemiese oksidasie van Rh(I) na Rh(III). Oplosmiddels wat oor beter doneringsvermoë beskik en dus ook beter koördineer, stabiliseer die gevormde Rh(III) wat die reduksie daarvan terug na Rh(I) bemoeilik.

Die twee-elektron onomkeerbare elektrochemiese oksidasie van Rh(I) na Rh(III) is tydens Totale-elektroliese en Sikliese Voltammetrie waargeneem waar $[B_ZN(Et)_3]^+Cl^-$ by die oplossing gevoeg is om die gevormde Rh(III) te stabiliseer.

´n Verhoging in die pKa-waarde van die β-diketoon het gelei tot ´n verhoging in die reaksietempo tydens oksidatiewe addisie. Elektron ontrekkende groepe gekoördineerd aan die Rodium metaal veroorsaak dat die Rodium senter ´n sterker Lewis-suur is en dus minder reaktief is ten opsigte van oksidatiewe addisie.

Die reaksietempo wat tydens oksidatiewe addisie van CH_3I aan Rh(I)(β-diketoon)(CO)(PPh_3) komplekse waargeneem is, is nie net afhanklik van die elektronies parameters nie, maar is ook afhanklik van steriese hindernisse wat deur gekoördineerde ligande veroorsaak word. Rh(btfa)(CO)(PPh_3) het dieselfde pKa-waarde as Rh(tfaa)(CO)(PPh_3), maar die oksidatiewe addisie reaksietempo van die eersgenoemde kompleks was baie stadiger as gevolg van steriese hindernis.

Die oksidasie potensiaal van Rh(btfa)(CO)(PPh_3) en Rh(tfaa)(CO)(PPh_3) wat oor identiese pKa-waardes beskik, was binne ´n eksperimentele fout dieselfde tydens elektrochemiese oksidasie. Alhoewel die elektroniese effek van die gekoördineerde β-diketone dieselfde resultate getoon het tydens chemiese- en elektrochemiese oksidasie, speel die steriese effek van gekoördineerde β-diketone nie ´n rol tydens elektrochemiese oksidasie nie.

Die eindproduk van oksidatiewe addisie is afhanklik van die aard en nukleofiliteit van die gekoördineerde ligande. In die geval van Rh(dbm)(CO)(PPh_3) en Rh(ba)(CO)(PPh_3) is die eindproduk die *cis*-Rh(III)-karbonielfosfien isomeer, maar in die geval van Rh(btfa)(CO)(PPh_3) en Rh(tfaa)(CO)(PPh_3) is die eindproduk die Rh(III)-asiel isomeer.